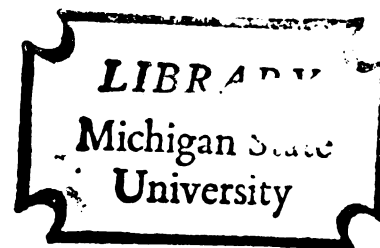


THESIS



This is to certify that the
thesis entitled
Two-Photon Spectroscopy of Linear Polyenes

presented by
Howard L. B. Fang

has been accepted towards fulfillment
of the requirements for

~~Ph.D.~~ degree in ~~Chemistry~~

A handwritten signature in cursive script, reading "G. B. Levi".

Major professor

Date 8/26/77

TWO-PHOTON SPECTROSCOPY OF LINEAR POLYENES

By

Howard Lih-Bao Fang

A DISSERTATION

Submitted to
Michigan State University
in partial fulfillment of the requirements
for the degree of

DOCTOR OF PHILOSOPHY

Department of Chemistry

1977

ABSTRACT

TWO-PHOTON SPECTROSCOPY OF LINEAR POLYENES

By

Howard Lih-Bao Fang

Linear, all-trans polyenes have received considerable attention because of their importance in photochemical and biological systems. Recent calculations and experiments indicate that, like the electronic ground state, the lowest excited singlet state in this centrosymmetric chromophore has A_g symmetry, and thus is forbidden in the normal electric-dipole absorption spectrum because the transition violates the $u \leftrightarrow g$ selection rule. However, ${}^1A_g \leftarrow {}^1A_g$ transitions are allowed in two-photon absorption, and it appeared that two-photon spectroscopy would enable direct observation of these hidden excited states.

Two types of linear polyenes were investigated in this research: diphenylsubstituted polyenes and retinyl polyenes. The two-identical-photon excitation (TIPE) spectrum of all-trans diphenyloctatetraene (DPO) in EPA at 77°K has been obtained over the spectral range 10500-12700 cm^{-1} . Near infrared radiation from a tunable dye laser pumped by a Q-switched ruby laser served as the excitation source. A sharp origin and distinct vibrational

structure were observed in the TIPE spectrum of DPO. The excited 1A_g state origin is about 2100 cm^{-1} below the 1B_u origin and is essentially coincident with the one-photon fluorescence origin. A low-lying 1A_g state in DPO has been confirmed.

Several retinyl polyenes of the vitamin A family (all-trans retinol and anhydrovitamin A), which are relevant to the mechanism of vision, have also been investigated in EPA at 77°K by TIPE spectroscopy. Each shows structure suggesting the presence of a 1A_g excited electronic state below the lowest 1B_u allowed state. The excited 1A_g state origin of anhydrovitamin A is about 1600 cm^{-1} below the 1B_u origin. The spectrum of retinol is too broad to establish the origin. The existence of these forbidden states appears to explain the anomalous fluorescence properties of these polyene molecules such as the huge Stokes shift, the very long fluorescence lifetime and the abnormal solvent shift behavior.

To My Parents

ACKNOWLEDGMENTS

I wish to express my most sincere gratitude to Professor George Leroi for his direction, encouragement, and patience. Without his help, this work could hardly have been completed.

I am also deeply grateful to Professor Schwendeman, who served as my second reader, for his valuable comments and guidance. Professor El-Bayoumi was most generous in lending me a fluorimeter instrument for some experiments. I would also like to thank Dr. Robert Thrash for his help in constructing the experimental apparatus, and for his suggestions and understanding. Other group members and our secretary, Mrs. Naomi Hack, deserve thanks for their friendship and stimulation.

Financial support from MSU and NSF is greatly appreciated. Finally, I wish to thank my wife, Julia, for her understanding and support while busily engaged in her own music career.

TABLE OF CONTENTS

	Page
LIST OF TABLES	v
LIST OF FIGURES	vi
 Chapter	
I. INTRODUCTION	1
II. A GENERAL SURVEY OF TWO-PHOTON ABSORPTION IN RELATION TO EXPERIMENTAL CONSIDERATION	15
A. Motivation	15
B. Experimental Methods	17
(1) Direct Measurement	18
(2) Indirect Measurement	26
(3) Parametric Mixing Measurement	34
III. EXPERIMENTAL APPARATUS	39
A. Absorption Spectra	39
B. Emission Spectra	39
C. Ruby Laser System	40
D. Dye Laser System	52
(1) Ruby Laser Pumped Dye Laser	58
(2) Nitrogen Laser Pumped Dye Laser	65
(3) Flashlamp Pumped Dye Laser	72
E. Materials	76
F. Two-Photon Excitation (TPE) Spectrometer	81
IV. THE TWO-PHOTON EXCITATION SPECTRUM OF DIPHENYLOCTATETRAENE	88
A. The Reason for Choosing DPO to Study	88
B. Results and Discussion	93
C. Conclusion and Implications	102
V. THE RETINYL POLYENES	105
A. Introduction	105
B. Results and Discussion	119
C. Summary and Conclusions	130
REFERENCES	133

LIST OF TABLES

Table		Page
1	Comparison of Vibrational Intervals Observed in TPE Spectrum with Those Observed in Fluorescence Spectrum for Diphenyloctatetraene	102

LIST OF FIGURES

Figure		Page
1	Excitation Energy Diagrams for Butadiene by Several Approximate Molecular Orbital Methods	4
2	Upper: A Diagram of Molecular Orbital Wavefunctions for Butadiene. Lower: Electronic Configurations of Butadiene .	5
3	Absorption and Emission Spectra of DPH in EPA at 77°K	8
4	Absorption and Emission Spectra of DPO in EPA at 77°K	9
5	Ground State and Four Lowest Excited States of Octatetraene: (a) Hartree-Fock Calculation; (b) PPP Semi-empirical Calculation with Singly Excited CI Included; (c) PPP with Doubly Excited CI Included	12
6	(a) Two-Photon Absorption (TPA) Effect (b) Some Scattering Effects might Compete with Direct TPA Measurement	20
7	Two-Photon Direct Absorption Measurement	22
8	Two-Photon Absorption Signal in 1-chloronaphthalene	23
9	Ruby Burst Spot after Thermal Blooming Effect.	25
10	Dual Beam Oscillogram of TPE Measurement	29
11	Fluorescence Peak Height as a Function of (b/τ)	31
12	Resonant and Nonresonant Processes in Three-Wave-Mixing. (a) Nonresonant Processes; (b) Raman Resonance; (c) TPA Resonance	35

Figure		Page
13	A Side-View Cross Section of the Ruby Laser Double Elliptical Cavity.	42
14	End-View of Double Elliptical Cavity . .	43
15	Flashlamp Excitation Pulse Forming Network.	45
16	Block Diagrams of the Ruby Power Supply and Triggering Systems	47
17	Automatic Firing Circuit	48
18	Transverse Pumping by a Cylindrical Lens Set	57
19	The Tuning Range and Relative Output Power of Several Dyes	60
20	Dye Laser Tuning System	62
21	Circuitry of the Blumlein Type N ₂ Laser .	67
22	(a) Side-View and (b) End-View of N ₂ Laser; (c) Output Window of N ₂ Laser . .	68
23	N ₂ Laser Pumped Dye Laser	71
24	Two-Dye-Laser (N ₂ Laser Pumped)-Photon Induced Fluorescence Measurement	73
25	Flashlamp Pumped Dye Laser	75
26	Sample Materials	77
27	Absorption Spectra of All-trans Anhydro-vitamin A (taken at 77°K in EPA) Before (—) and After (---) Lengthy Exposure to Room Light at Room Temperature	80
28	Two-Photon Spectrometer of a Ruby Laser Pumped Dye Laser	83
29	Fluorescence Housing for TPE Measurements	84
30	Energy Gap Between the Absorption Origin and the Fluorescence Origin of Diphenyl Polyenes as a Function of the Number of Carbon-Carbon Double Bonds	90

Figure		Page
31	Diffuse Band Appears on the Low Energy Side of the Absorption Origin of DPO at High Concentration ($C = 2 \times 10^{-4}M$)	95
32	Two-Photon Excitation Spectrum of DPO in EPA at 77°K.	97
33	Square Dependence of Two-Photon Induced Fluorescence of DPO	99
34	Absorption and Emission Spectra of All-trans Retinol in EPA at 77°K	108
35	Absorption and Emission Spectra of All-trans Retinal in EPA at 77°K	109
36	(a) The Absorption and Emission Spectra of Axerophthene in EPA at 77°K (ref. 33). (b) The Absorption Spectra of Retinol (—) and 5,6-dihydroretinol (---) in Ethanol of Room Temperature (ref. 132) . .	111
37	Absorption and Emission Spectra of All-trans Anhydrovitamin A in EPA at 77°K . .	113
38	Torsional Potential for the β -ionylidene Ring in Retinal (Ref. 124b)	114
39	One Photon Excitation Spectrum of All-trans Retinal in EPA at 77°K	117
40	The Absorption Spectrum of All-trans Anhydrovitamin A in EPA at 77°K as Concentration Increases ($\sim 5 \times 10^{-5}M$) . . .	121
41	Two-Photon Excitation Spectrum (in unit of $\ln(I_f/I_D^2)$) and the Lowest Energy One-Photon Absorption Band (in unit of relative absorbance) in EPA at 77°K	122
42	TPE Spectrum of All-trans Retinol in EPA at 77°K.	126
43	Square Dependence of Two-Photon Induced Fluorescence of All-trans Retinal	128
44	Two-Photon Excitation Spectrum of All-trans Retinal in EPA at 77°K	129

CHAPTER 1

INTRODUCTION

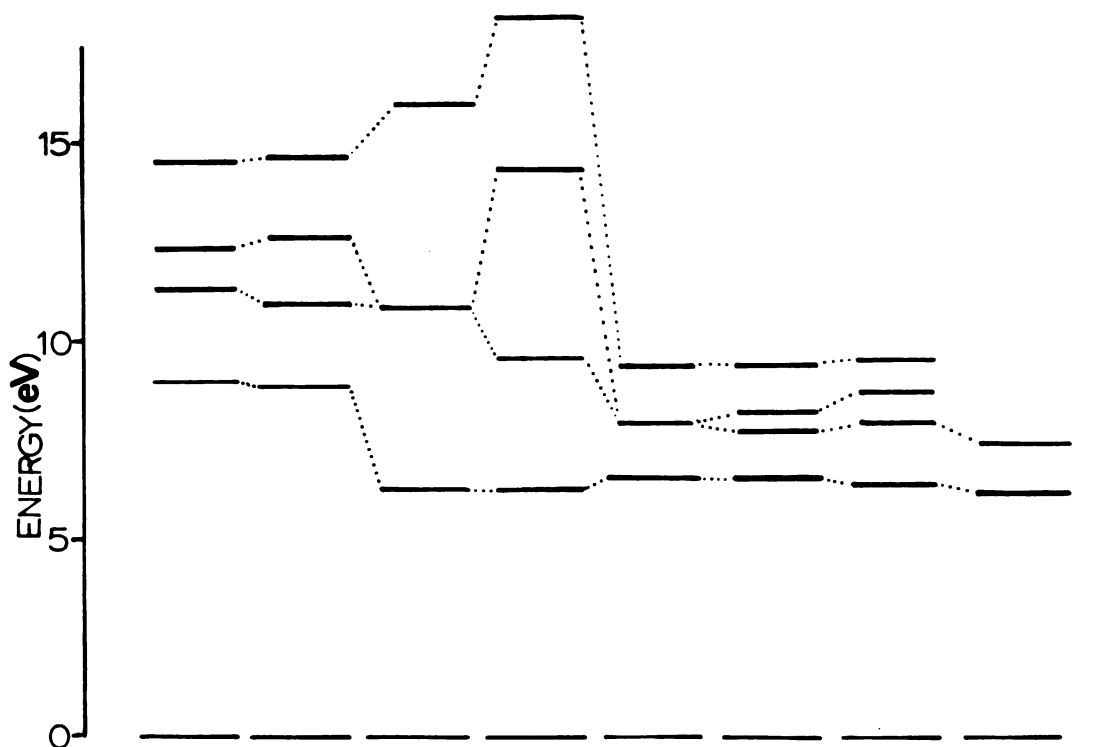
A linear polyene is a chain of conjugated carbon-carbon double bonds with an unbranched π electron system. The spectroscopy of this conjugated system in the near UV and visible regions can be described by considering only the π electron structure of the molecule. Considerable attention has been paid to the electronic spectroscopy of polyenes because of their importance as chromophores in photochemical and biological systems.¹⁻³ Polyenes are involved in many different kinds of photochemical and biological functions including cis-trans isomerization, plant and animal coloration, photosynthesis, phototropism, and vision. All of these processes involve interaction of the polyene molecules with light or with excited states of other molecules. For example, carotenoid polyenes are known to be active in photosynthesis,^{4,5} and 11-cis retinal in rhodopsin is the visual pigment in vertebrate retina.^{6,7} However, the mechanism by which light energy absorbed by carotenoids is transferred to chlorophyll in order for photosynthesis to proceed is still not perfectly understood. Also, the molecular basis of how an excited state of rhodopsin creates a visual response is an unsolved problem in

sensory physiology.⁸

The photochemical interconversion of cis-trans isomers of polyenes is of fundamental importance because it is the most basic step in most chemical and biological transformations. A basic understanding of all these aspects depends on an understanding of the electronic structure of the molecules involved. The first systematic study of polyene electronic spectroscopy, including the measurement of absorption and fluorescence spectra, investigation of the solvent dependence of spectral properties, vibrational analysis of electronic bands, and the establishment of trends with number of double bonds and end substitution, was made by Hausser, R. Kuhn, A. Smakula and co-workers in the 1930's.⁹⁻¹⁴ The primary spectral feature is a strongly allowed transition in the near UV or visible region whose intensity increases (hyperchromicity) and whose energy decreases (bathochromicity) as the chain length increases. As the chain length becomes very long, the transition energy approaches an asymptotic value of almost 18000 cm^{-1} .

Several theoretical calculations based on either neglecting electron-electron interaction or taking such electronic interaction terms into account in an approximate way have been carried out.^{2,3,15-17} Consider the example of trans-butadiene, which is the simplest prototype of linear polyenes. We may compare the calculated

electronic state energies for butadiene in different molecular orbital approximations. These approximate MO methods include Hückel MO theory (Mulliken),^{16,17} Free Electron MO theory (Kuhn¹⁸ and Bayliss¹⁵), the Pariser-Parr-Pople^{17,19} method with and without singly excited configuration interaction (Sidman²⁰), and an ab initio calculation (Buenker and Whitten²¹). The first five energy levels in different MO theories are compared to the limited experimental values²² in Figure 1, where $\beta = -4.854$ eV has been used for the Hückel calculation, and $L = 5.4$ Å as the one dimensional box length for the Free Electron model. These parameters were chosen to fit the energy of the first 1B_u state to the experimental value. Butadiene has four π electrons moving in a fixed core with nuclei and σ electrons. In this idealized planar geometry, the four π electrons form a centrosymmetric chromophore and belong to C_{2h} symmetry, as is assumed for all-trans linear polyenes. Linear combinations of these four π atomic orbitals form four molecular orbitals which are alternately a_u and b_g in character,²³ as shown in Figure 2. From these MO's, four singly-excited singlet electronic configurations can be obtained. The wavefunctions for the ground state and the four excited states are also sketched in Figure 2. In all calculations, the lowest singlet excited state of trans butadiene is 1B_u . The transition from the



States	ab initio ¹ (NoCI)	ab initio ¹ (1stCI)	Hückel	FEMO	ppp ² (NoCI)	ppp ² (1stCI)	ppp ³ (1stCI)	Experimental ⁴
¹ A _g (ψ_0)	0	0	0	0	0	0	0	0
¹ B _u (ψ_1)	9.04	9.03	6	6	6.3	6.3	6.21	6.0
¹ A _g (ψ_2)	11.34	10.99	10.85	14.4	7.8	7.7	7.87	7.2
¹ A _g (ψ_3)	12.29	12.64	10.85	9.6	7.8	7.9	8.51	
¹ B _u (ψ_4)	14.58	14.59	15.71	18	9.4	9.4	9.50	

1) R. J. Buenker and J. L. Whitten, J.C.P. 49, 5381 (1968).

2) J. W. Sidman, J. C. P. 27, 429 (1957).

3) R. Pariser and R. G. Parr, J. C. P. 21, 767 (1953).

4) R. S. Mulliken, Rev. Mod. Phys. 14, 765 (1942).

Figure 1. Excitation Energy Diagrams for Butadiene by Several Approximate Molecular Orbital Methods.

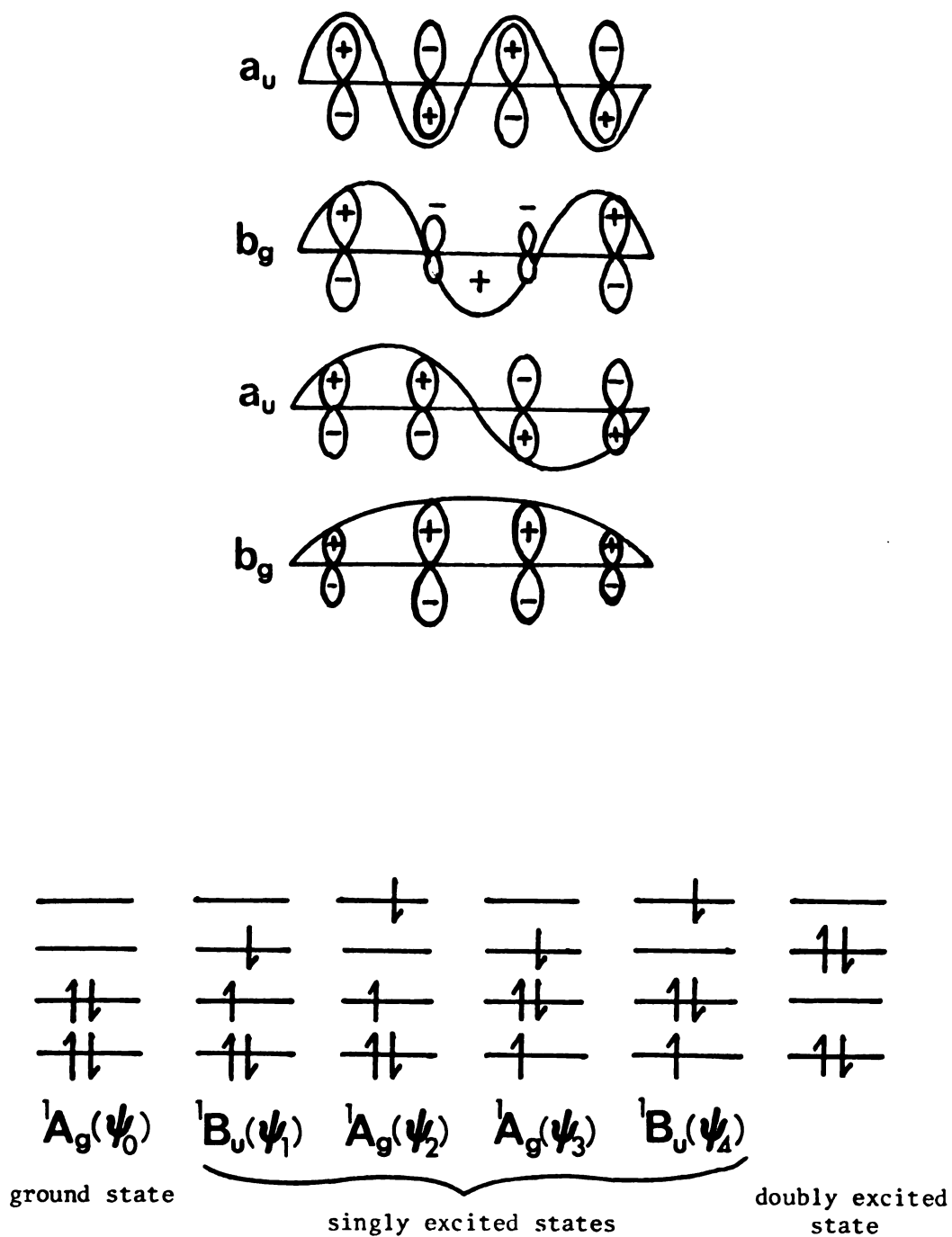


Figure 2. Upper: A Diagram of Molecular Orbital Wavefunctions for Butadiene.
 Lower: Electronic Configurations of Butadiene.

ground state (1A_g) to 1B_u is strongly symmetry allowed and corresponds to the intense lowest energy absorption band normally observed in polyenes. The next two states (ψ_2 and ψ_3) are 1A_g , and correspond to excitation from the highest filled to second unfilled orbital and from the second highest filled to lowest unfilled orbital. Their energies are very close (they are degenerate in Hückel and PPP MO theories) and transitions to these states from the ground electronic state are symmetry forbidden. The linear combination of these two states, $\psi_2 + \psi_3$ (${}^1A_g^+$) and $\psi_2 - \psi_3$ (${}^1A_g^-$) are also excited electronic states. One of these two 1A_g states, the ${}^1A_g^+$, becomes allowed if the polyene chain contains cis double bonds which destroy the inversion symmetry of the molecule.²⁴ It usually gives rise to the so-called "cis peak", having a transition energy between those of the two lowest 1B_u states (ψ_1 and ψ_4). The other linear combination, ${}^1A_g^-$, had not been observed in polyene spectra until recently, when Hudson and Kohler reported its determination in diphenyloctatetraene.^{25,26}

All the theoretical calculations just presented indicate that the lowest excited singlet state in linear polyenes is of B_u symmetry, which corresponds to the strongly allowed bands observed in the visible or near UV regions. The polarization character predicted for such transitions is also in agreement with the experiments.²⁷ However, an examination of the fluorescence

properties of linear polyenes shows several discrepancies between the expected and observed results. These discrepancies are: (1) a large "Stokes shift" between the lowest energy peak of the absorption spectrum and the highest energy peak of the emission spectrum (examples of diphenyloctatetraene and diphenylhexatriene in EPA at 77°K are shown in Figures 3 and 4); (2) an extremely long intrinsic fluorescence lifetime, which is much longer than would be expected from the accepted formula²⁸ relating the lifetime to the measured absorption intensity; (3) an abnormal solvent shift behavior, where the absorption peak is sensitive to changes in the solvent properties but the fluorescence peak is almost unaffected. Several possibilities have been postulated to explain the anomalous behavior, which is common to linear polyenes. The very long intrinsic fluorescence lifetimes suggest that the transition is symmetry forbidden, since the intrinsic fluorescence lifetime is inversely proportional to the absorption oscillator strength. However, the magnitude of the absorption oscillator strength of most polyenes is very large ($f \sim 1.0$) which makes this assumption very unlikely. Moreover, it does not account for the other two discrepancies mentioned above. The lack of overlap between absorption and emission spectra could be a consequence of an electronic transition involving a large change in the molecular geometry which gives

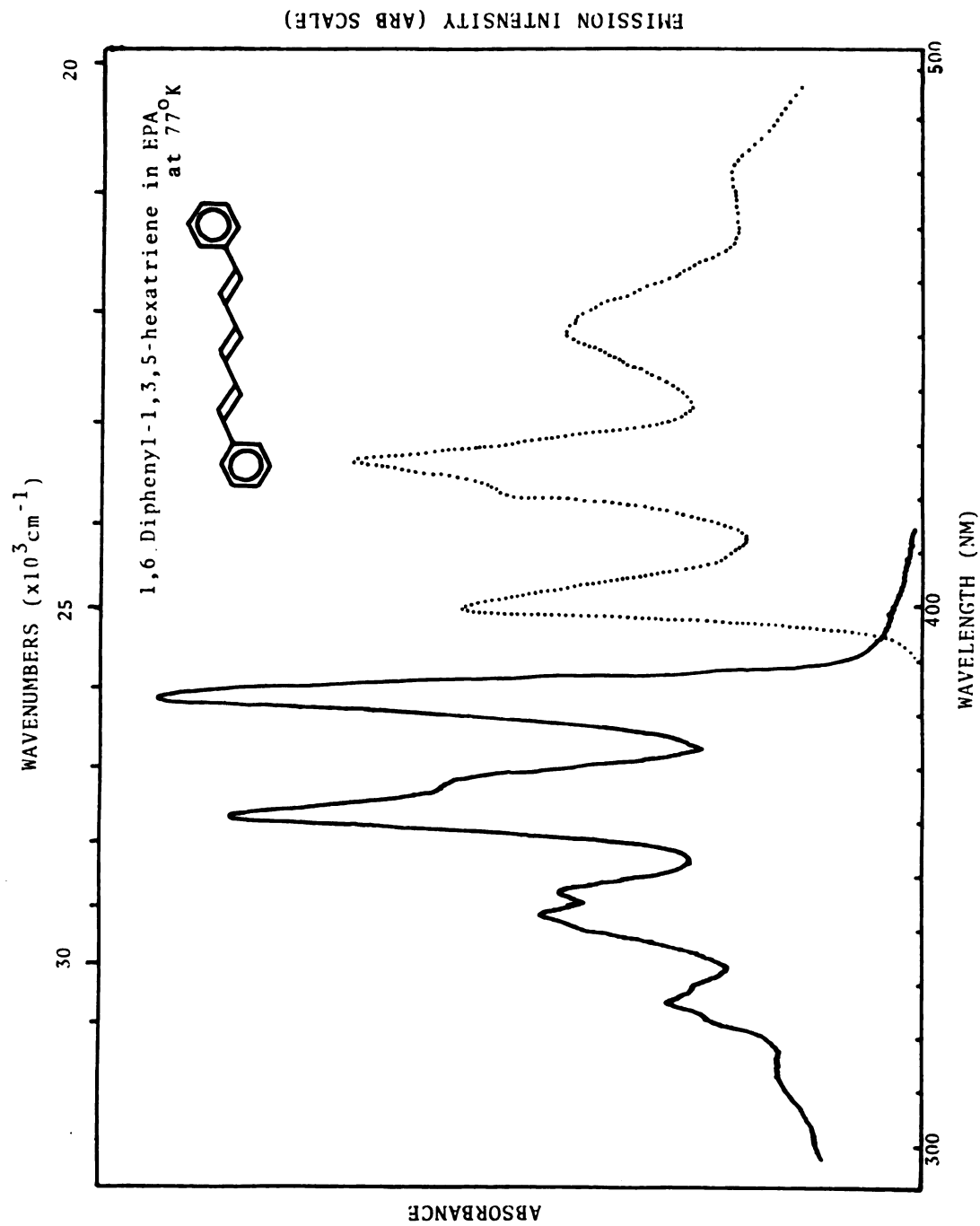


Figure 3. Absorption and Emission Spectra of DPH in EPA at 77°K.

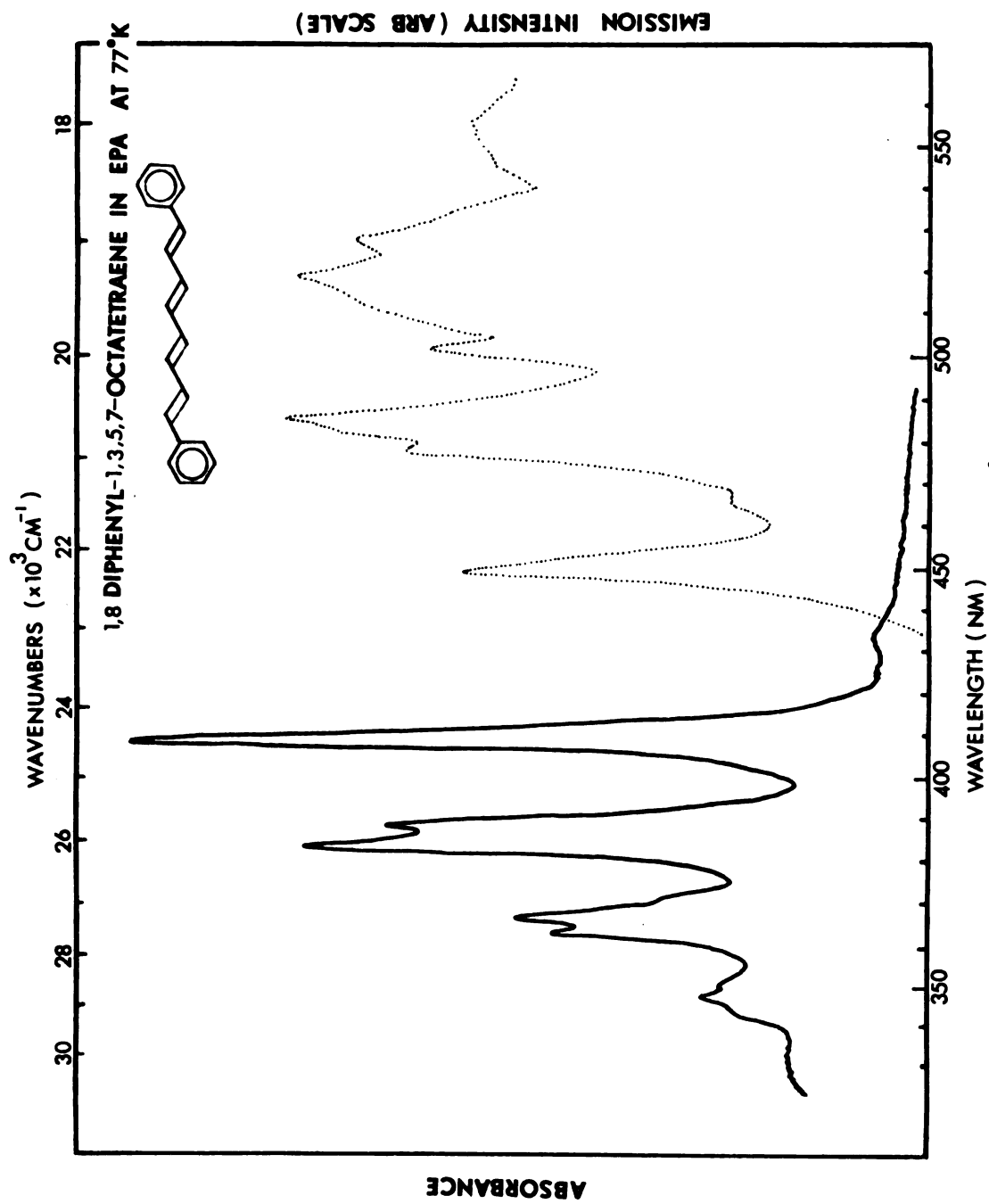


Figure 4. Absorption and Emission Spectra of DPO in EPA at 77°K.

rise to the Franck-Condon forbiddenness. Franck-Condon forbidden electronic transitions usually exhibit long progressions in one or more vibrational modes with smoothly varying intensity, because as the vibrational quantum numbers become higher, the vibrational energy levels become more closely-packed. However, for most polyenes, the absorption and fluorescence spectra show only three or four quanta, and this vibrational structure is sharp and discretely varying in one or two normal modes. Furthermore, the onsets of both absorption and emission are sharp and strong. Therefore, this possibility is not likely, either.

All these discrepancies can be explained by a third possibility: the existence of a low-lying symmetry-forbidden electronic state. This forbidden state is close in energy to the strongly allowed 1B_u state, but lies below it. The observed fluorescence comes from this symmetry-forbidden state through vibronic coupling with allowed neighboring states. The intrinsic fluorescence lifetime is long because the fluorescence comes from a symmetry-forbidden state. The Stokes shift is large because the absorption and emission involve two different excited electronic states, and the fluorescent origin lies below that of the 1B_u absorption state. The solvent shift behavior is different for absorption and emission spectra because the upper states involve two different

dipole moments, which give rise to different interactions with the environment. If the existence of this low-lying symmetry-forbidden state is correct, the lowest excited singlet state is no longer the 1B_u state, but is of A_g symmetry. Transitions to such states are normally forbidden by one-photon selection rules because the electronic ground state is 1A_g , and only $u \leftrightarrow g$ transitions are permitted for centrosymmetric chromophores.²⁹ This explanation suggests that a fundamental modification of state energy ordering in polyene molecules is needed.

Several recalculations of the polyene energy ordering have been carried out.³⁰⁻³² The calculations have included not only singly excited configurations, but also configuration interaction with both singly and doubly excited states.²¹ One interesting result is that the inclusion of at least double excitation lowers the energy of the $^1A_g^-$ state to an extent that it becomes the lowest excited singlet state. A typical example, calculated for octatetraene by Schulten and Karplus^{30,32} using a double CI PPP method, is shown in Figure 5. Ab initio molecular orbital calculations for butadiene with doubly excited configuration interaction included²¹ also indicate the lowering characteristic of $^1A_g^-$, although the calculated excitation energy for the 1B_u state is about 4 eV higher than the experimentally observed value.

Although the transition from the ground state to

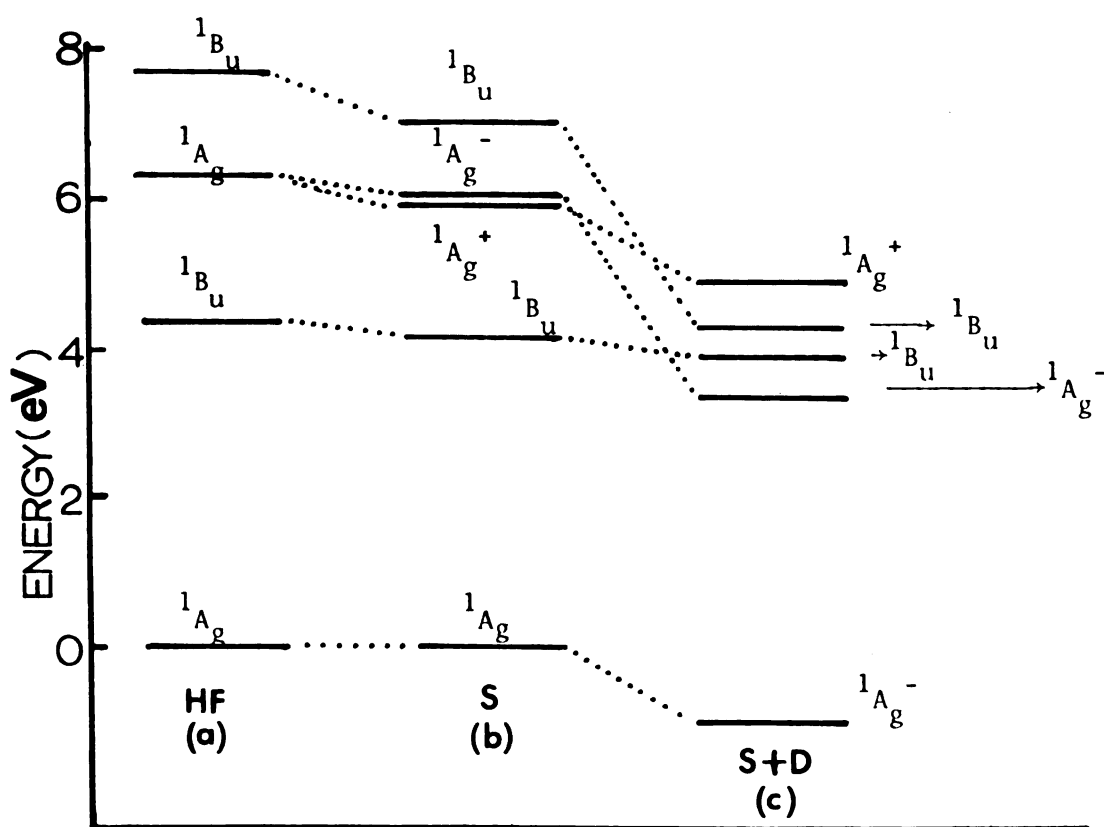


Figure 5. Ground state and four lowest excited states of octatetraene: (a) Hartree-Fock calculation; (b) P-P-P semi-empirical calculation with singly excited CI included; (c) P-P-P with doubly excited CI included. (reference 30)

Butadiene		Hexatriene		Octatetraene	
<u>S</u>	<u>S+D</u>	<u>S</u>	<u>S+D</u>	<u>S</u>	<u>S+D</u>
0.000($1A_g$)	0.000 ^a ($1A_g$)	0.000($1A_g$)	0.000 ^b ($1A_g$)	0.000($1A_g$)	0.000 ^c ($1A_g$)
5.465($1B_u$)	5.408($1A_g$)	4.633($1B_u$)	4.731($1A_g$)	4.112($1B_u$)	4.422($1A_g$)
7.371($1A_g$)	5.860($1B_u$)	6.591($1A_g$)	5.182($1B_u$)	5.926($1A_g$)	4.830($1B_u$)
7.624($1A_g$)	7.836($1A_g$)	6.672($1A_g$)	5.630($1B_u$)	6.058($1A_g$)	5.268($1B_u$)
9.582($1B_u$)	9.408($1A_g$)	7.485($1B_u$)	7.204($1A_g$)	7.010($1B_u$)	5.890($1A_g$)

a) The ground state energy is lowered by 0.554 eV relative to S.

b) The ground state energy is lowered by 0.817 eV relative to S.

c) The ground state energy is lowered by 1.068 eV relative to S.

the $^1A_g^+$ state can be observed as cis peaks when some cis isomers are present, the $^1A_g^-$ state remains forbidden even in the cis isomers of polyenes. Recently, low temperature, high resolution polyene absorption and fluorescence spectra have been obtained by Hudson, Christensen and Kohler,^{25,33-37} using a mixed crystal technique. The compounds isolated in Shpol'skii hosts included diphenylhexatriene,³⁷ diphenyloctatetraene,²⁵ 2,10-dimethylundecapentaene,³⁴ 2,4,6,8-decatetraene,³⁶ and 2,12-dimethyltridecahexaene.³⁵ These studies reveal a series of weak absorption lines on the red shoulder of the strongly allowed transition, which roughly show a mirror image of the emission spectra. In order to more easily observe such low-lying symmetry-forbidden transitions, a method which does not abide by the one-photon optical selection rules is necessary. Specialized techniques such as electron impact spectroscopy (EIS) and magnetic circular dichroism (MCD), which do not follow optical selection rules, might be used to locate optically-forbidden states. However, EIS³⁸ and MCD³⁹ have insufficient resolution to identify the low-lying $^1A_g^-$ states of linear polyenes. Two direct and promising methods to observe such states have been developed in this laboratory: two-photon spectroscopy^{40,41} and preresonance Raman excitation profile spectroscopy.^{42,43} The unique even-parity selection rule of two-photon spectroscopy and the electronic

transition enhancement of resonance Raman excitation profiles reveal important information regarding such "hidden" states. In this thesis, the observation of a hidden electronic state by two-photon excitation spectroscopy will be described.

This work contains two parts: (1) the two-photon excitation (TPE) spectroscopy of all-trans diphenyl substituted polyenes such as 1,8-diphenyloctatetraene, and (2) the TPE spectroscopy of all-trans retinyl polyenes such as retinol (Vitamin A) and anhydrovitamin A. The TPE spectra of these compounds in EPA (ether-isopentane-ethanol, 5:5:2 by volume) have been obtained at 77°K over the spectral range 10000-12500 cm^{-1} . Near infrared radiation from a tunable dye laser pumped by a Q-switched ruby laser served as the excitation source. The medium-resolution TPE spectra show the existence of low-lying 1A_g states in each compound studied.

The presence of an excited singlet state in linear polyenes at an energy below that of the 1B_u state not only explains the apparently anomalous fluorescence properties of polyenes but also provides a fundamental modification of electronic state ordering in polyenes. Calculations which include doubly excited configuration interaction are apparently able to account for the presence of this low lying state, but the present theoretical picture is by no means complete.

CHAPTER II

A GENERAL SURVEY OF TWO-PHOTON ABSORPTION IN RELATION TO EXPERIMENTAL CONSIDERATIONS

A. Motivation

The high light intensities available from powerful lasers have opened several new nonlinear spectroscopic techniques which involve a nonlinear response of a medium to applied irradiating fields. Here nonlinearity means that the electric polarization or the induced electric dipole density of the medium is a quadratic, cubic or higher order function of the electric field amplitude. The response functions to the fields can be calculated quantum mechanically by higher-order, time-dependent perturbation theory.^{44,45} An early example is the calculation of two-photon absorption (TPA) intensity by Goeppert-Mayer in 1931.⁴⁶ Compared to many other second order and higher order nonlinear optical processes, two-photon spectroscopy is relatively amenable to both experimental observation and theoretical interpretation. Indeed, TPA serves as a prototype for many other nonlinear processes.

The limitations of linear optics have made the study of two-photon spectroscopy inevitable. Although one-photon spectroscopy is very successful in helping

understand matter, it explores only a fraction of the possible eigenstates. There are still many forbidden transitions which cannot be detected. However, allowed transitions in TPA cover a much wider range, usually that range inaccessible to allowed one-photon absorption. For example, in centrosymmetric molecules TPA permits a direct examination of those states having the same parity as the ground state, whereas one-photon transitions to such states violate the Laporte symmetry rule. Additionally, polarization analysis provides more information for two-photon than for one-photon processes. Polarization studies in random gases, liquids and glasses are uninformative in one-photon absorption because of an averaging out of polarization effects. The one-photon transition probability $\omega^{(1)}$ from ground state $|g\rangle$ to final state $\langle f|$ is proportional to $|\vec{\lambda} \cdot \vec{\mu}_{fg}|^2$ where $\vec{\lambda}$ is the polarization vector of the absorbed photon and $\vec{\mu}_{fg}$ is the transition vector between states g and f . In randomly oriented systems, $\omega^{(1)}$ must be averaged over all orientations of the molecules to obtain $\langle \omega^{(1)} \rangle$. The result is $\langle \omega^{(1)} \rangle = \frac{1}{3} (\vec{\lambda} \cdot \vec{\lambda}^*) (\vec{\mu}_{fg} \cdot \vec{\mu}_{fg}^*)$. Since $\vec{\lambda} \cdot \vec{\lambda}^* = 1$ for all polarization (linear, circular or elliptical), the absorption then is completely independent of polarization. In TPA, the two-photon transition probability $\omega^{(2)}$ is proportional to $|\vec{\lambda} \cdot \vec{S}_{fg} \cdot \vec{\mu}|^2$, where $\vec{\lambda}$ and $\vec{\mu}$ are the polarization vectors of the two absorbed photons and \vec{S}_{fg} is the

two-photon transition tensor. The average value of $\langle \omega^{(2)} \rangle$ is a linear function of two variables $|\vec{\lambda} \cdot \vec{\mu}|^2$ and $|\vec{\lambda} \cdot \vec{\mu}^*|^2$, where $\vec{\mu}^*$ is the complex conjugate of $\vec{\mu}$.⁴⁷⁻⁵⁰ A complete polarization study of two-photon transitions by suitable selections of polarization vectors $\vec{\mu}$ and $\vec{\lambda}$ provides enough information to permit an unequivocal identification of the symmetry species of the excited states in a random system. Therefore, TPA in randomly oriented phases can uniquely identify the symmetry of eigenstates of matter in situations where the direction of the polarization vectors can be independently varied. TPA then becomes a powerful tool to supplement one-photon spectroscopy.

B. Experimental Methods

Since the first observation of TPA by Kaiser and Garrett,⁵¹ who showed that the simultaneous absorption of two ruby photons by Eu^{++} in crystalline CaF_2 leads to blue fluorescence, a considerable amount of work has been done, both on the study of the absorption process and on its application to spectroscopic purposes. The basic quantity of TPA is the two-photon cross section, δ , which relates the two-photon transition probability per unit time, $\omega^{(2)}$, to the product of the photon fluxes F_1 and F_2 by $\omega^{(2)} = \delta F_1 F_2$. At the time of writing, there are three general ways to observe two-photon cross sections:

(1) direct measurement,^{52,53} (2) indirect measurement,⁵⁴⁻⁵⁶ and (3) parametric mixing measurement.^{57,58}

(1) Direct Measurement:

In a direct measurement,⁵⁹ two light beams are directed onto the sample, one a continuous probe beam and the second a powerful, pulsed pump beam, and the intensity change of the probe beam is monitored during the pulse of the pump laser. The fraction of the probe beam intensity absorbed is related to the two-photon absorption cross section δ by $\delta = (\Delta I/I)/ClF$, where C is the sample concentration in molecules/cm³, l is the length of the sample cell in cm, and F is the photon flux of the pump laser in photons/cm² sec. The units of δ in this case are cm⁴sec photon⁻¹molecule⁻¹. An absorptivity of 10⁻⁵⁰ in these units is known informally as 1 maria.

Ideally, two-photon direct absorption measurements should provide absolute values of the δ 's. However, the technique suffers several substantial experimental difficulties which make direct measurement experimentally impractical. The limiting factors are: (1) relatively low sensitivity, which prevents the study of molecules in dilute solutions, (2) inevitable side effects in the sample which increase the uncertainty in the determination of δ , and (3) uncertainties in the spatial and temporal properties of each individual laser beam which strongly

influence the δ value.⁶⁰

The TPA cross sections for most organic molecules are on the order of a few marias. In order to overcome such small values of δ , a powerful, Q-switched pump laser is necessary. Even for a good probe beam detector, a realistic value of the intensity change would be at least $\frac{\Delta I}{I} = 10^{-2}$ (a 1% dip in the probe beam). If $C = 10^{22}$ molecules/cm³ (a neat fluid sample) and $l = 1$ cm, the corresponding photon flux of the pump laser must be $F = 10^{26}$ photons/cm² sec, which is 20 Mw/cm² in the visible region. In other words, even for a megawatt pump laser, a highly concentrated sample is required for direct measurement of two-photon absorption. This precludes the possibilities of observing direct absorption in solutions.

As the power of the pump laser increases, several side effects such as stimulated scattering and thermal heating of sample may occur. These effects include the production of stimulated Raman scattering which depletes the laser intensity in the sample,⁶¹ self-focusing which enhances the laser intensity,^{62,63} sample filamentation,⁵⁹ and the formation of shock waves.^{59,64} All increase the uncertainty in determination of TPA δ 's. In addition, many competing processes are of the same order of magnitude as TPA.^{65,66} Some competitive effects are shown schematically in Figure 6(b). In many cases, it is

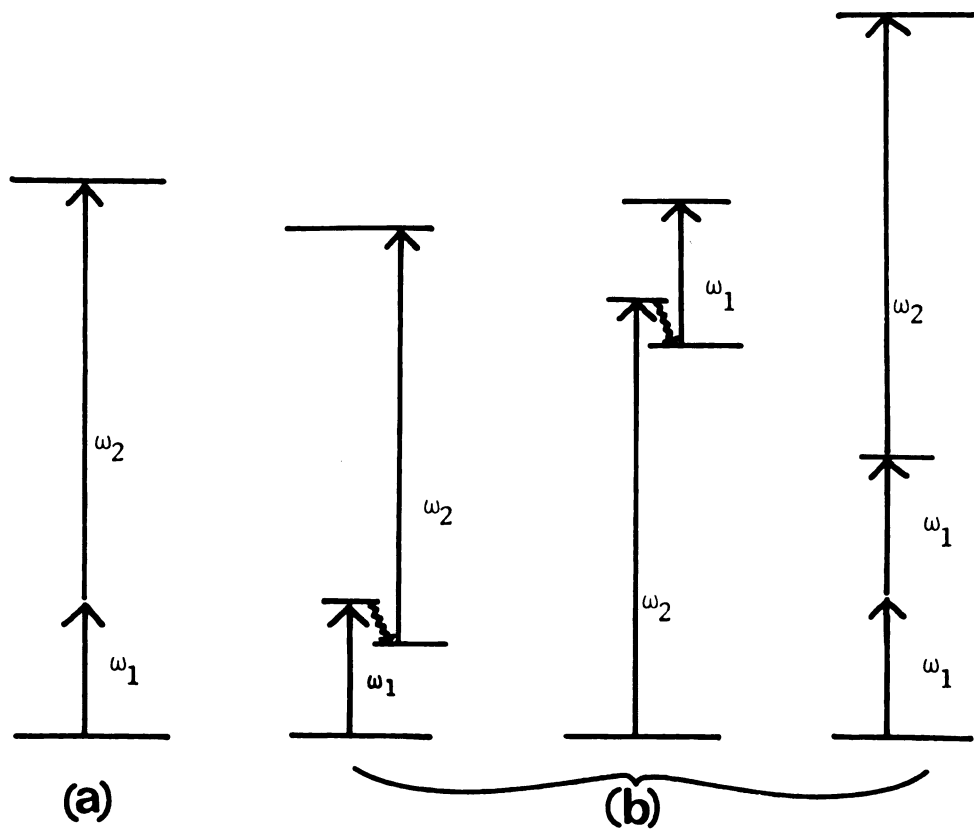


Figure 6. (a) Two-Photon Absorption (TPA) Effect
(b) Some Scattering Effects might Compete with Direct TPA Measurement

impossible to distinguish, or to estimate the relative size of these competing processes. Therefore, the experimentally determined value of the two-photon cross section contains contributions from unwanted processes, and is not an absolute TPA cross section.

The third uncertainty in determination of δ arises from some characteristics of the lasers used. Any erratic temporal or spatial behavior of the excitation source can strongly affect the experimental value of the observed cross section. This intrinsic uncertainty of the laser beam is serious and cannot be completely resolved. It affects all kinds of TPA measurements, not solely direct measurement. Further discussion will be found in the next section, on the indirect measurement technique.

An experimental example of the determination of δ at a single wavelength is schematically shown in Figures 7 and 8. The sample was pure fluid α -chloronaphthalene in a 1 cm long cuvette. The 4765 Å line from cw argon ion laser served as the probe beam. The pump beam was a Q-switched ruby laser. In order to obtain an entire two-photon direct absorption spectrum, the single wavelength probe beam should be replaced by a tunable light source (either a stable cw dye laser or a conventional light source). Careful protection of the detector (the photodiode P_2 in Figure 7) against the huge noise spike coming

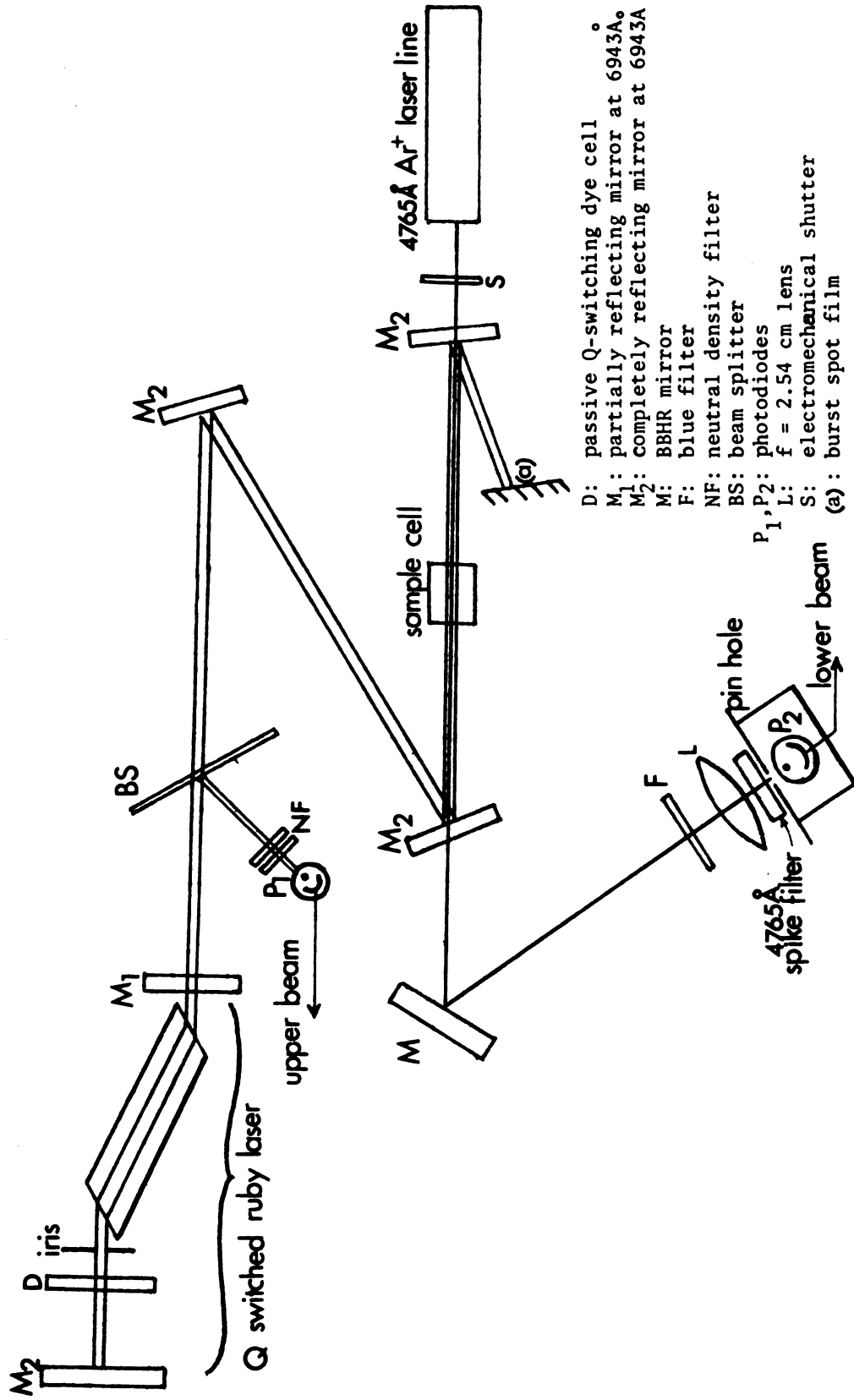


Figure 7. TWO-PHOTON DIRECT ABSORPTION MEASUREMENT

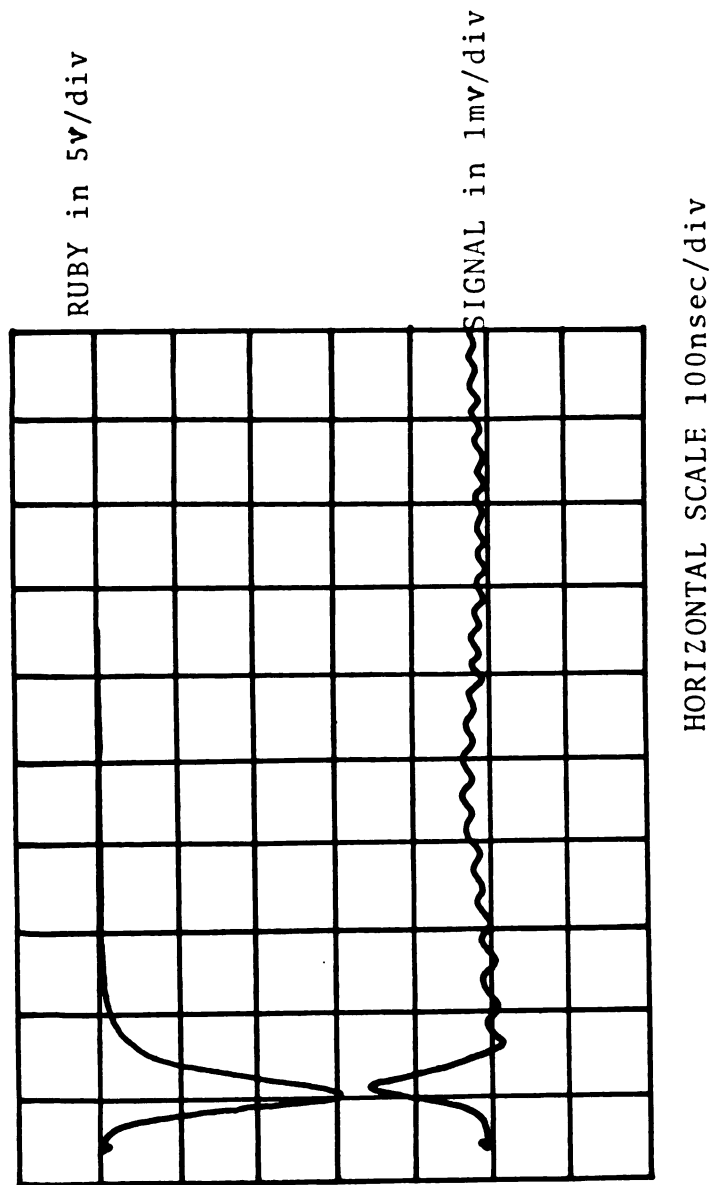


Figure 8. TWO PHOTON ABSORPTION SIGNAL IN 1-CHLORONAPHTHALENE

$$\Delta \frac{1}{I} = \delta C I F_{\text{ruby}} \quad \delta = 1.1 \times 10^{-50} \text{ cm}^4 \text{ sec/photon, molecule}$$

Probe laser beat frequencies at $\sim 50 \text{ MHz}$ can be seen on the signal trace. This beat can be eliminated by placing an etalon inside the Ar^+ laser cavity.

from the pump laser, and of the sample from overheating by the probe beam was required. Several ruby light rejection filters followed by a narrow-band 4765 Å spike filter and a 100μ pinhole were placed in front of the photodiode to eliminate pulsed ruby light at the detector. An electromechanical shutter which was synchronized with the triggering system of the ruby laser was placed in front of the Ar⁺ laser to avoid overheating the sample by the probe beam. Just before the ruby was ready to fire, the shutter was opened. Then, the probe beam passed through the sample and filters and finally was focused by a lens through the pinhole onto the surface of the photodiode. Without the shutter, the heat generated in the sample, which has very low but finite absorptivity, caused a refractive index gradient which made the sample behave like a divergent lens. This phenomenon is well known as the thermal blooming effect.⁶³ When the ruby laser pulse passed through this divergent lens, the intensity distribution of the original Gaussian mode was slightly deflected, and took on a "donut" shape with less intensity in the center. A burst spot obtained by inserting a piece of film at position (a) in Figure 7 looked like:



Figure 9. Ruby Burst Spot After Thermal Blooming Effect.

The thermal blooming effect definitely affects the measurement of two-photon cross sections because the photon flux in the middle of a donut-shaped distribution is much lower than that in a Gaussian distribution. In other words, the sample molecules sitting along the center of the probe beam cannot see the pump laser efficiently. Therefore, the measured value of δ will be slightly smaller than the true value.

The two-photon spectrum of neat α -chloronaphthalene was studied by Monson and McClain^{47a} using the direct measurement technique. Three two-photon absorption bands were observed, at 42600, 37700 and 34400 cm^{-1} . A complete polarization study was done to assign the symmetry of the transitions.⁴⁷⁻⁴⁹ The two bands, 42600 and 37700 cm^{-1} , correspond to $^1A_g + ^1A_g$ and $^1B_{1g} + ^1A_g$ transitions which are totally forbidden in one-photon spectroscopy. The weak absorption at 34400 cm^{-1} is probably due to a vibronically induced $^1B_{2u} + ^1A_g$ transition. The combination of a 4765 Å Ar^+ laser and a 6943 Å ruby laser described

in Figure 6 gives an energy of 35400 cm^{-1} which falls in the vibronically induced $^1B_{2u} \leftarrow ^1A_g$ transition. The measured two-photon cross section at this wavelength, $1.1\text{ m}^2\text{ mol}^{-1}$, is in agreement with McClain's value.^{47a}

(2) Indirect Measurement:

Indirect measurement monitors consequences of laser-induced nonlinear processes initiated by primary two-photon absorption. Among two-photon induced secondary processes are optical emission,^{54,55} ionization,^{67,68} photodetachment^{69,70} and photochemical reactions.⁷¹ Each process has its own setup and detection system. A typical example is the two-photon excitation (TPE) indirect measurement. It is based on the experimental study of the energy dependence of two-photon fluorescence spectra induced by tunable lasers, and is the technique used in determining the low-lying forbidden electronic states of polyenes described in this thesis. The usual experimental arrangement⁷² is the following: the sample under study is irradiated by light from one or two lasers, at least one of which is tunable; part (but not all) of the two-photon induced fluorescence is collected by an optical system, and after appropriate filtering (either selected optical filters or a monochromator), is detected by a photomultiplier. Compared

with the TPA direct measurement, TPE is much more easily detected. This is readily understood upon substitution of typical experimental parameters into the TPE rate equation: $\omega^{(2)} = Q\delta NF_1F_2$, where Q is the fluorescence quantum yield and N is the number of sample molecules in the active region. For an ordinary pulsed dye laser with power ≈ 20 kw in the visible region, the photon flux is correspondingly about 10^{24} photons/cm² sec if the dye laser is partially focused into a volume of approximately 0.1 cm³. The number of sample molecules in a 10^{-3} M solution within this region of focus is almost 10^{17} . Even if the cross section of the sample is only 0.1 mm², the rate of two-photon fluorescence induced from this single laser pulse would still be $\omega^{(2)} = Q \times 10^{-51} \times 10^{17} \times (10^{24})^2 = 10^{14}Q$. Therefore, TPE should be relatively easy to study under the influence of a tunable, moderate power (~ 50 kw) dye laser. However, TPE still has a serious problem, the stability and reproducibility of the laser pulse, mentioned earlier in relation to TPA direct measurements.⁶⁰ The temporal characteristics of a laser pulse, which strongly influence the experimental data, will be discussed from a theoretical standpoint in the following paragraphs.

In the time domain, the ordinary shape of a laser pulse can be described by a Gaussian beam: $I(t) = a \exp(-t^2/2b^2)$ where a is a constant and b is the root-mean-

square deviation of t from the mean of the Gaussian distribution. Since two-photon induced fluorescence can be related to $I^2(t)$ by a time correlation function, one can apply the well-known deconvolution technique^{73,74} to the TPE fluorescence signal giving by: $F(t) = \int_{-\infty}^t I^2(t')K(t-t')dt'$ where K is the fluorescence correlation function. Usually the fluorescence function is simply an exponentially decaying function.⁷³ Then the correlation function can be represented by: $K(t-t') = \frac{1}{\tau} \exp(-\frac{t-t'}{\tau})$, where τ is the measured fluorescence lifetime of the sample molecule. Substituting the input Gaussian beam $I(t)$ and the fluorescence correlation function $K(t-t')$ into the integral of $F(t)$ and evaluating leads to the relationship:

$$F(t) = \frac{a^2}{\tau} e^{-t/\tau} \int_{-\infty}^t [\exp -(\frac{t'}{b} - \frac{b}{2\tau})^2 + \frac{b^2}{4\tau^2}] dt'$$

$$= \frac{\sqrt{\pi} a^2 b}{\tau} e^{-t/\tau} e^{b^2/4\tau^2} [\frac{1}{2} + \frac{1}{\sqrt{2\pi}} \int_0^{Z(t)} e^{-Z^2} dZ]$$

where $Z(t) = (\frac{t}{b} - \frac{b}{2\tau})$. The integral here is the standard error function, which can be evaluated from mathematical tables.⁷⁵ The fluorescence response $F(t)$, then, is dependent on three variables (t, b, τ) . For each particular choice of b and τ , (b_i, τ_i) , the fluorescence response function $F(t, b_i, \tau_i)$, shows a peak in the time domain. This peak is designated $F_{\max}(t, b_i, \tau_i)$, and is the fluorescence peak height seen on the oscilloscope. If a TPE

experiment is monitored by observing both the laser and fluorescence signal on a fast oscilloscope, where the upper trace shows the laser pulse and the bottom trace shows the fluorescence pulse, the oscillogram looks like:

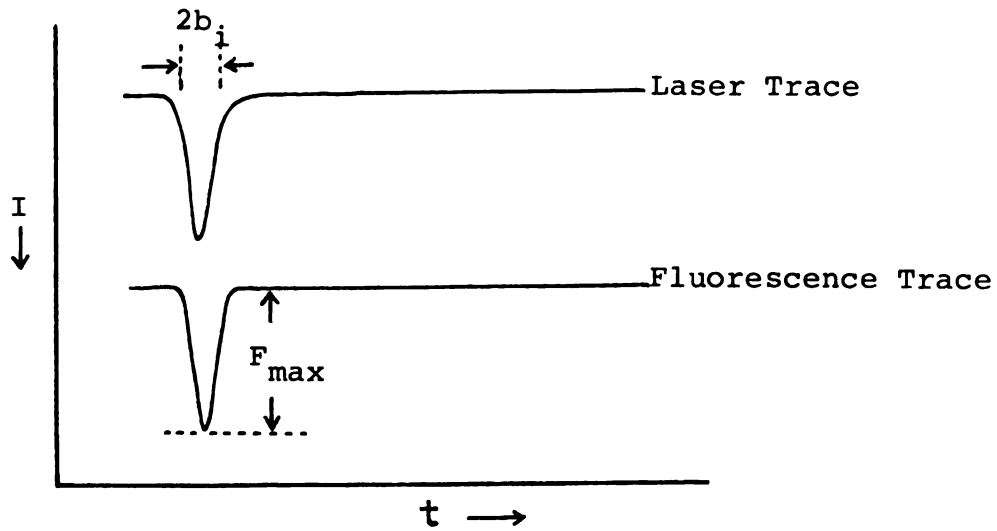


Figure 10. Dual Beam Oscillogram of TPE Measurement.

The measured fluorescence peak height $F_{\max}(t, b_i, \tau_i)$ is strongly dependent on the values of b_i and τ_i . If the laser pulse shape, b_i , changes, the fluorescence peak height will change too. In other words, the fluorescence intensity will depend strongly on the laser pulse shape. If the laser pulse is not reproducible, the measured fluorescence intensity will fluctuate from

pulse to pulse. A quantitative plot of $F_{\max}(t, b, \tau)$ as a function of the ratio of the laser pulse width to the fluorescence lifetime, $\frac{b}{\tau}$, has been calculated by Swofford et al.⁶⁰ and is shown in Figure 11.

When the $\frac{b}{\tau}$ value is greater than 2 (that is the laser pulse width is at least twice the fluorescence lifetime of the sample), only a small variation appears in fluorescence peak intensity F_{\max} . As the $\frac{b}{\tau}$ value becomes smaller and smaller (the laser pulse width approaches the fluorescence lifetime), large fluctuations are expected in F_{\max} . In order to obtain reliable TPE measurements, two conditions are required: (a) a stable pulse laser, and (b) the pulse width of excitation laser must be longer than the fluorescence lifetime of the molecule under study. This indicates that subnanosecond pulses such as mode-locked laser pulses cannot be used to induce the TPE peaks. As the laser pulse becomes really sharp, the pulse peak will be a short spike and cannot be detected by a photodiode and oscilloscope because it is faster than the risetime of these detectors. Therefore, any erratic temporal behavior of the tunable laser source can introduce serious errors into the observed TPE spectrum.

In the TPE experiments described in this thesis, the fluorescence lifetimes of the samples studied (diphenyl polyenes and retinyl polyenes) are shorter (< 8

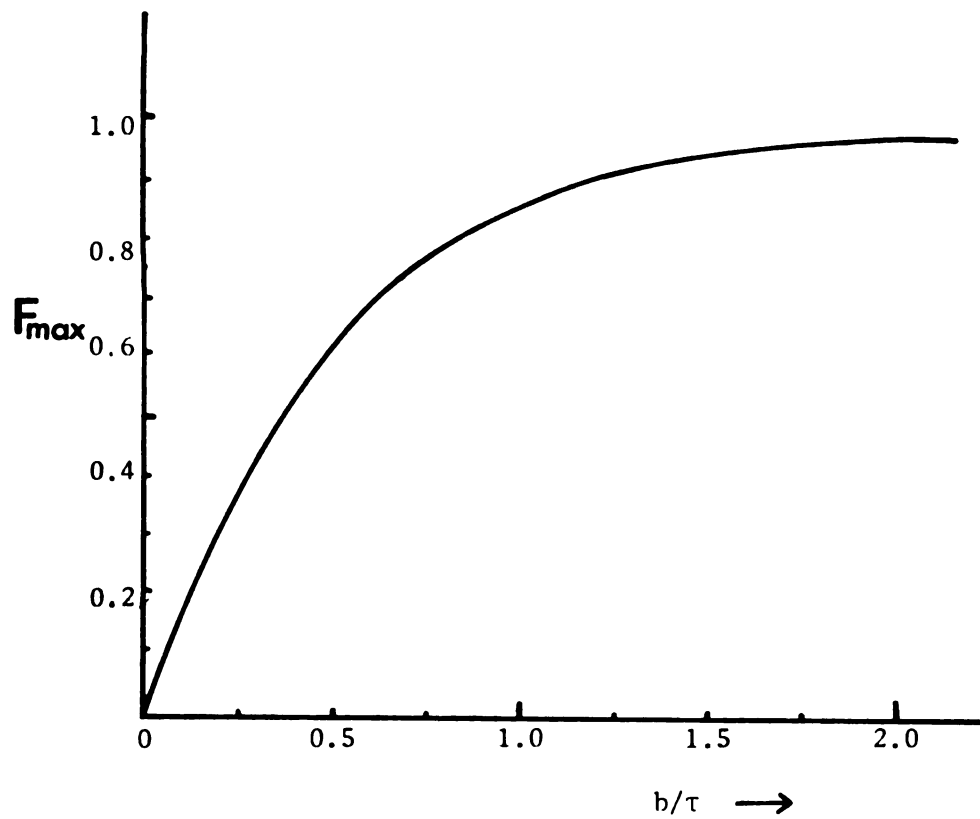


Figure 11. Fluorescence Peak Height as a Function of (b/τ) .

nsec) than the pulse width of the dye laser, which is about 30 nsec. The ratio $\frac{b_i}{\tau_i}$ is thus greater than 4, and the fluctuation of the fluorescence peak height caused by the variation in the pulse width of the dye laser should be negligible.

The measurement of the peak height of both the laser beam and the two-photon induced fluorescence can be easily made from a photograph of a fast oscilloscope trace. This method is relatively simple but suffers difficulties if the pulse width of the dye laser fluctuates markedly. This is particularly true for a pulsed dye laser which has relatively poor beam quality. Dye laser fluctuations arise mainly from the quality of the excitation source, if the other parameters of the dye laser are fixed. Although the pulse shape of a ruby laser, such as that used in this work, changes from pulse to pulse, under the conditions of a good quality ruby rod and a uniform flash-lamp pumping system, the variation is not great. The primary problem is the Q-switching dye of the ruby laser. If the Q-switching dye is not well adjusted, or the Q-switching dye cell is not in an appropriate position, the ruby output might contain either multiple pulses or sharp spikes, superimposed on a single pulse. These spike pulses are usually very short compared with τ , and increase the fluorescence signal by an unpredictable amount. Thus, short duration laser fluctuations produce

false peak heights in fluorescence measurements.

A method⁷⁶⁻⁷⁹ which overcomes pulse shape fluctuation problems involves the simultaneous measurement of the fluorescence peak height from a standard "reference" of already known absolute cross section and fluorescence quantum yield, and that of the sample. If the ratio of fluorescence peaks from the unknown sample and the standard reference is taken shot by shot, one will get effective cancellation of the pulse width irregularities of the dye laser. This will be true if the fluorescence lifetimes of unknown and reference are similar. However, the use of this method requires accurately known two-photon standards, which are unavailable at the present time. Also, if the lifetimes of unknown and reference are somewhat different, the correction procedure begins to breakdown.

Although the fluorescence peak height is sensitive to the laser pulse shape, the total number of fluorescence photons emitted from the sample still should be accurately proportional to the square of the total number of laser photons. Therefore, if it is possible to integrate both the upper trace and lower trace on the oscilloscope through fast integrator circuits, one should be able to determine the TPE cross section, $\delta \propto \frac{\int F(t)dt}{\int I^2(t)dt}$, very accurately. With high repetition rate pulsed dye lasers and fast integrating devices such as the boxcar

integrator, several compounds have been studied in this way.^{80,81}

(3) Parametric Mixing Measurement:

Recently, a great deal of attention^{44,57,82} has been paid to the creation of light at $\omega_3 = 2\omega_1 \pm \omega_2$ when two intense laser beams at ω_1 and ω_2 interact with matter. These experiments have been called four-wave mixing (4WM) for the case $\omega_3 = 2\omega_1 + \omega_2$, and three-wave mixing (3WM) for the case $\omega_3 = 2\omega_1 - \omega_2$. In both cases the induced polarization in the material is a cubic function of the electric field amplitudes. In cartesian coordinates, the i th component of the polarization is written in terms of the third-order susceptibility:⁴⁴

$$P_i(2\omega_1 \pm \omega_2) = \sum_{jkl} \chi_{ijkl}^{(3)}(-\omega_3, \omega_1, \omega_1, \pm\omega_2) E_j(\omega_1) E_k(\omega_1) E_l(\pm\omega_2)$$

where $i, j, k, l = x, y, z$. The third-order nonlinear susceptibility is a fourth-rank tensor and contains information regarding the interference between various resonant and nonresonant processes. In 3WM, for centrosymmetric materials, there are three primary contributions to $\chi^{(3)}$: The nonresonant electronic processes (Figure 12a), stimulated Raman scattering when $\omega_1 - \omega_2$ corresponds to a Raman-active mode (Figure 12b), and two-photon

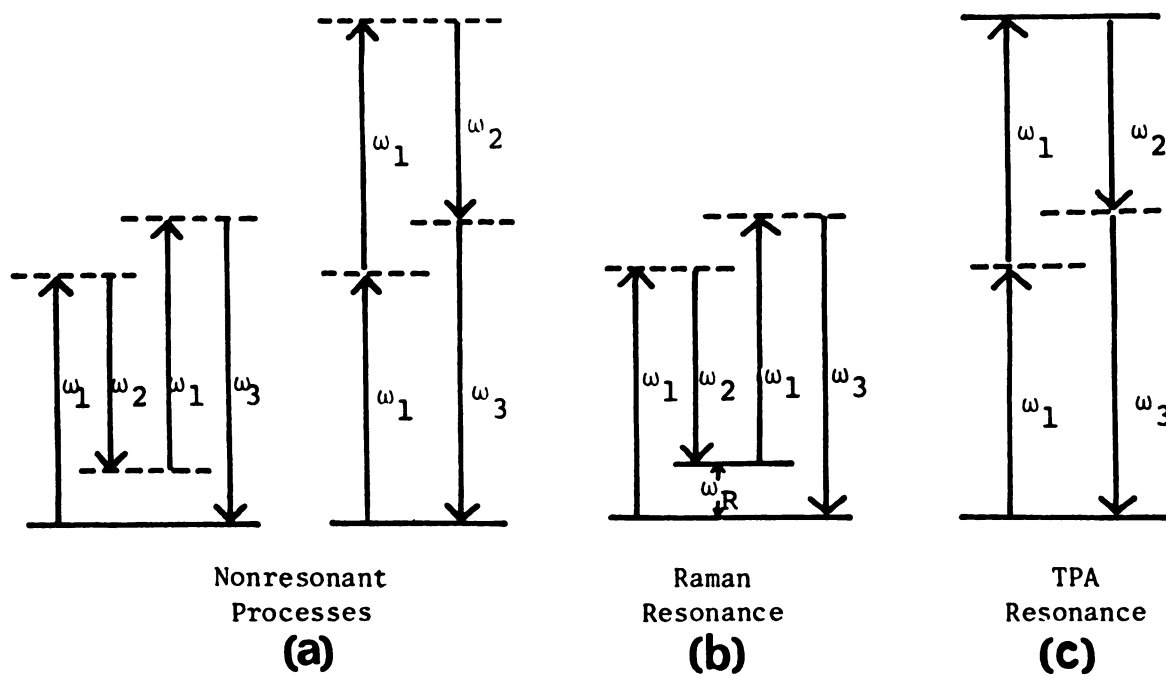


Figure 12. Resonant and Nonresonant Processes in Three-Wave-Mixing.
 (a) Nonresonant Processes; (b) Raman Resonance;
 (c) TPA Resonance

absorption when $2\omega_1$ corresponds to the energy difference of a TPA-allowed electronic transition (Figure 12c).

Then the total third order susceptibility can be represented as $\chi^{(3)} = \chi_{NR}^{(3)} + \chi_{Raman}^{(3)} + \chi_{TPA}^{(3)}$.

The second case (Figure 12b) has also been called CARS (coherent anti-Stokes Raman spectroscopy). When the frequency difference $\omega_1 - \omega_2$ is tuned through the region of a Raman active transition ($\omega_1 - \omega_2$ is tuned from below to above ω_R), the observed intensity at frequency ω_3 , $I(2\omega_1 - \omega_2)$, which is proportional to $|\chi^{(3)}|^2$, should show a minimum on the high frequency side of $\omega_1 - \omega_2 = \omega_R$.⁵⁸ In other words, a plot of the shape of the 3WM susceptibility $\chi^{(3)}$ vs $\omega_1 - \omega_2$ in the vicinity of a Raman resonance should show a dispersion curve which has a maximum and minimum. The reason for this behavior is that the real part of the Raman susceptibility is positive for $\omega_1 - \omega_2 < \omega_R$ and negative for $\omega_1 - \omega_2 > \omega_R$. According to formal perturbation theory, if neither frequency ω_1 nor ω_2 is close to any real electronic transition of the material the nonresonant contribution, $\chi_{NR}^{(3)}$, will be a slowly varying function. If the Raman resonance contribution is the only resonance process, the dispersion minimum is caused by partial cancellation of $\chi_{NR}^{(3)}$ by the negative contribution of the Raman term. However, if when tuning frequency ω_1 the value of $2\omega_1$ approaches a two-photon allowed level, a sudden change in the shape of the minimum

will occur. Therefore, the position and magnitude of this minimum can probe the TPA resonance contribution to $\chi^{(3)}$. The application of 3WM in the determination of two-photon absorption is based simply on this idea.^{58,58,83}

In contrast to traditional TPA methods, the mixing technique does not involve any change in the quantum state of the material; the ground state is both the initial and final state. (In both direct and indirect measurements, the final state is either a real two-photon allowed state or a vibronic induced state.) Therefore, the competing processes represented in Figure 6(b) will not influence the measurement of $\chi^{(3)}$. For this reason the 3WM technique can provide a more accurate two-photon cross section than the other methods. However, the 3WM technique has some disadvantages too. In addition to several experimental difficulties, 3WM can be used only to determine TPA information in the vicinity of a Raman active mode. It is useful only for a selected wavelength.⁸⁴

Several good reviews have been written on one or another aspect of the two-photon process, including those of Peticolas⁵⁴ (1967), Jortner⁸⁵ (1969), Gold⁵³ (1969), Frohlich⁸⁶ (1970), Worlock⁸⁷ (1972) and Mahr⁵⁶ (1975). The theoretical aspects of TPA are well covered in these reviews, and will not be repeated here. Two-photon effects in the microwave region are not reviewed here because

the electronic region of absorption is emphasized in this work.⁸⁸

CHAPTER III

EXPERIMENTAL APPARATUS

A. Absorption Spectra

All absorption spectra were recorded on a Cary 15 spectrometer. For low temperature measurements, the sample was dissolved in EPA ($\sim 10^{-6}$ M.) and placed in a square quartz cell with 1 cm width and 0.75 mm wall thickness. The sample cell was immersed in liquid N_2 in a cylindrical, partly-silvered Dewar which was placed in the sample compartment of the Cary instrument. This quartz Dewar was 24 cm long and 5.7 cm in outside diameter. It had 4 windows, 2 on each side, for light to enter and exit. Helium gas was blown over the surface of the liquid N_2 to prevent bubbling. Nitrogen gas was also blown into the sample compartment to reduce moisture condensation on the windows. In order to obtain a homogeneous glass phase without any internal cracking and imperfection, the sample cell was slowly and carefully immersed into the liquid N_2 .

B. Emission Spectra

Low resolution emission spectra were obtained with an Aminco spectrofluorimeter. High resolution fluorescence

spectra were obtained with a system comprised of the following components located in the laboratory of Prof.

A. El-Bayoumi of the MSU Biophysics Department: The excitation source was a 900 W Xenon lamp. Excitation wavelengths were selected by a 0.5 m B & L monochromator with a 600 l/mm grating blazed at 3000 \AA . The excitation illumination was focused on the sample whose fluorescence emission was collected at 90° from excitation and focused onto the entrance slit of the emission monochromator. The latter was a 1 m Spex 1700 II with a 1200 l/mm grating blazed at 5000 \AA . The emission detector was an air-cooled EMI 9558 QA photomultiplier tube which was normally operated at 1.1 KV. Signals from the phototube were fed to a PAR HR-8 lock-in amplifier followed by a strip chart recorder, while the reference signals were provided by a light chopper placed between the excitation monochromator and the sample. For low temperature fluorescence measurements, samples were immersed in the same liquid N_2 Dewar described in the previous paragraph.

C. Ruby Laser System

A melt grown Czochralski ruby rod (0.05% Cr_2O_3) with dimensions $5/8$ " diameter \times $6 \frac{1}{2}$ " long was purchased from the Linde Crystal Products Division of the Union Carbide Corp. Both ends were cut at Brewster's angle (60° for the ruby-to-air interface) to avoid internal

self-lasing. The ruby was excited by pump radiation from two linear high energy flash lamps (EG & G FX-47C-6.5 Xenon flash lamps). The ruby rod and flash lamps were placed at the 3 foci of a double elliptical configuration to obtain more efficient coupling of the pump light to the laser rod. Polished Alcoa Alzak Aluminum lined the inner surface of the dual elliptical cavity to increase the reflectivity.⁸⁹ A totally reflecting concave rear mirror with 8 m radius of curvature and a 35% R partially reflecting mirror for the emergent beam formed the ruby resonant cavity.

The dual elliptical cavity was made of brass and contained 2 end plates, a brass back template and a ceramic front template (Figure 13). The ceramic front template, made from Corning machinable glass ceramic, served as an insulator for the high voltage of the flash lamp trigger wires. Cylindrical quartz tubing surrounded both flash lamps and the ruby rod, and served to circumscribe the water cooling system shown in Figures 13 and 14. Viton O-rings between the flash lamps and quartz tubing prevented water leakage. The ruby was held with Teflon O-rings, each set in a groove in a brass cylinder which closely fit the ends of the ruby quartz tubing. A tiny amount of Torr Seal cement was used to seal the ends of the tubing to the two brass holders to prevent water leakage. A side-view cross-section of the ruby laser

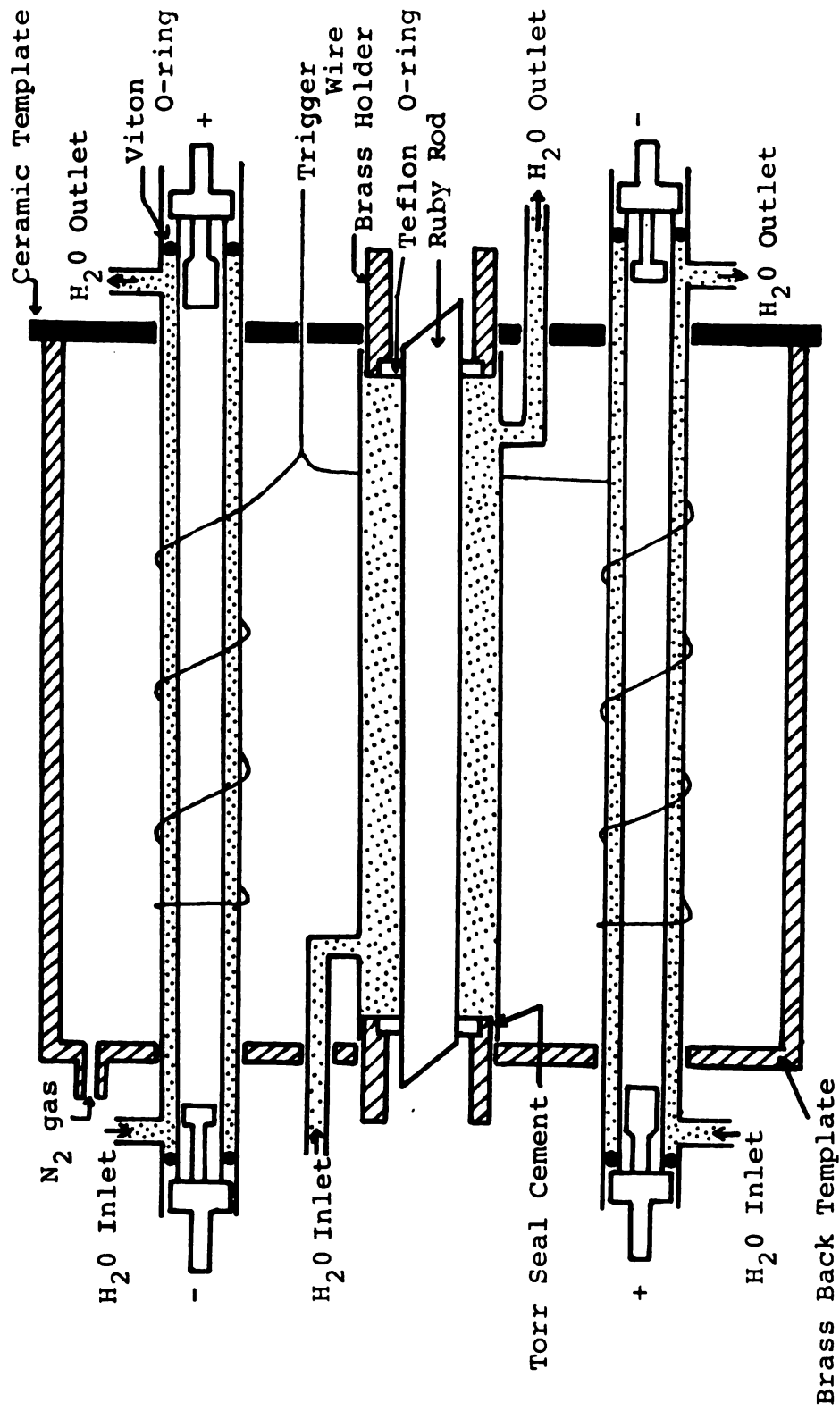


Figure 13. A Side-View Cross Section of the Ruby Laser Double Elliptical Cavity.

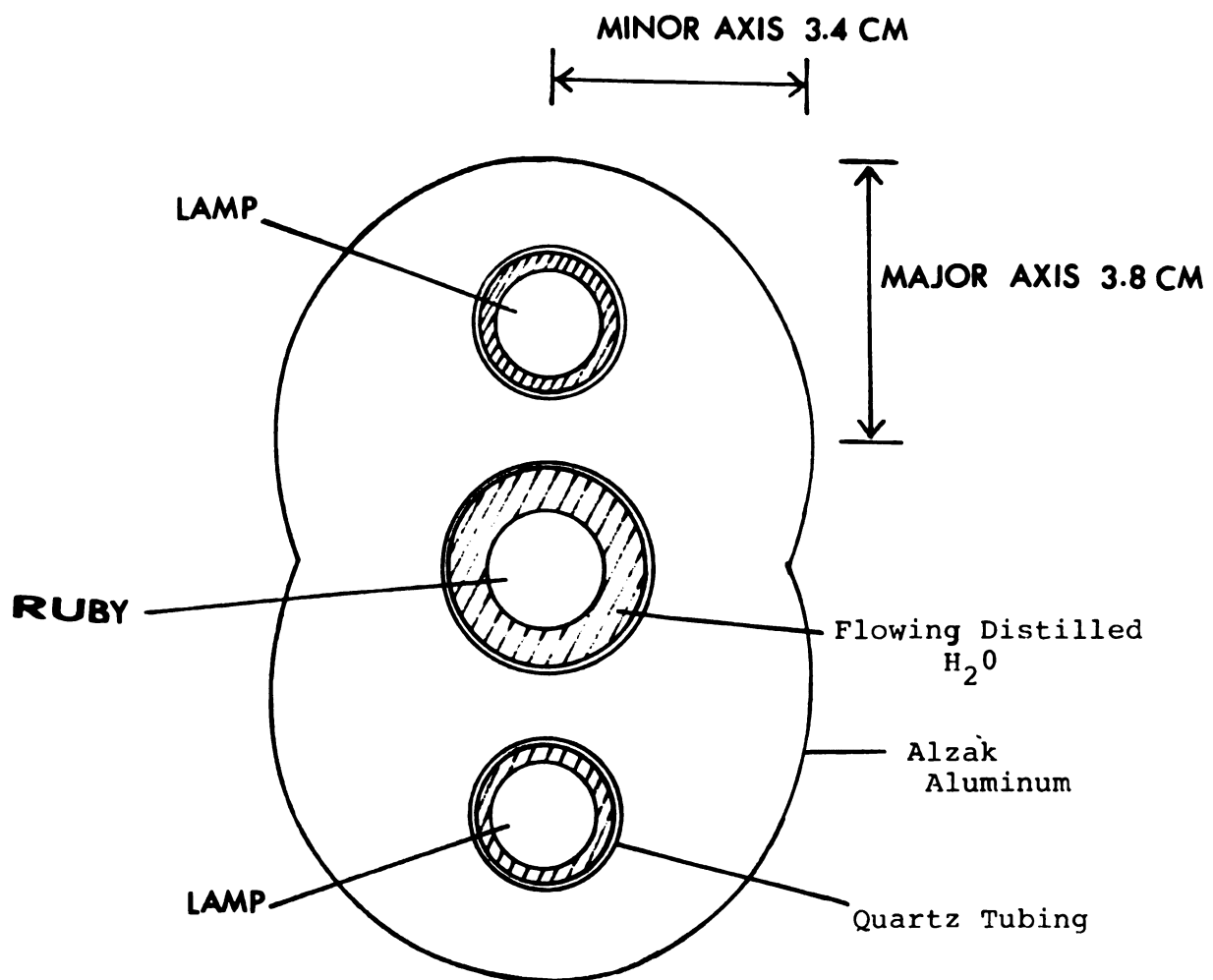


Figure 14. End-view of Double Elliptical Cavity.

cavity is shown in Figure 13. Two small pieces of metal foil (not shown in the figure) were also wrapped around the outside of the ends of the quartz tubing to cover the sealing zone and protect the cement from damage caused by heat and the high radiant intensity from the flash lamps. Flowing distilled water circulated through the quartz cylinders by a peristaltic pump to remove the heat generated by the lamps and the ruby.

The two flash lamps were wired in series and were charged by a 5kv, 1280 μ F capacitor bank drawn schematically in Figure 15. In order to maintain a uniform input energy for the excitation of the ruby, several coil inductors were introduced into the circuit to impede sharp changes in discharging current. In addition, a constant voltage firing circuit was placed between the ruby power supply and the triggering system (Figure 15). The constant voltage and slow discharge rate gave a nearly uniform flash lamp energy input for the ruby pump radiation. The typical pulse width of the Xenon flash lamps was ~300 msec. Two kinds of triggering systems were employed. For an internal trigger, the lamp discharge was triggered by a high voltage surge through the lamp circuit, generated by a high voltage relay inside the ruby power supply. For an external trigger, the breakdown was initiated by a high ac voltage provided by a Tesla coil discharge through the trigger wires surrounding

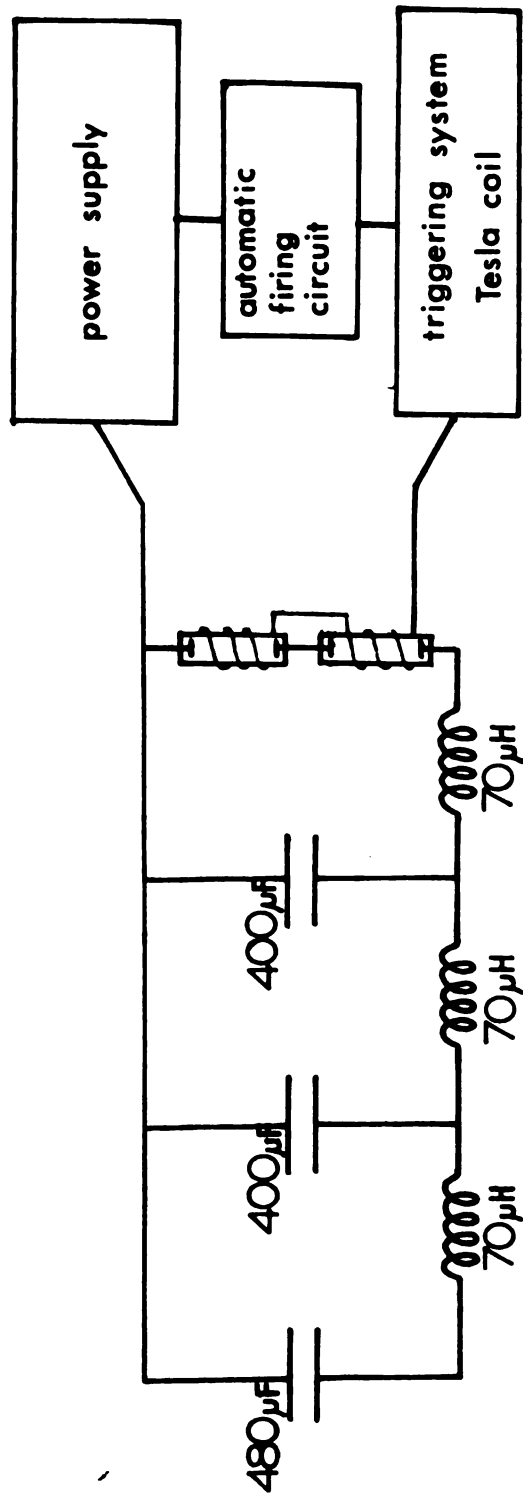


Figure 15- Flashlamp Excitation Pulse Forming Network.

both flash lamps. When high time resolution was desired the external triggering was preferable because of the lower noise level. The high voltage surge in the internal trigger usually produced a rather high noise background. It was necessary to carefully shield and ground all electronic components. The discharging voltage of the flash lamps was controlled either by a manual variac on the power supply control panel or by the automatic firing circuit. Figures 16 and 17 show block diagrams of the ruby power supply and the automatic firing circuit.

In order to compensate for the low efficiency of two photon processes, high power ruby laser radiation was required. Giant pulse techniques were used, which are based on blocking and unblocking (Q-switching) the optical path between the cavity mirrors within a desired period of time so that a higher population inversion can be built up.⁹⁰ This enables most of the stored energy to be released in an intense, short duration pulse. Bleachable dyes served as passive Q-switches. The Q-switching dye, cryptocyanine dissolved in controlled concentrations in methanol,⁹¹ was placed within the optical cavity between the ruby and the totally reflecting mirror. The laser pulse characteristics are extraordinarily sensitive to the operating parameters of the component which make up the laser cavity. Each cavity configuration, distance between mirrors, mirror reflectivity, variation of the

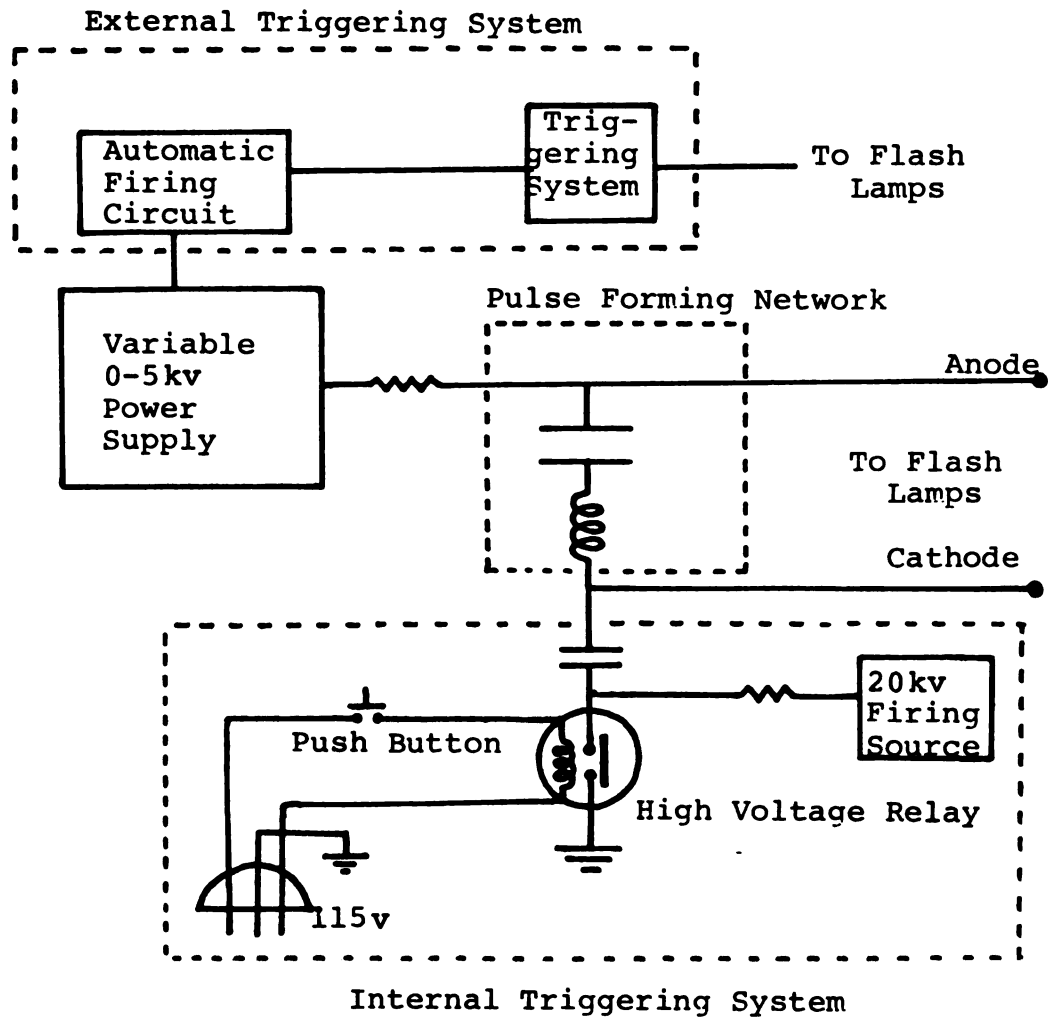


Figure 16. Block Diagrams of the Ruby Power Supply and Triggering Systems.

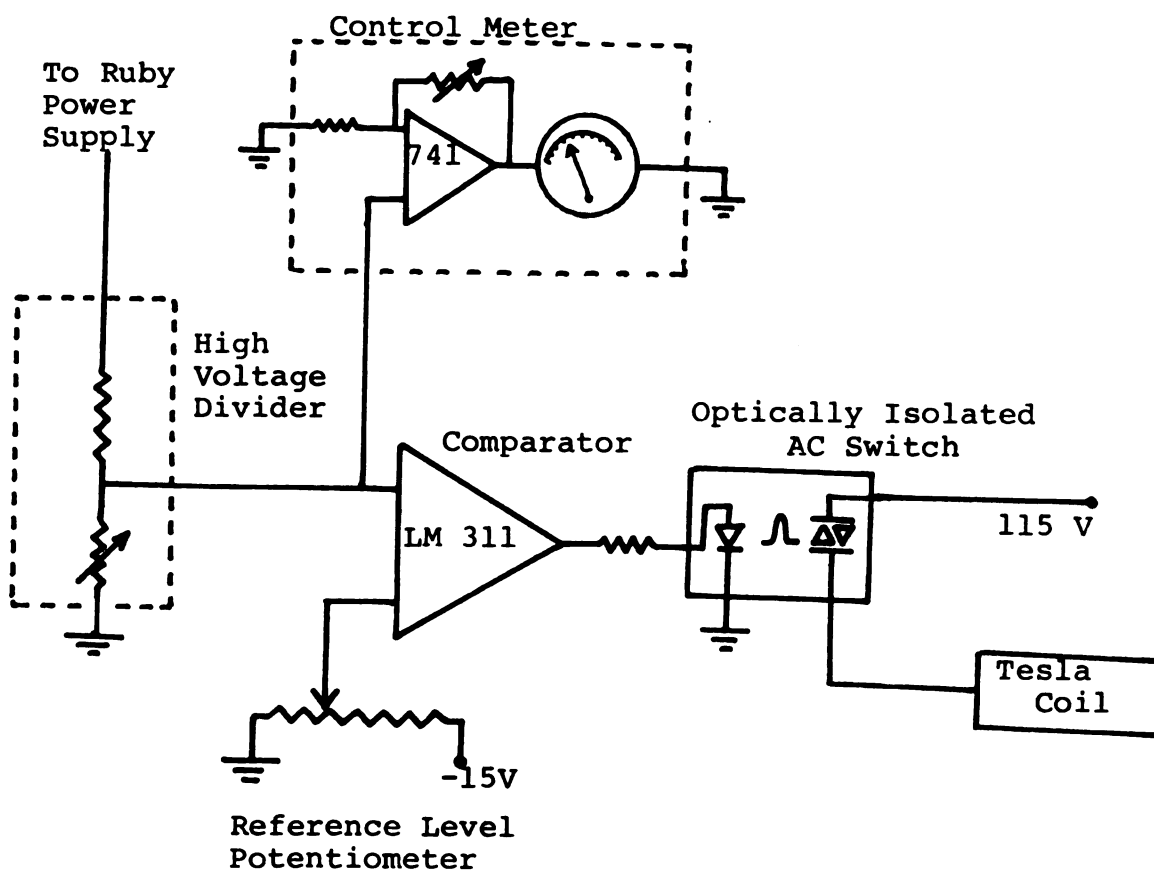


Figure 17. Automatic Firing Circuit.

Q-switch dye, etc. had its own impact on the laser power and pulse shape. The most critical factor for obtaining short pulse duration was the choice of the saturable absorber, its concentration and solvent.^{92,93}

The Q-switch dye cell was 0.3 cm long with two parallel quartz windows. Mode locking was avoided by placing the cell in the laser cavity so that the windows were perpendicular to the laser beam. The quality of the output pulse was determined by the time shape of the pulse and the burst spot on a piece of film. The output pulse shape was measured by diverting a small portion of the radiation with a beam splitter through neutral density filters to a photodiode followed by a Tektronix 519 or 555 oscilloscope. The pulse width was very sensitive to the concentration of the saturable dye. At relatively low concentration, multiple pulses and a long overall pulse width was obtained. As the concentration of the dye was increased a single giant pulse was observed. When the concentration was further raised the pulse became sharper, but the flash lamp discharge threshold also increased significantly. The optimum concentration at 2.5kv firing voltage was $5 \times 10^{-6} \text{M}$ in methanol; under these conditions the pulse width (FWHM) was around 50 nsec. Below $1 \times 10^{-6} \text{M}$, at least 2 or 3 pulses with different widths were observed. Above $8 \times 10^{-5} \text{M}$, the power level obtained was near the ruby damage threshold. In fact, a

cryptocyanine concentration of $5 \times 10^{-6} \text{M}$ in methanol was not the best choice for obtaining a short pulse. Narrower pulses ($\sim 30 \text{ nsec}$) could be obtained by slightly increasing the concentration. However, at the higher concentration the dye solution degraded after the first few shots.⁸⁹ After these few shots, the pulse duration time became longer and the power dropped quickly. Variation in the Q-switch characteristics definitely influenced the stability of output power. As described earlier in the discussion of methods for measuring TPA, temporal fluctuations of the excitation laser causes uncertainty in determining the two-photon cross sections. A stable and reproducible ruby laser was necessary for the TPE experiments described in this thesis. With $5 \times 10^{-6} \text{M}$ cryptocyanine concentration the dye endurance was long, almost 30 shots without refilling, and the pulse width was reasonably reproducible. A second reason for using this slightly low concentration as the optimum was to control the pulse duration. As noted earlier, short pulses should be avoided in two-photon peak height measurements. For the ruby pumped dye laser, the pulse width of dye laser was shorter than that of the ruby pulse by about a factor of 2. In addition to the peak height fluctuations which occur when the pulse width approaches the fluorescence lifetime of the sample, the TPE peak shows a very short spike when the dye laser pulse is really sharp. This

spike could not be observed when it was shorter than the risetime of the photodiode and oscilloscope detectors, thus producing inaccurate values of the emission intensity.

Burst spots in Polaroid film were used to determine the mode structure of the ruby laser emission. An iris with diameter of 3 mm was placed within the cavity to select the TEM_{00} mode. The shape of the burst spot was very sensitive to mirror alignment. The output of the ruby laser was determined by the ratio of the total energy obtained by an energy receiver to the pulse width observed with an oscilloscope. A calibrated Quantronix 500 energy receiver (5.4 mV/Joule) with Quantronix 503 control unit, followed by a chart recorder, was used to measure the total energy. The voltage threshold for the Q-switched ruby to begin lasing at the optimum concentration of the dye was 2.37 kv on the 1280 μ F capacitors, giving an input energy of ~3600 Joules. The energy output of the ruby determined by the energy receiver was usually ~1.2 Joules. If only 10% of the input energy was transferred into the ruby, the conversion efficiency of the ruby laser was less than 0.3%.

The alignment of the ruby laser was very critical. A small He-Ne laser with a pinhole over the output was used to direct a 6328 Å beam through the center of the ruby. The polarization vector of the ruby rod was parallel to the optical table. A polarizer was put in

front of the He-Ne laser to select the \vec{E} vector of the 6328 Å beam in the same direction. The ruby rod was rotated until the transmitted He-Ne beam was precisely parallel to the table. Cavity alignment was accomplished in the following order: The reflected light of the He-Ne laser beam from the front mirror of the ruby laser cavity was adjusted to be coincident with the pinhole by rotating the mirror micrometer mount. Then the same reflection from the Q-switch dye cell was adjusted to coincide with the incident light. Finally, the same procedure was used to align the back mirror. After placing the iris inside the cavity, the alignment was completed.

D. Dye Laser Systems

Many dye molecules are high gain laser active media. For a large dye molecule in a condensed phase, collisional and electrostatic perturbations caused by the surrounding solvent molecules broaden the individual vibrational modes of the dye in each electronic state. Each vibronic sub-level has superimposed on it many rotational states. Therefore there is a quasi-continuum of states superimposed on every electronic state. If the fluorescence band of the dye solution is utilized in a laser, the allowed transition from the lowest vibronic level of the first excited singlet state to some higher vibronic level of the ground electronic state will provide a broad tuning energy range, usually in

the tens of nanometers.⁹⁴ Organic dye lasers can be optically pumped to laser threshold by either other lasers or by flash lamps. Although dye lasers are high gain lasers, in order to design a stable laser cavity, several oscillation conditions must be satisfied.

(a) A fast rising, high power and short duration optical pump pulse is necessary to raise the dye to laser threshold. The risetime of the excitation pulse must be sufficiently short to satisfy the condition $t < \frac{10}{k_{ST}}$, where k_{ST} is the rate constant for intersystem crossing of dye molecules from the singlet state to lower-lying triplet states. For most organic dyes, the value of $\frac{10}{k_{ST}}$ is around 1 μ sec; thus the excitation pulse must be shorter than 1 μ sec.^{94,95} For a laser pumped dye laser, this condition is easily reached. Both Q-switched ruby pulses and N_2 laser pulses are shorter than 50 nsec. However, a flashlamp-pumped dye laser satisfies this condition only by the utilization of a specially designed pumping system,^{96,97} or by the addition of some triplet state quencher.⁹⁸⁻¹⁰⁰

The rise time requirement insures that the population of excited triplet states of the dye molecules remains low. The excitation pulse must pump sufficient dye molecules to the first excited singlet state to reach the laser threshold. Some excited singlet state population will go to triplet states through intersystem crossing. If the

increase in triplet state population is fast, two consequences arise. First, it dramatically reduces the population of the excited singlet state, and hence decreases the dye laser gain factor. Second, it enhances the triplet-triplet absorption rate, and hence increases the dye laser loss factor because some of the stimulated emission has been utilized for triplet-triplet absorption. When the triplet-triplet absorption rate becomes equal to the laser stimulated emission rate, the laser will definitely stop. Thus, if the risetime of the excitation pulse is longer than $\frac{10}{k_{ST}}$, stimulated emission cannot start because all of the laser light has been used for providing triplet-triplet absorption. One or more of several means of quenching the triplet state concentration rapidly enough so that $t < \frac{10}{k_{ST}}$, such as chemical additives or rapid flow of the dye through the excitation region, must be provided in order to maintain the dye laser efficiency.

(b) Although dye lasers are high gain lasers, certain conditions must be achieved to match the parameters of the dye resonator. The simplest form of a dye laser consists of a cuvette of length l containing dye of concentration n and of two parallel reflectors possessing a total reflectivity R ($R = R_1 R_2$, the product of reflectivities of both mirrors). The condition for laser action can be written in the form:⁹⁴

$$\exp(-\sigma_a(\hat{\nu})n_o l) R \exp(\sigma_{em}(\hat{\nu})n_l l) \geq 1, \quad (3.1)$$

where $\sigma_a(\hat{\nu})$ and $\sigma_{em}(\hat{\nu})$ are the cross sections for absorption and stimulated emission at $\hat{\nu}$ respectively, and n_0 and n_1 are the populations of the ground and first excited states. The first exponential factor represents the loss factor which is mainly due to reabsorption of the fluorescence emission by the long-wavelength tail of the absorption band. The second factor represents the cavity loss factor. Usually we define a constant $S = \frac{1}{\ell} \ln(\frac{1}{R})$ which gives $R = e^{-S\ell}$ and contains only parameters of the cavity. The third factor represents the laser gain factor. This condition then becomes:

$$\sigma_{em} n_1 \ell - \sigma_a n_0 \ell - S \ell \geq 0 \quad (3-2)$$

If we assume that the cross-sections for absorption and emission are approximately equal ($\sigma_a \approx \sigma_{em}$), and rearrange equation (3-2) to the form:

$$\frac{S/n + \sigma_a}{\sigma_a + \sigma_{em}} \leq \frac{n_1}{n} < 1,$$

then $S/n < \sigma_{em}$. This allows a quick estimate of the feasibility of laser action for a given resonator (defined reflectivities and cavity length) and dye concentration. For any dye laser, the condition $S/n < \sigma_{em}$ must be achieved.

(c) The behavior of a dye laser depends not only on the choice of coupling coefficient (i.e. mirror reflectivity), but also on the geometry of the cavity (the distance

between mirrors and shape of the cavity, i.e. plane, spherical, confocal, etc.). A parameter, the Fresnel number, which relates the stability of a laser to the configuration of the cavity is defined as $F = \frac{a^2}{\lambda d}$, where λ is the output wavelength, a is the radius of the circular aperture of the laser beam, and d the distance between the two reflectors. The Fresnel number of a dye laser must not be too small or the laser will be unstable.¹⁰¹ For example, if we expand and focus the ruby laser to form a uniform plane to pump a dye laser by passing the ruby radiation through 2 cylindrical lenses as shown in Figure 18, $a \sim 0.15$ cm and $\lambda \sim 8 \times 10^{-5}$ cm. In order to obtain a reasonably large F value, such as 20, the distance between the cavity mirrors can be only $d < 14$ cm. In other words, the cavity length of the pulsed dye laser must be compact. For a N_2 laser pumped dye laser, this requirement is even more critical because the N_2 laser beam has to be focused into dye solution to a rather smaller region (a is smaller).

A ruby pumped dye laser, a N_2 laser pumped dye laser, and a flashlamp pumped dye laser have been built in the course of this work. In addition to the powerful ruby pumped dye laser, the N_2 laser pumped dye laser has been used to detect two-photon induced fluorescence. However, difficulties in tuning the N_2 -pumped dye laser limited its utility for TPA measurements to several restricted wavelengths.

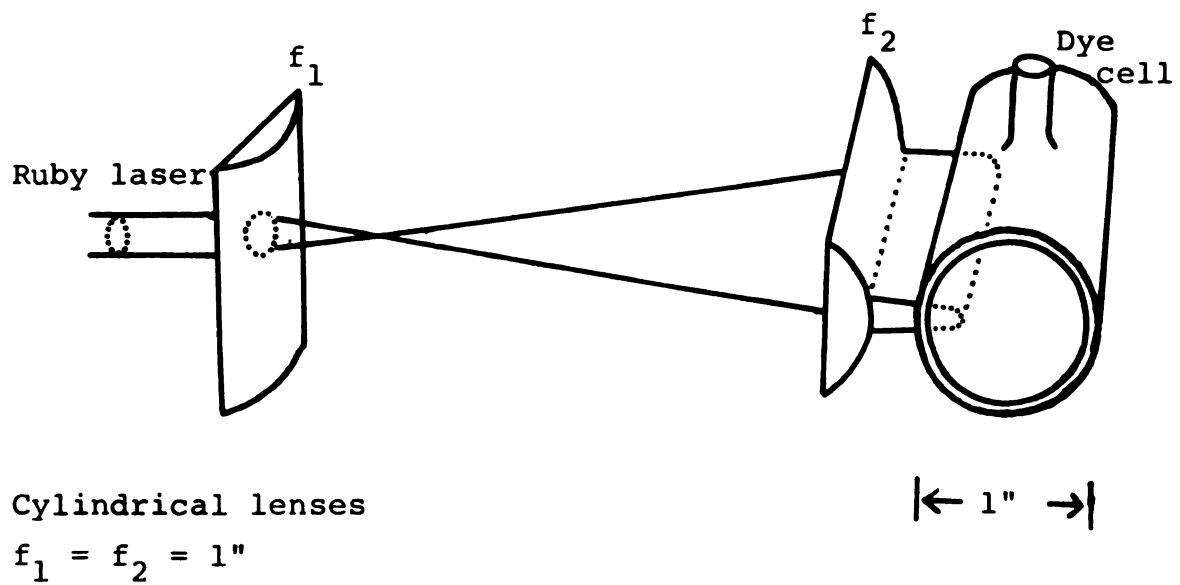


Figure 18. Transverse Pumping by a Cylindrical Lens Set.

(1) Ruby Laser Pumped Dye Laser

As shown in Figure 18, cylindrical lenses focused the ruby pulse into the dye cell. The quartz dye cell was 2" long and 1" in diameter, and had windows tilted 10° from perpendicular in order to prevent self-lasing. In order to obtain a reasonable value for the dye laser Fresnel number, the ruby pulse was not simply focused on the front surface of dye cell. Rather, it was focused inside the dye solution at a depth of almost 1 cm, enabling a larger aperture for the dye active region to be obtained. The burst spot of a typical dye pulse, obtained by focusing the pulse on a piece of film, looked like:



The 15 cm long dye laser cavity was formed by a rotatable grating¹⁰² (1200 ℓ /mm blazed at 5000 \AA) and a fixed output mirror (a 100% R ruby mirror at 6943 \AA) which had 50% R at 900 nm and 40% R at 800 nm. Dyes¹⁰³ used to cover the wide spectral range required for this work were DDI (1,1'-Diethyl-2,2'-dicarbocyanine iodide), DTTC (3,3'-Diethylthiatricarbocyanine iodide), Candela #4 (3,3'-Diethyl-2,2'-(4,5,4',5'-dibenzo) thiatricarbocyanine iodide), #10 (1,1'-Diethyl-2,2'-quinotricarbocyanine iodide), #11 (1,1-Diethyl-4,4'-quinotricarbocyanine

iodide), #17 (1,3,3,1',3',3'-Hexamethyl-2,2'-indotri-carbocyanine iodide) and Eastman IR-140. DDI and DTTC were stable at room temperature, while the polymethine dyes (the Candela dyes) were stored in a freezer. The output power and tuning range for these dyes in their optimum solvents are shown in Figure 19. DDI, like cryptocyanine, lases only in a viscous solvent such as glycerol or ethylene glycol; the recovery time of DDI in glycerol after each shot was rather long. Candela dyes 10 and 11 are both weak. The output powers of these two dyes were an order of magnitude less than the powers of other dyes. The tuning range of DTTC and Candela #17 shifted to the blue by $\sim 50 \text{ \AA}$ when the solvent was changed from DMSO to acetone.

The alignment method for the dye laser is critical and therefore requires a detailed description. First the dye cell was filled with the appropriate solvent (DMSO or acetone). He-Ne laser light collimated through a pinhole which was sitting 1 m away from the output mirror of the dye laser was then passed through the dye cell at a distance only few millimeters (2~3 mm) from the left edge of the cell. The perpendicular adjustment knob of the dye cell was adjusted until the 6328 \AA beam inside the cell was completely parallel to the cell axis. Then the horizontal adjustment knob of the dye cell was turned until the reflected light from the front window of the

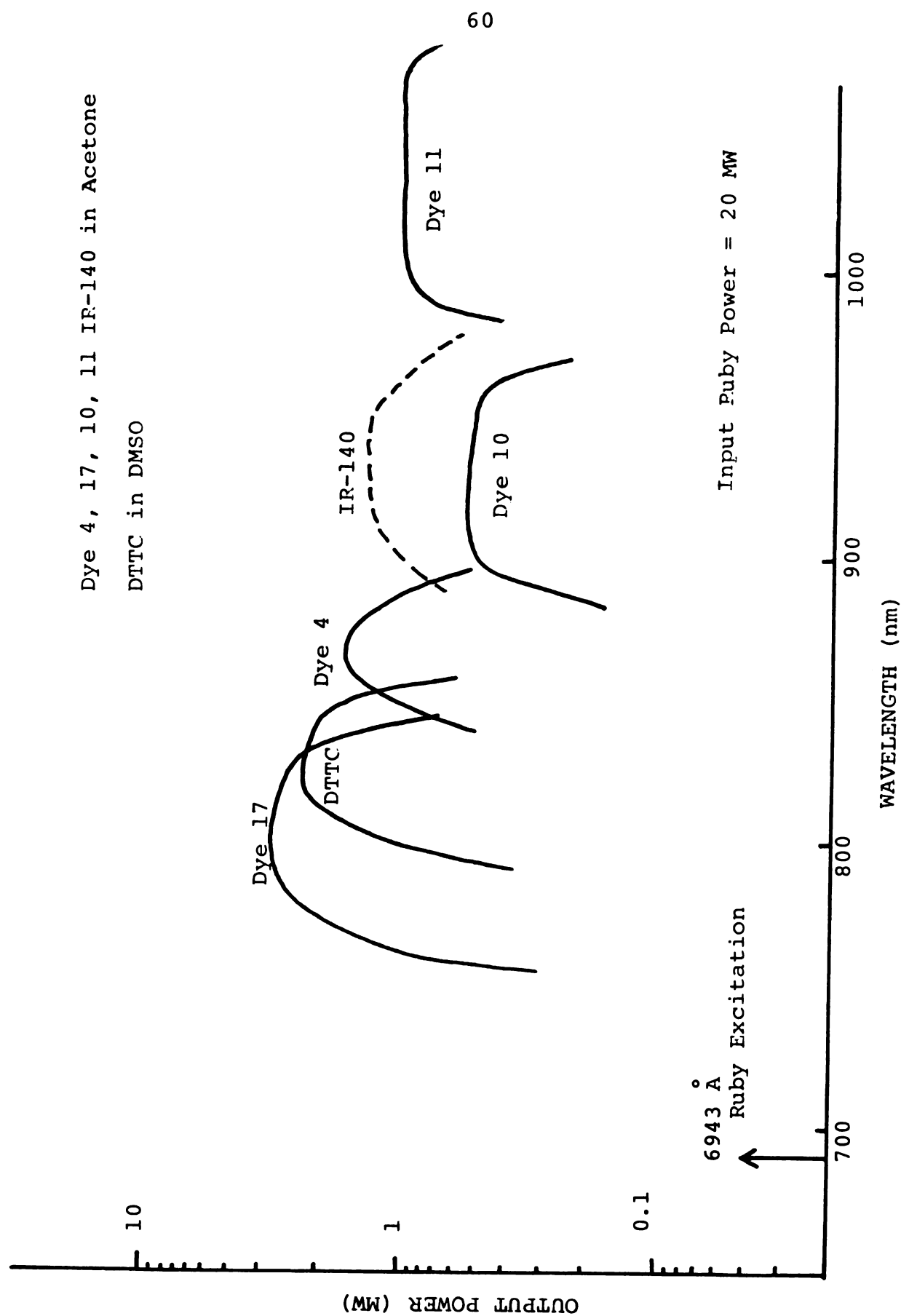


Figure 19. The Tuning Range and Relative Output Power of Several Dyes.

dye cell was lying with the incident beam in the same plane perpendicular to the floor. The He-Ne laser beam passed through the dye cell filled with pure solvent and hit the grating. The grating rotation was selected so that the first-order diffracted light was coincident with the incident light. This coincidence could be checked by observing the reflected first-order light from the grating which passed back through the cell and provided an image spot on the surface of the pinhole plate. The grating was further rotated and checked by this coincidence procedure for zeroth order light and second order light to make sure that the grating surface was precisely perpendicular to the dye laser pathway. After alignment of the grating with the dye cell, the dye laser front mirror was reinserted and adjusted so that the reflected light from the inner surface of the mirror coincided with the pinhole. (Note: there were 2 reflection spots from the two surfaces of the mirror; the brighter one was chosen.) Finally, the grating was rotated to the desired angle and several drops of the desired dye solution were added to the dye cell. This completed the alignment procedure. The selection of rotation angles for the grating and the tuning method are discussed in the following section.

Two He-Ne alignment lasers were used as reference beams to do the tuning. The first laser beam (laser 1 in Figure 20) passed through the dye cell and served as an

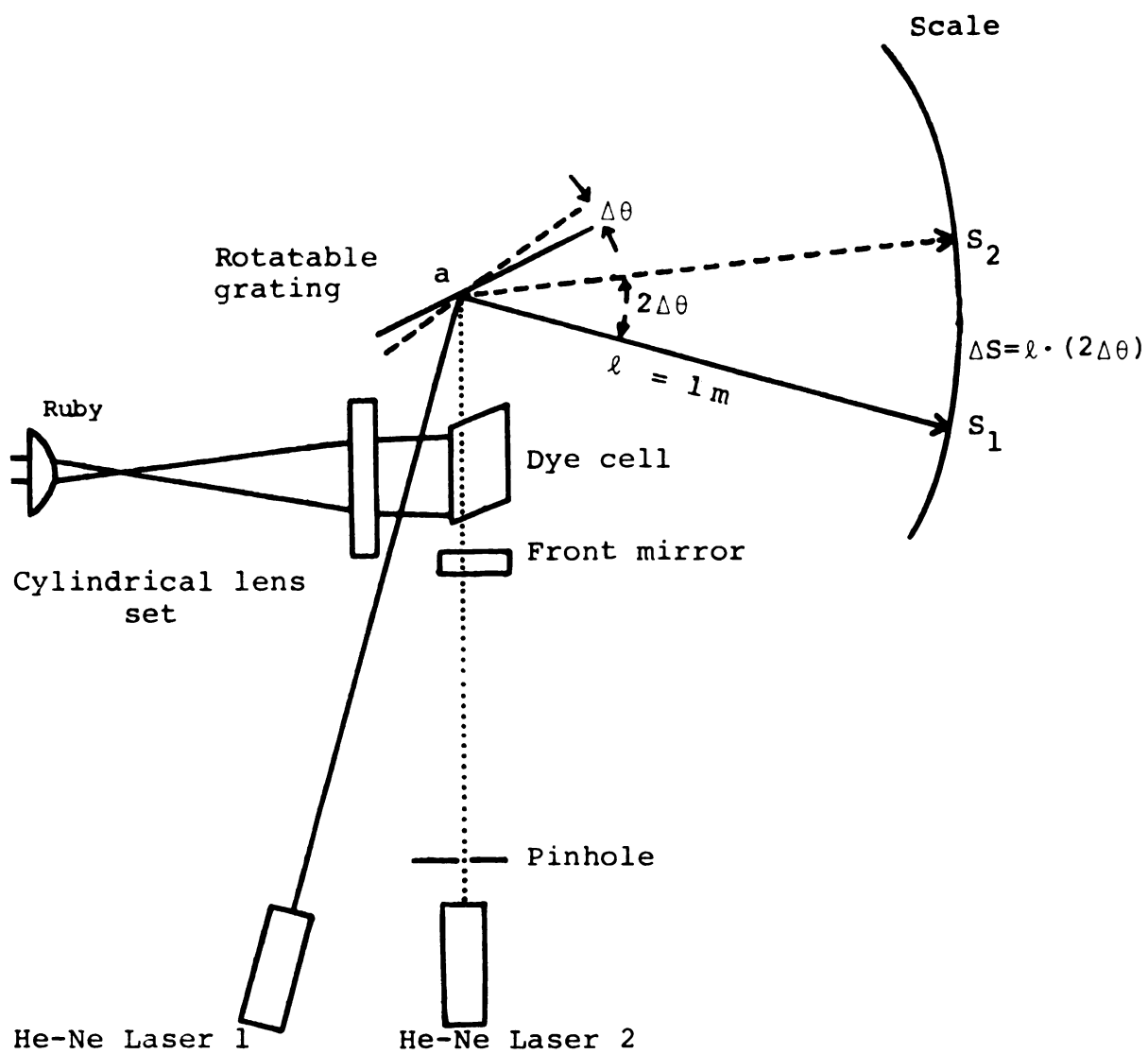


Figure 20. Dye Laser Tuning System.

alignment laser, as described above. Light from the second He-Ne laser (laser 2), directed onto the grating from the side of the dye cell, served as a tuning reference beam. This beam from laser 2 hit the grating at the same point at which the dye laser would hit. The zeroth order diffraction light of laser 2 from the grating was reflected onto scale S, where it served as a marker. This scale was a circumference meter with its circular center at point a; i.e. the radius of circle ℓ (the distance from point a to any point on the scale) was exactly 1 m. A rotation angle $\Delta\theta$ of the grating would provide a rotation of $2\Delta\theta$ for zeroth order reflected light of laser 2 from the grating. Therefore, as the grating rotated by an angle $\Delta\theta$, the reference beam scanned a distance $\Delta S = \ell \cdot (2\Delta\theta)$ on the scale. From the value of ΔS , the angle $\Delta\theta$ could be calculated. The tuning theory was simply based on this relationship. The tuning procedure was as follows: First, the grating rotation was set so that the 1st order diffracted light from the alignment laser (laser 1) was coincident with the pinhole. The grating at this position had an angle θ_1 determined from the well-known grating formula: $\lambda_1 = 6328 \times 10^{-8} = 2d \sin \theta_1$, where the groove distance $d = \frac{0.1}{1200}$ cm because this grating had 1200 ℓ/mm . So, $\theta_1 = 22^\circ 19'$ or $\sin \theta_1 = 0.3797$. When the grating was at this position, the zeroth order diffracted light of laser 2 fell at a point S_1 on

the scale. When the grating was rotated to another position, the zeroth order diffracted light of laser 2 shifted to another point S_2 . Therefore $\Delta S = S_2 - S_1 = \lambda \cdot 2(\theta_2 - \theta_1)$ or $\theta_2 = \theta_1 + \frac{\Delta S}{2\lambda} = 22^\circ 19' + \frac{\Delta S}{200}$. If we knew θ_2 , we could calculate the corresponding wavelength λ_2 by using the formula $\lambda_2 = 2d \sin \theta_2$. However, the wavelength corresponding to rotating the grating an angle $\Delta\theta$ from θ_1 can also be related directly to the only variable which could be observed on the scale, ΔS , by the formula $\lambda_2 = \sin(22^\circ 19' + \frac{\Delta S}{200}) \cdot 2d$. After substituting numerical values, the final formula was $\lambda_2(\text{\AA}) = \sin(22.3167^\circ + \Delta S \times 0.2874) \times 16666.6$. The accuracy of this tuning technique was checked by diverting a small portion of the dye laser output with a beam splitter to a Heath monochromator. The difference between calculated and observed values of the dye laser wavelength was zero in the 800 nm region and was only 1 \AA in the 900 nm region. Hence the uncertainty in wavelength was within 0.1 nm.

The bandwidth of the ruby laser pumped dye laser was also ascertained in this way. The observed bandwidth throughout the range throughout the range 760-1050 nm was less than 2 \AA . The temporal behavior of the ruby and dye lasers were recorded using silicon photodiodes (Hewlett Packard PIN photodiodes) and a Tektronix 555 oscilloscope. The pulse durations of the dye lasers were around 30 nsec, shorter than the ruby pulse by about a factor of 1.5 to

2. Dye laser output power was in excess of 200 kw. High power ruby excitation light was avoided because as the dye power became too high it would cause damage to the grating surface if a telescope expander was not used. The tuning range was very sensitive to the alignment and dye concentration. As the dye concentration was slightly increased, the tuning range would shift to red.⁹⁴ If the alignment was not perfect, the tuning range declined in both wavelength extrema. For low-gain regions, such as those encountered near the limits of a dye's tuning range, the pulse width decreased and the pulses became sharper than those in the high-gain regions. As mentioned in chapter II, when the excitation pulses became sharper, the fluctuation of measured TPA cross sections increased. Therefore, the side wings of a given dye tuning range should be avoided in two-photon applications; this can be accomplished by increasing the overlap between dyes. If such overlap is not available, a slightly increased dye concentration will extend the tuning range to the red and will thus enable a broader spectral range to be covered at optimum pulse widths.

(2) Nitrogen Laser Pumped Dye Laser

A transversely excited (TE) Blumlein type¹⁰⁴ nitrogen laser, which emits radiation at 3371 \AA , was constructed. The circuitry for the operation of the N_2 laser is shown

in Figure 21. Two capacitors, C_1 and C_2 , were interconnected electrically by a coil of copper wire. A high voltage power supply (40 kv, 2 mA, EOS Model ILM-70) served to charge both capacitors to the same potential and the same polarity. No potential difference existed across the electrodes. As the voltage was increased the air between the electrodes of the spark gap (~2 cm gap) suddenly began to break down. Then the potential drop across capacitor C_2 suddenly was released. Shortly after the onset of conduction in the spark gap the voltage difference abruptly shifted to the center of the discharge gap between the two electrodes because the charge on capacitor C_1 could not be drained away through a small coil of wire in a short period of time. For changes that occurred within nanoseconds the wire acted as an open circuit. Finally the voltage across the capacitor C_1 discharged abruptly through the 2 electrodes and excited the N_2 molecules within the laser cavity. The experimental setup is schematically depicted in Figure 22. The capacitors were made from 4 pieces (2' x 3') of 3/32" thick epoxy circuit board which were clad with copper on both sides. The copper was etched from a 1" margin around the perimeter of each board, and two boards were combined to form one capacitor. The laser discharge channel was a gastight rectangular box of dimensions 2" x 4" x 72". It consisted of two strips of brass electrodes connected

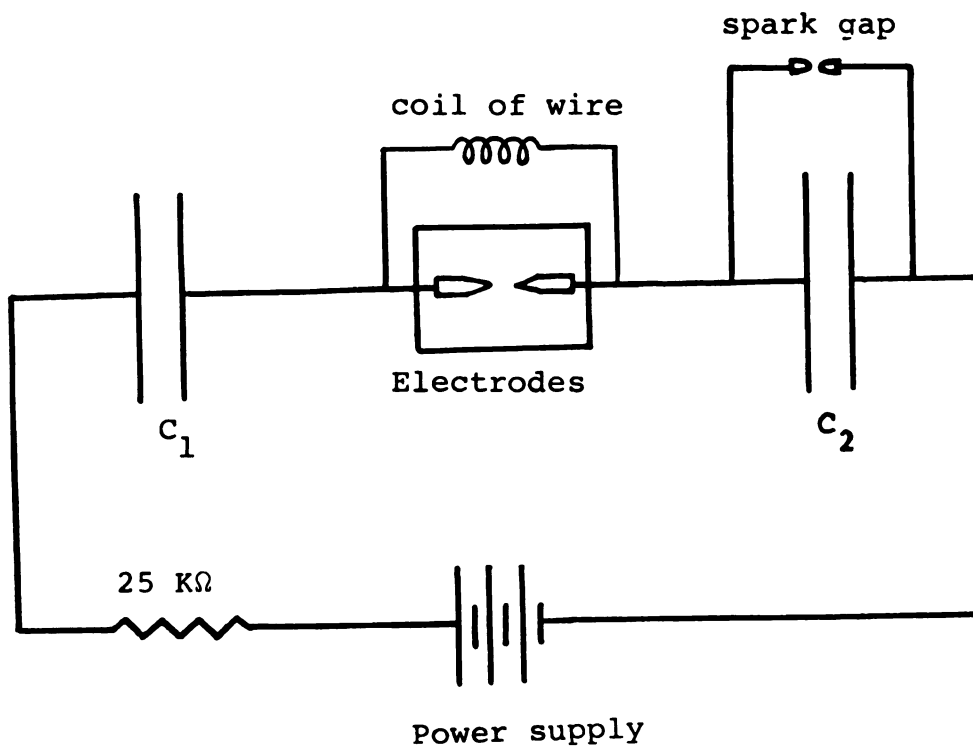
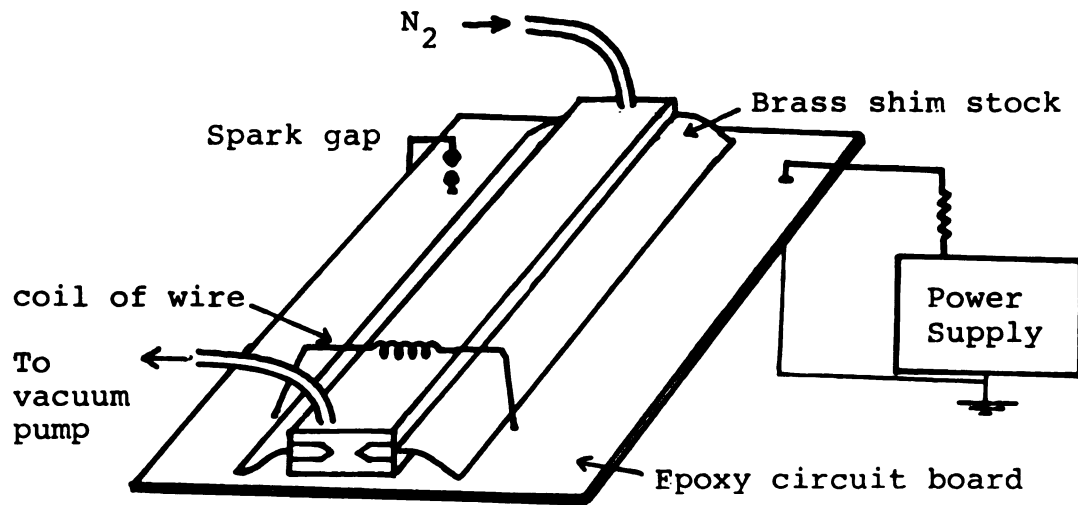
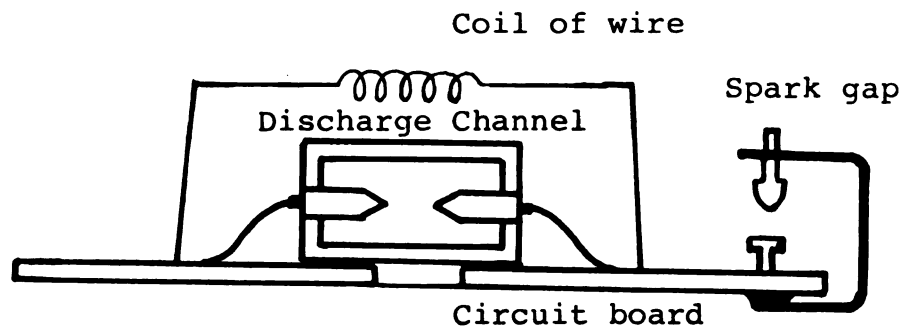


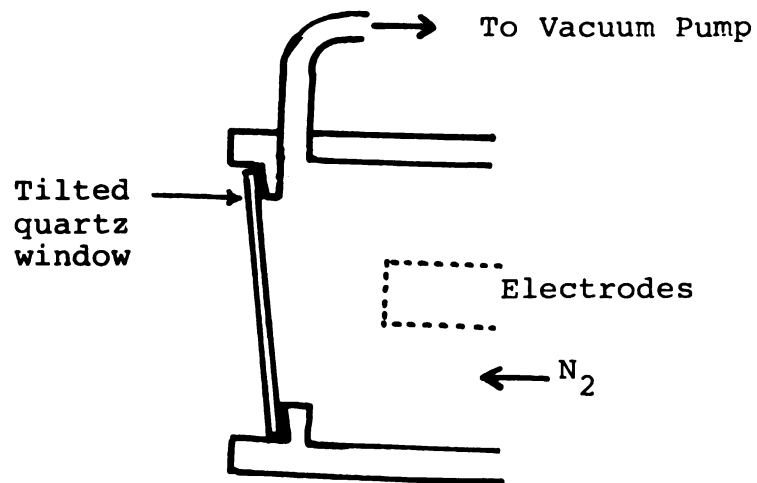
Figure 21. Circuitry of the Blumlein Type N_2 Laser.



(a)



(b)



(c)

Figure 22. (a) Side-View and (b) End-View of N₂ Laser;
(c) Output Window of N₂ Laser.

to the circuit board by brass shim stock. The head of each electrode was sharpened to a knife edge. These two electrode knife edges were carefully aligned to form a straight plane throughout the channel. The distance between electrodes was 1" at the back end and was 1.1" at the output end of the N_2 laser. The entire cell was assembled by cementing together strips of plexiglass with epoxy glue. End plates with tilted quartz windows (15° from perpendicular to the laser beam) were cemented on both ends of the channel. Each plate contained a hose connection which served as inlet and outlet for the flowing N_2 gas. The outlet hose was connected to a vacuum pump and the inlet hose to a N_2 gas tank. The optimum N_2 gas pressure was between 50 and 70 torr. An Aluminum mirror was used as the back reflector. No front mirror was needed, since the pulsed N_2 laser is superradiant. The switching device was a spark gap with an adjustable gap distance. The output power and the repetition rate of the pulsed N_2 laser were determined by the gap distance. As gap distance became small, the firing voltage decreased and the repetition rate increased. For example, the repetition rate increased from 1 Hz to 20 Hz as the voltage decreased from 20 kv to 16 kv. High voltage (> 24 kv) should be avoided because it might cause the breakdown of the epoxy circuit board.

The total input energy was calculated by $E = \frac{1}{2} CV^2$, where the capacitance C of the circuit board was derived by measuring the area of the whole plate A and the thickness of the plate d . ($C = \frac{\epsilon KA}{d}$, where the dielectric constant K of epoxy is about 4.5 and the permittivity ϵ is 8.854×10^{-12} farad/m.) The capacitance in this configuration was about 0.035 μF and the total input energy at a firing voltage of 18 kv was almost 5.5 Joules. The pulse width of the N_2 laser, measured by an oscilloscope, was between 10 and 15 nsec. Assuming 0.08% conversion efficiency of N_2 laser,¹⁰⁵ the energy output of each pulse should be approximately 4.4 mJ and the corresponding output power for a 15 nsec pulse will be about 300 kw.

The 3371 Å output of the N_2 laser was focused into the dye cell to pump the dye laser. Various dye laser geometries were tested, the most reliable tuning method being the transverse pump configuration shown in Figure 23. The N_2 laser light was focused through a $f = 30$ cm spherical lens and a $f = 2.54$ cm cylindrical lens to form an almost 1 cm wide plane entering the dye cell. The latter was an ordinary 1 cm² commercial cuvette, tilted at an angle about 15° from vertical to prevent self-lasing. A quartz plate and a rotatable grating formed the dye laser cavity. In order to maintain a reasonable Fresnel number, the cavity length should not be longer than 20 cm. For the most popular Hänsch design¹⁰⁶ of the N_2 -laser

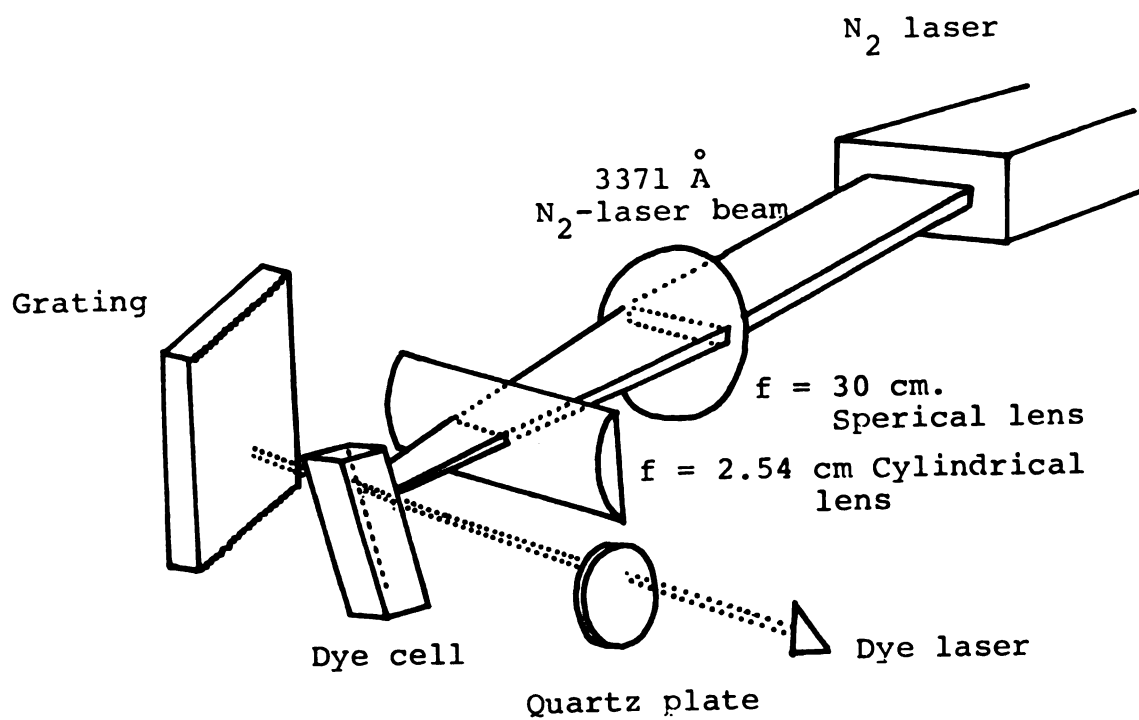


Figure 23. N_2 Laser Pumped Dye Laser.

pumped dye laser, a telescope expander should be inserted between the dye cell and the grating. However, for medium resolution measurements, the dye laser was still tunable without the expander. For example, with this setup, R6G can be easily tuned from 5750 Å to 6050 Å. Several measurements of two-photon induced fluorescence signals excited by two N₂ laser pumped dye laser photons were made. In particular, some preliminary data demonstrating the fluorescence of α -chloronaphthalene induced by two dye laser photons at several different wavelengths have been obtained. Sample fluorescence was collected at 90°, passed through a Corning 7-59 filter and Spex single monochromator, and detected by a RCA C31034 photomultiplier (as shown in Figure 24). However, the spark gap of the N₂ laser produced a tremendous amount of noise which completely precluded accurate measurements of these weak two-photon induced fluorescence signals. Either extensive shielding of the whole circuit board or the use of a thyatron tube in place of the spark gap must be incorporated in order for the N₂ laser to be a viable dye pump for two-photon experiments.

(3) Flashlamp Pumped Dye Laser

A flashlamp pumped dye laser was also built. The excitation source was a EG & G FX38C-3 Xenon flash lamp connected to several low inductance, fast risetime

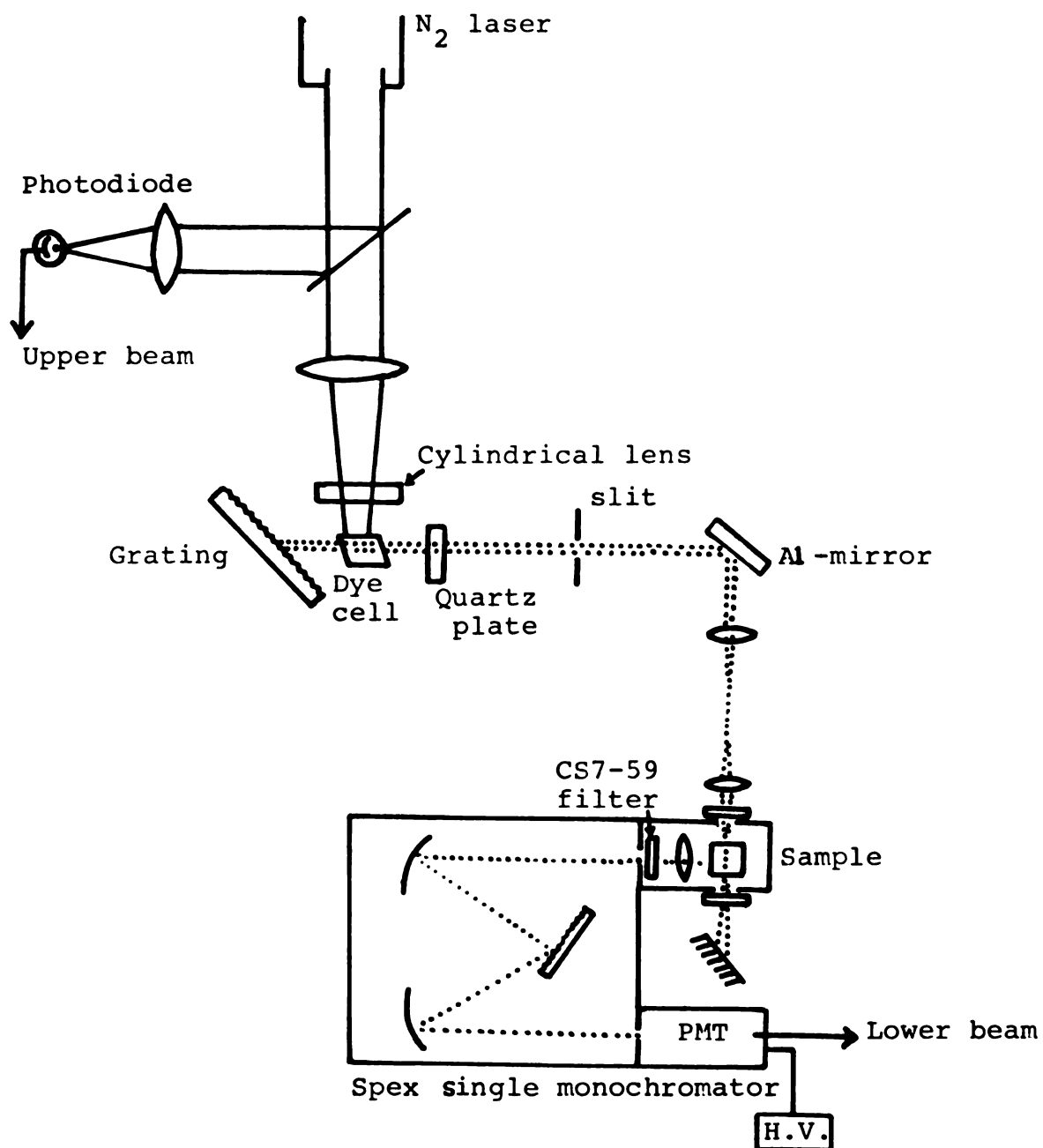


Figure 24. Two-Dye-Laser (N₂ Laser Pumped)-Photon Induced Fluorescence Measurement.

capacitors ($2\mu\text{F} + 2\mu\text{F} + 1\mu\text{F}$ in parallel) which were charged by a 5 kv power supply. In order to obtain a fast discharge time, the conductance of the wires connecting the flashlamp to the electrodes of the capacitors must be high. Two copper plates were used to replace the ordinary low conductance wire, and the distance between the flashlamp and the capacitors was made as short as practicable. An elliptical cavity with polished Aluminum inner surface was used to cover the flashlamp and the dye cell, which were placed along the two foci. An external triggering system consisting of a Tesla coil and a trigger wire wrapped around the flashlamp was used. The dye cell was a 3" long, 0.5 cm radius quartz tube, tightly fitted into Teflon holders into which quartz windows were also placed and through which the dye solution flowed. A schematic view of the flashlamp pumped dye laser is given in Figure 25. A methanol solution of the dye ($\sim 10^{-3}\text{M.}$) was circulated through the cell. A front mirror and a rotatable back grating formed the dye laser cavity. The dye output was detected by a photodiode protected with neutral density filters, followed by a Tektronix 519 oscilloscope. A typical flashlamp pumped dye pulse was almost 2-3 μsec in half width. The threshold voltage was about 2.5 kv and the threshold input energy was $\frac{1}{2} CV^2 = 15.6 \text{ J.}$ Assuming 0.02% conversion efficiency of flashlamp pumped dye laser,^{94,95} the dye

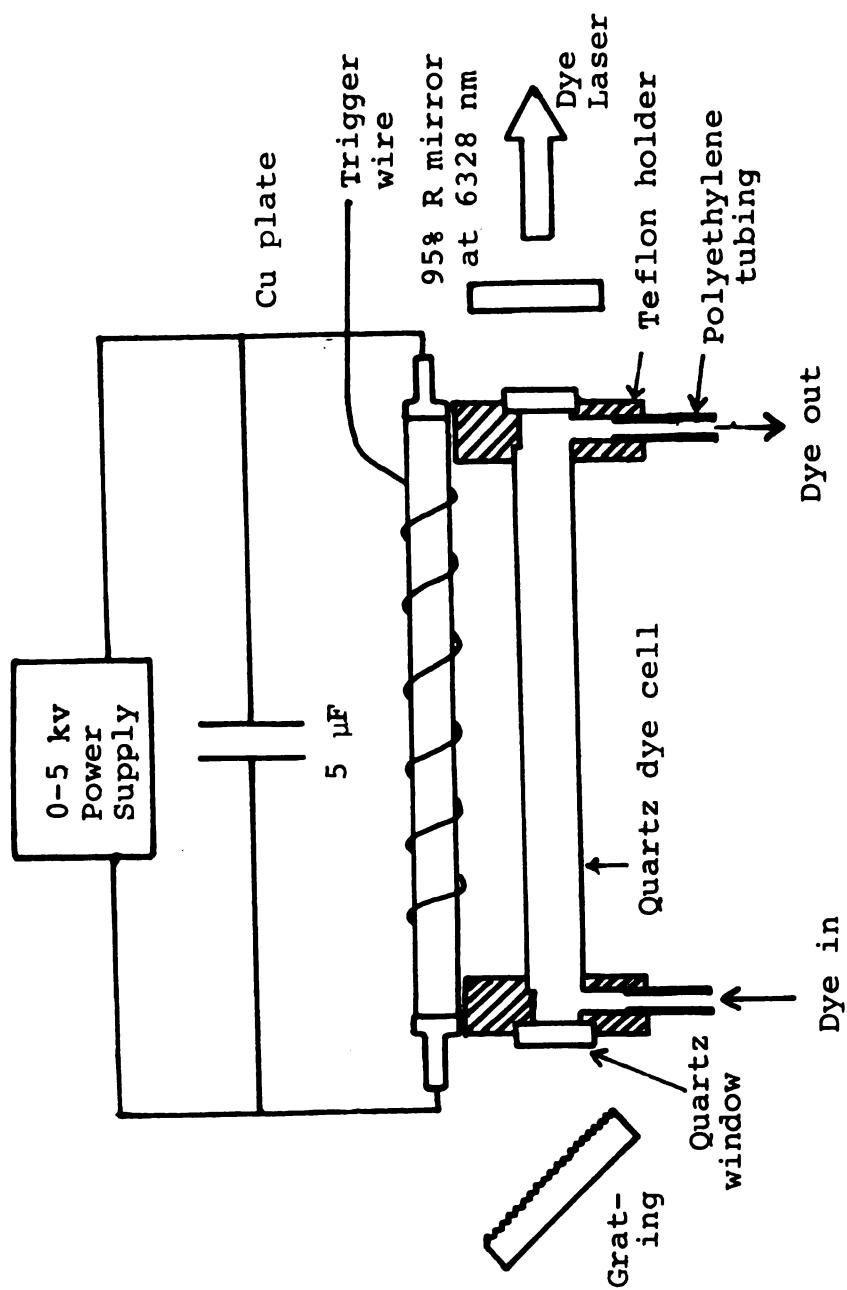
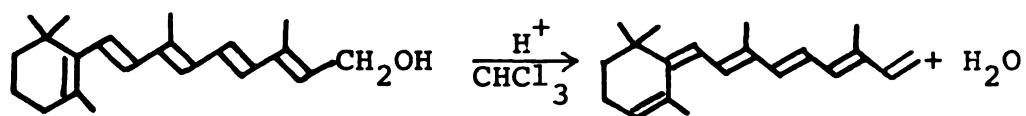


Figure 25. Flashlamp Pumped Dye Laser

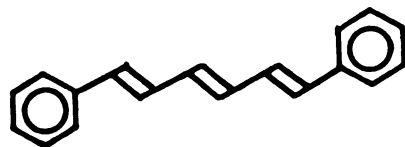
laser output energies per pulse should be 3 mJ and the corresponding output power for a 2 μ sec pulse will be about 1.5 kw. This output power is low for two-photon measurements.

E. Materials

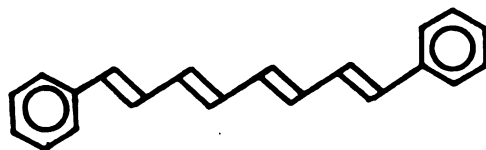
Structural formulas for the molecules studied in this work are shown in Figure 26. All-trans diphenylhexatriene and diphenyloctatetraene were purchased from Aldrich Chemical Co. and used without further purification. All-trans retinol and retinal were obtained from Sigma Chemicals and were used in most experiments without further recrystallization. All-trans anhydrovitamin A was rather simply synthesized from all-trans retinol by the following reaction:^{33,107}



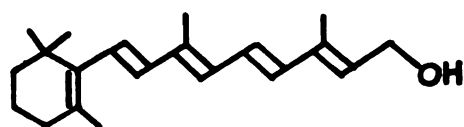
1 g of all-trans retinol was dissolved in 250 ml CHCl_3 . About 2 ml of a CHCl_3 solution saturated with HCl gas (HCl gas bubbling through it for 1 hr.) was added dropwise while stirring in darkness. Too much acid was avoided since vigorous dehydration might cause formation of some side products. The solution was stirred in the dark for 15 min. The reaction was then stopped by adding a small amount of water and drying with Na_2SO_4 . The CHCl_3



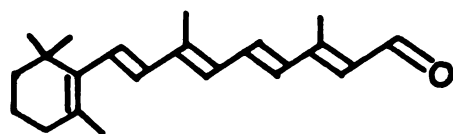
1,6-diphenylhexatriene



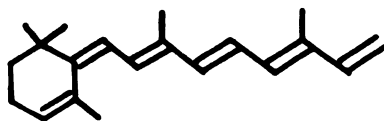
1,8-diphenyloctatetraene



All-trans Retinol



All-trans Retinal



All-trans Anhydrovitamin A

Figure 26. Sample Materials.

solution was concentrated by using a rotating evaporator until the volume of the solution had decreased to a few mls. The concentrated solution was then transferred to a chromatography column (180 ml alumina with mesh number 80-200) where the anhydrovitamin A was separated from reactants by elution with a 5% (ether-hexane 5:95 by volume) solution. The anhydrovitamin A came off the column first and left behind any unreacted vitamin A. The anhydrovitamin A obtained from the first column contained several isomers and was therefore rechromatographed through a second column containing 100 ml Woelm alumina (activity 1) to separate the all-trans fraction. The carrier solution was an ether-hexane mixture with gradually increasing ether concentration (5-25%). The first pale yellow portion (~10%) consisted of unwanted cis isomers, followed by the all-trans portion (~70%) and a second cis isomer (~20%). The all-trans anhydrovitamin A fraction was dark yellow color and was concentrated by evaporation to a very small volume of about 1 ml.

If a few mls petroleum ether were added to this concentrated solution, beautiful orange needle-shaped crystals of all-trans anhydrovitamin A could be obtained by cooling the resultant solution for 48 hrs. at -78°C (dry ice in acetone). The crystals were dried by decanting the solution and blowing dry Helium gas over the solid, or by vacuum desiccation. Anhydrovitamin A is

stable for extended periods at room temperature only in oil solution. Other concentrates and the crystalline preparation will either absorb water vapor to reform all-trans retinol, or degrade to other cis-isomers. In a sealed cell filled with dry Helium gas and stored in a freezer, all-trans anhydrovitamin A will last for weeks. Its isomeric purity can be easily checked by its distinctive, vibrationally resolved absorption spectrum. Anhydrovitamin A is the only compound in the retinyl family which has a well resolved electronic absorption spectrum. All other retinyl polyenes show remarkably diffuse spectra when compared to those of unsubstituted or diphenyl-substituted polyenes of approximately the same size. Also, the absorption spectra of the cis isomers of anhydrovitamin A are bluer than that of the all-trans compound. For example, after lengthy exposure of the isomer to ultraviolet light, the electronic absorption spectrum shows a decrease in resolution and an increase in broadness in the blue region, as illustrated in Figure 27.

Solutions for low temperature studies were prepared by using MCB spectrograde EPA (ether-isopentane-ethanol, 5 : 5 : 2 by volume). To avoid effects caused by sample decomposition or degradation, fresh solutions were prepared just prior to each experiment and handled under safelights.

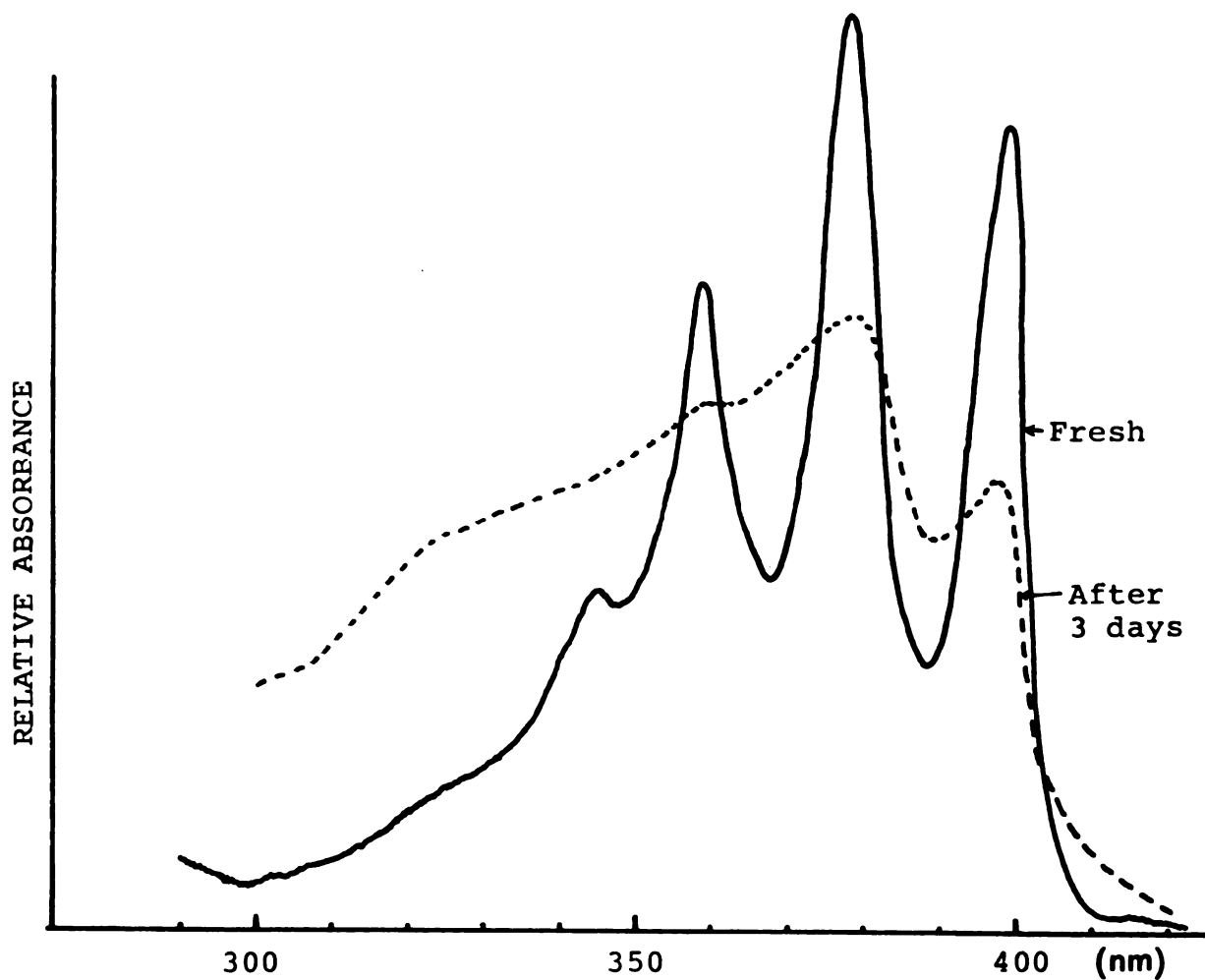


Figure 27. Absorption Spectra of All-trans Anhydrovitamin A (taken at 77°K in EPA) Before (—) and After (---) Lengthy Exposure to Room Light at Room Temperature.

F. Two-Photon Excitation (TPE) Spectrometer

Because of the even-parity selection rule, two-photon absorption is an ideal way to observe and locate low-lying "forbidden" ${}^1A_g \leftrightarrow {}^1A_g$ transitions. At the present time, the TPE technique, in which two-photon induced fluorescence is monitored is still the best method for detecting TPA processes because of its simplicity and high sensitivity. (Direct absorption measurements are still in the early stages of development.) In order to use TPE to observe low-lying 1A_g states of all-trans linear polyenes, several conditions must be met: (1) A near infrared tunable and powerful dye laser is needed. The best candidates for the study of low-lying 1A_g states are polyenes of medium size ($n = 4\sim 6$). (Examples will be discussed in chapter IV.) For these medium size polyenes, the absorption origins are in the range 3500 \AA to 4200 \AA . Assuming that the low-lying 1A_g states are 1000 cm^{-1} to 3000 cm^{-1} below the origin of the lowest one-photon absorption, the two-photon tuning range of interest is from 14500 cm^{-1} to 11000 cm^{-1} , which is in the near infrared region. Therefore a ruby laser pumped dye laser is an excellent choice for the excitation source.

(2) The polyene molecule selected for study must be fluorescent, and have a reasonably high two-photon cross section. (3) The noise level of the excitation source

must be low. Although TPE is a sensitive technique, after appropriate filtering (filters or a monochromator) only part of the selected fluorescence will be detected by a photomultiplier. If the noise is similar in magnitude to the signal, no spectrum can be obtained. This is the reason why an external triggering system was used for the ruby laser, since it provided a much lower noise level than was possible with internal triggering.

The experimental apparatus is schematically depicted in Figure 28. Near infrared radiation from a tunable dye laser pumped by a Q-switched ruby laser served as the excitation source. Cylindrical lenses focused the ruby pulse inside the dye cell, which was within a resonant cavity formed by a rotatable grating (1200 l/mm) and fixed output mirror. The ruby laser and dye laser have been described in sections C and D of this chapter.

The fluorescence housing, shown in Figure 29, contained a spherical collection lens ($f = 5$ cm) which focused the two-photon induced fluorescence radiation emitted at 90° from the dye laser beam onto the photomultiplier. The 1P28 photomultiplier was normally operated at 1020 v. Three Corning colored glass filters, CS 4-76, 4-94, and 4-96, were mounted between the collection lens and the PMT. Fluorescence in the 380-560 nm region, only, reached the phototube. Another filter, CS 2-60, was placed outside the entrance of the

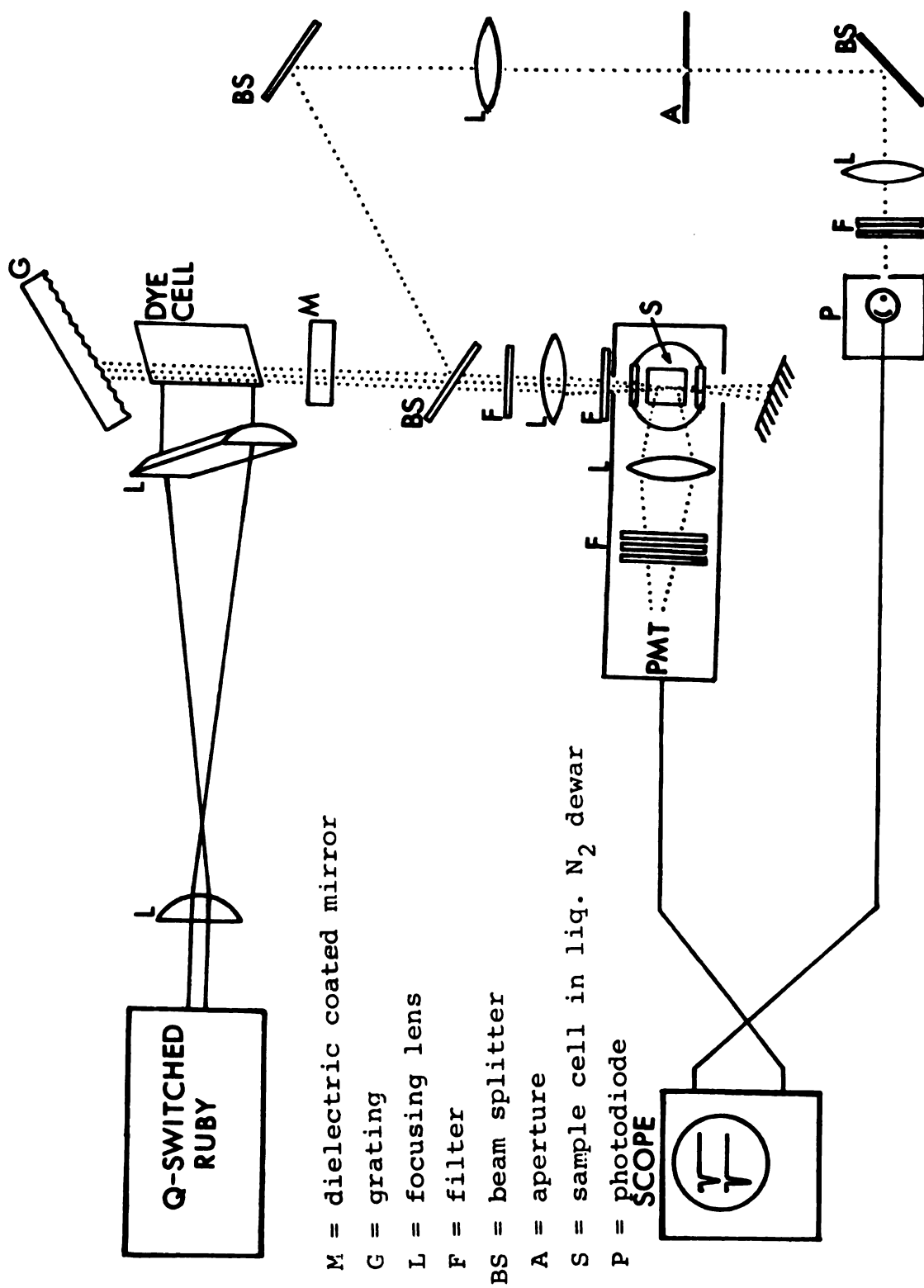


Figure 28. Two-Photon Spectrometer of a Ruby Laser Pumped Dye Laser.

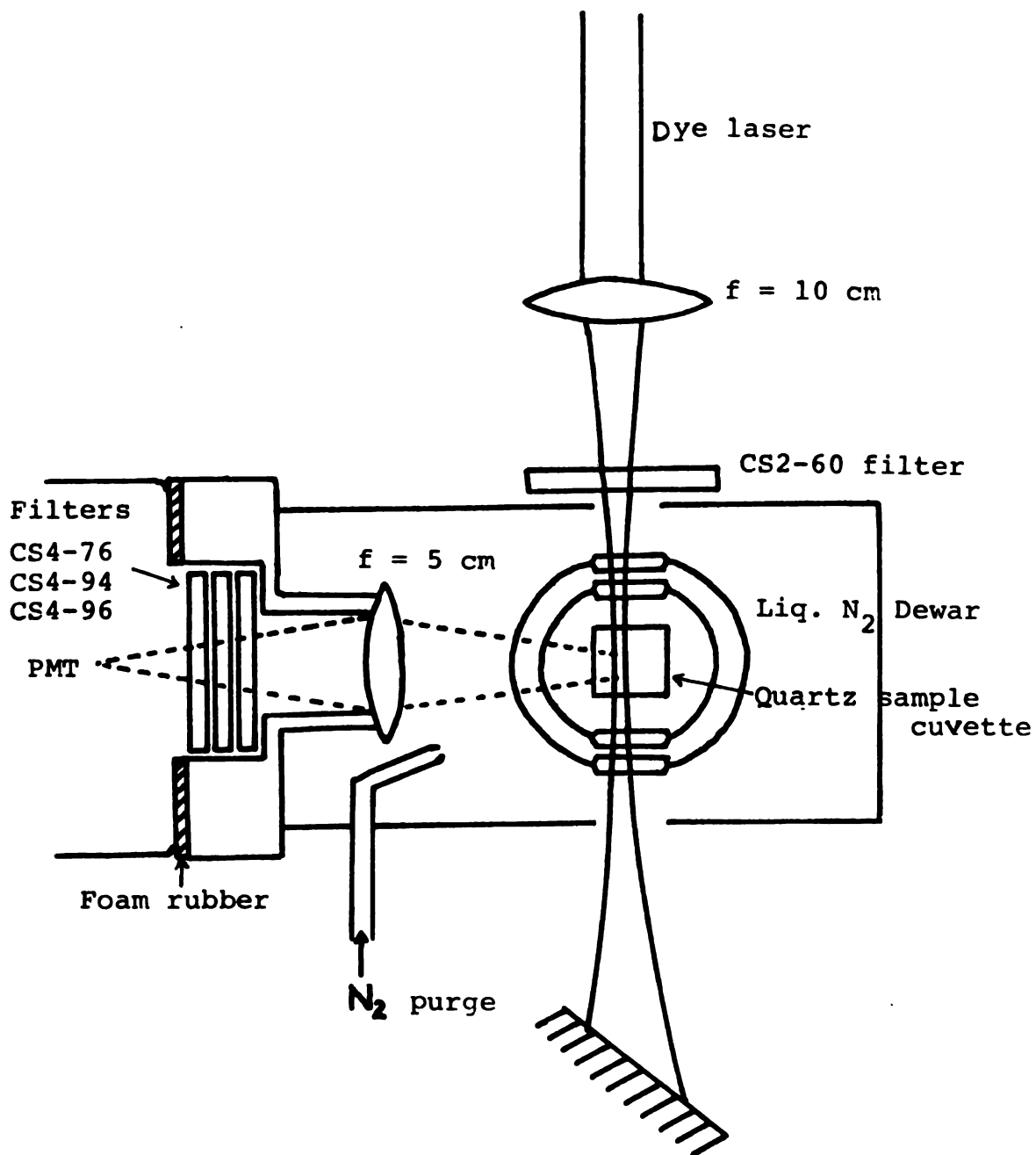


Figure 29. Fluorescence Housing for TPE Measurements.

fluorescence housing to eliminate stray visible and UV light from the ruby and pass only the near infrared dye laser radiation. The dye laser radiation was focused in the middle of a 1 cm^2 quartz sample cell which was immersed in the liquid N_2 Dewar. The fluorescence housing was purged with dry nitrogen gas to reduce moisture condensation on Dewar windows. Helium gas was blown across the top of the Dewar to minimize bubbling.

Dye laser intensity was measured by diverting a small portion of the radiation with several beam splitters through neutral density filters to a photodiode. The neutral density filters were adjusted so that the dye signal displayed on an oscilloscope did not exceed 1 v. The photodiode voltage was normally 40 v. Since the dye laser aperture was larger than the photodiode area, it was necessary to focus the dye laser onto the photodiode in order to measure the total dye intensity, rather than only some portion of the inhomogeneous dye laser beam. At high dye laser powers, a neutral density filter was also placed before the sample cell to avoid saturation of the fluorescence signal.

A typical experimental procedure may be described as follows: First, the ruby laser is operated under normal conditions, in order to optimize both temporal and spatial characteristics by adjusting the concentration of the Q-switched dye solution and the ruby alignment so that

a good pulse is observed on the oscilloscope and a uniform burst spot is formed on the film. Second, the alignment and the concentration of the dye laser is adjusted until a dye pulse is shown on the oscilloscope with suitable temporal characteristics and the desired tuning range. Third, a sample cell containing a pure EPA solution is placed in the liquid N_2 Dewar to check the noise background. Without the sample, a good EPA glass (immersed in liquid N_2 at a very slow speed to prevent cracking or other crystalline imperfection) ordinarily shows a noise signal of only a few mv on the lower beam of a dual beam oscilloscope. (With a sample such as DPO, a several hundred mV signal can be obtained.) This noise might come from either in situ second harmonic generation of the dye laser light in the sample cell, or two-photon induced fluorescence from some impurities in either EPA or the quartz cell.¹⁰⁸ However, at high sample signal levels the noise can be neglected. After the blank background is checked, a fresh sample is placed in the sample cell and the measurement formally started.

As mentioned earlier, the TPE spectrum consists of a plot of the two-photon induced fluorescence intensity as a function of excitation energy. Two-photon excitation requires that the fluorescence intensity be proportional to the square of the dye laser intensity. It is necessary to record the ratio of the measured fluorescence

intensity (fluorescence peak height, I_f) to the square of the measured dye laser intensity (square of the dye peak height, I_D^2). Thus $\ln(I_f/I_D^2)$ is plotted point-by-point vs twice the incident dye photon energy to obtain the TPE spectrum. The square dependence of the fluorescence intensity on the dye laser intensity was checked at several incident wavelengths by plotting $\ln I_f$ vs $\ln I_D$. Straight lines with slopes ~ 2 were obtained, indicating that second order processes were responsible for the fluorescence.

At each dye wavelength selected, several data points were taken. The repetition rate at which the ruby laser was operated was one or two shots per minute. Polaroid high speed 410 film was used to photograph each oscillogram. Typically, 3 or 4 hours were needed to measure a TPE spectrum over one dye tuning region. Usually three or four dyes are required to cover the spectral region of interest for the investigation of a low-lying 1A_g state. Therefore, at least 10 hrs., which does not include data treatment time, is needed to obtain one TPE spectrum for one compound. (Automation of the apparatus^{80,81,108} would relieve much of the tedium involved in these experiments; this would be rather difficult to accomplish for the present instrumentation.) The results described in the succeeding chapters justify the experimental effort expended.

CHAPTER IV

THE TWO-PHOTON EXCITATION SPECTRUM OF ALL-TRANS DIPHENYLOCTATETRAENE

As noted earlier, several recent calculations³⁰ and experiments^{25,26,33-35,76} indicate that the lowest excited singlet state of linear, all-trans polyenes is of A_g symmetry. Thus 1A_g state, which has the same symmetry as the electronic ground state, is hidden in the normal electricdipole absorption spectrum because the transition violates the $u \leftrightarrow g$ selection rule. However, ${}^1A_g \leftrightarrow {}^1A_g$ transitions are allowed in two-photon absorption, and two-photon excitation (TPE) spectroscopy thus may enable direct observation of this hidden excited state.⁵⁹

A. The Reason for Choosing DPO to Study

The TPE method, based on an investigation of the energy dependence of two-photon fluorescence spectra induced by tunable dye lasers, is a powerful and sensitive technique as has been described in chapter II. The primary requirements for organic molecules which are amenable to TPE measurements are: (1) reasonably large two-photon cross sections for transitions from the ground

state to the excited singlet states of interest; (2) a relatively high fluorescence quantum yield from the lowest excited singlet state; (3) no apparent wavelength dependence of the fluorescence quantum yield from excitation in the energy range of interest; (4) higher excited states are photochemically stable and exhibit no decomposition or photochemical reaction. The choice of a particular polyene or a particular set of polyenes for study should be considered first. There are several reasons why diphenyloctatetraene has been chosen for investigation. Consider first the Stokes shift, one of the anomalies in fluorescence spectra of linear polyenes. At least at relatively small values of n , the separation between the absorption origin and the fluorescence origin increases with polyene chain length. In the range $3 \leq n \leq 6$ the gap roughly approaches a linear dependence on chain length as has been plotted by Hudson and Kohler.²⁶ Figure 30 shows the energy gap of the diphenyl polyenes as a function of the number of carbon-carbon double bonds. When the chain length is short ($n < 3$), the fluorescence origin is very close to the strongly allowed absorption ($^1B_u + ^1A_g$) origin. If the fluorescence comes from a low-lying hidden 1A_g excited state, the origin of the transition ($^1A_g + ^1A_g$) would be very close to the $^1B_u + ^1A_g$ origin. According to the two-photon selection rule, the vibronic symmetry of the excited states must

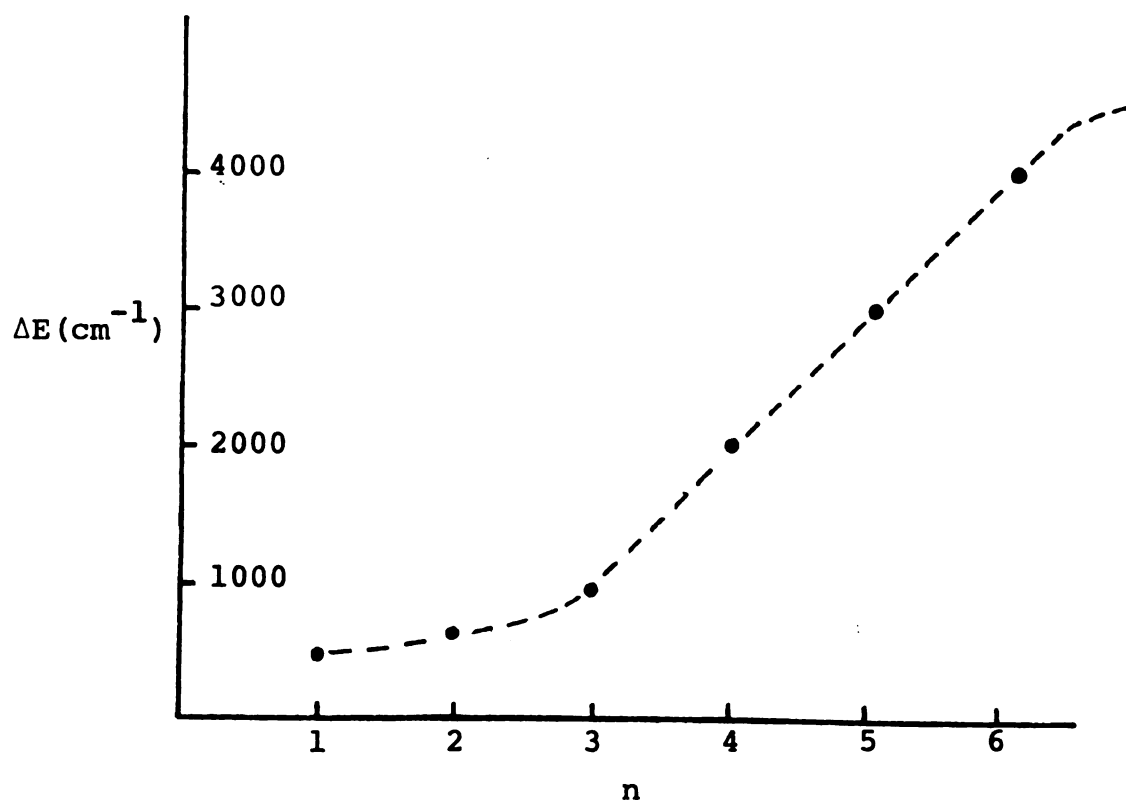


Figure 30. Energy Gap Between the Absorption Origin and the Fluorescence Origin of Diphenyl Polyenes as a Function of the Number of Carbon-Carbon Double Bonds.

be g. Thus the origin of the 1B_u state should be symmetry-forbidden in the TPE spectrum. However, certain low frequency skeletal bending or torsional modes of the polyene chain in the 1B_u state are still two-photon allowed and may become observable in the TPE spectrum if their total vibronic symmetry is g. For short polyenes, then, the 1A_g origin may be combined with or covered by low-frequency vibrational modes of the ${}^1B_u + {}^1A_g$ transition, and the data cannot provide conclusive evidence of the existence of a low-lying 1A_g state. Another reason for not choosing short diphenyl substituted polyenes is that the energy states of the benzene ring substituents will interfere with the energy states of the polyene chain.¹⁰⁹ In stilbene¹⁰⁹ and diphenylbutadiene,¹¹⁰ absorption characteristics of the polyene chain are severely perturbed by excitation involving the terminal phenyl groups. At least three or four double bonds are needed in the polyene chain before mixing between the benzene and polyene states becomes insignificant. As the chain length increases, the polyene absorption band shifts toward the visible, which emancipates it from the bondage of benzene. (The lowest ${}^1B_{2u}$ energy state of benzene¹¹¹ is at 4.9 eV, which is in the near UV.) When the chain length becomes relatively long ($n \geq 6$), the ${}^1B_u + {}^1A_g$ energy gap increases, which causes the low-lying 1A_g state to lie much closer to the ground state than in shorter fluorescent

polyenes. The increasing number of vibrational modes as the molecular size becomes larger, and the decreasing energy gap between the 1A_g excited state and the ground state might well provide a great rate of internal conversion of the excitation energy, thereby decreasing the fluorescence quantum yield. This may be the reason that longer polyenes, such as β -carotene and lycopene, are non-fluorescent molecules¹¹² (fluorescence quantum yield $< 10^{-5}$). Therefore, only medium size diphenyl substituted polyenes are good model candidates for two-photon excitation investigations. As a practical consideration, the solubility of the polyenes decreases as the chain length increases. This will severely influence the TPE measurements for longer polyenes.

As unsubstituted or dimethyl polyenes are concerned, it is well known that short unsubstituted polyenes are nonfluorescent.¹¹³ None of the dimethyl polyenes are commercially available. They have to be synthesized through a Wittig reaction by combining a short polyene aldehyde with a short polyene phenylphosphonium chloride.¹¹⁴ Also, dimethyl polyenes are unstable even below 0°C. The unsubstituted polyenes are also fairly difficult to synthesize and are unstable as well.¹¹⁵ Octatetraene is explosive in pure form.

Compared with these potential model polyenes, diphenyloctatetraene (DPO) is stable at room temperature,

easy to purify, and available commercially. Another reason for choosing DPO is that the original motivation for this work was to understand the electronic states of the visual pigments. DPO is an excellent prototype because it has about the same number of double bonds as the polyene chromophore in the visual pigments. The two-photon cross section of DPO is fairly large. According to the most recent 3WM (three-wave mixing) measurement, δ is about 60 marias.¹¹⁶ The fluorescence quantum yield of DPO, 0.15 in benzene^{28a} and 0.09 in cyclohexane,¹¹⁷ is reasonably high. Also it shows no apparent wavelength dependence. The one photon excitation and absorption spectra of DPO are essentially identical over the range of interest.^{33a} Therefore DPO is an ideal candidate for a TPE study.

B. Results and Discussion

The one-photon absorption and fluorescence spectra of DPO in EPA (either-isopentane-absolute ethanol at 5:5:2) glass at 77°K are shown in Figure 3. The absorption spectrum was recorded on a Cary 14 spectrometer with sample concentration $\sim 2 \times 10^{-6}$ M. The emission spectrum was recorded on a component system fluorimeter (see chapter 3) with sample concentration $\sim 5 \times 10^{-6}$ M, the exciting wavelength was 3500 Å. The absorption transition corresponds to the ${}^1B_u \leftarrow {}^1A_g$ strongly allowed transition.

The absorption origin is at 24420 cm^{-1} , and is followed by 1200 and 1600 cm^{-1} vibrational progressions. These correspond to C-C and C = C stretching modes in the excited electronic state. At least three quanta of the C = C symmetric stretching vibration are present, as are several combination bands. The fluorescence origin is at 22280 cm^{-1} , again followed by lines separated by about 1200 and 1600 cm^{-1} . The intensities of the higher vibrational quantum numbers of the progression are greater in emission than in absorption. Thus, the mirror image symmetry is not precisely followed. The large Stokes shift (2140 cm^{-1}) is a typical characteristic of polyene spectroscopy.

As the concentration of DPO in EPA was gradually increased, a weak and diffuse band was found on the low energy side of the absorption origin (Figure 31). It was possibly due to some vibrational modes of a low-lying 1A_g state. This feature was not found on the high energy side of the fluorescence origin. The energy gap between the absorption and fluorescence origins is strongly solvent dependent. For example, the energy gap at room temperature in methanol is 3200 cm^{-1} and in CS_2 1500 cm^{-1} .²⁶ In all cases it is the absorption origin which shows significant solvent dependence; the fluorescence origins hardly change.

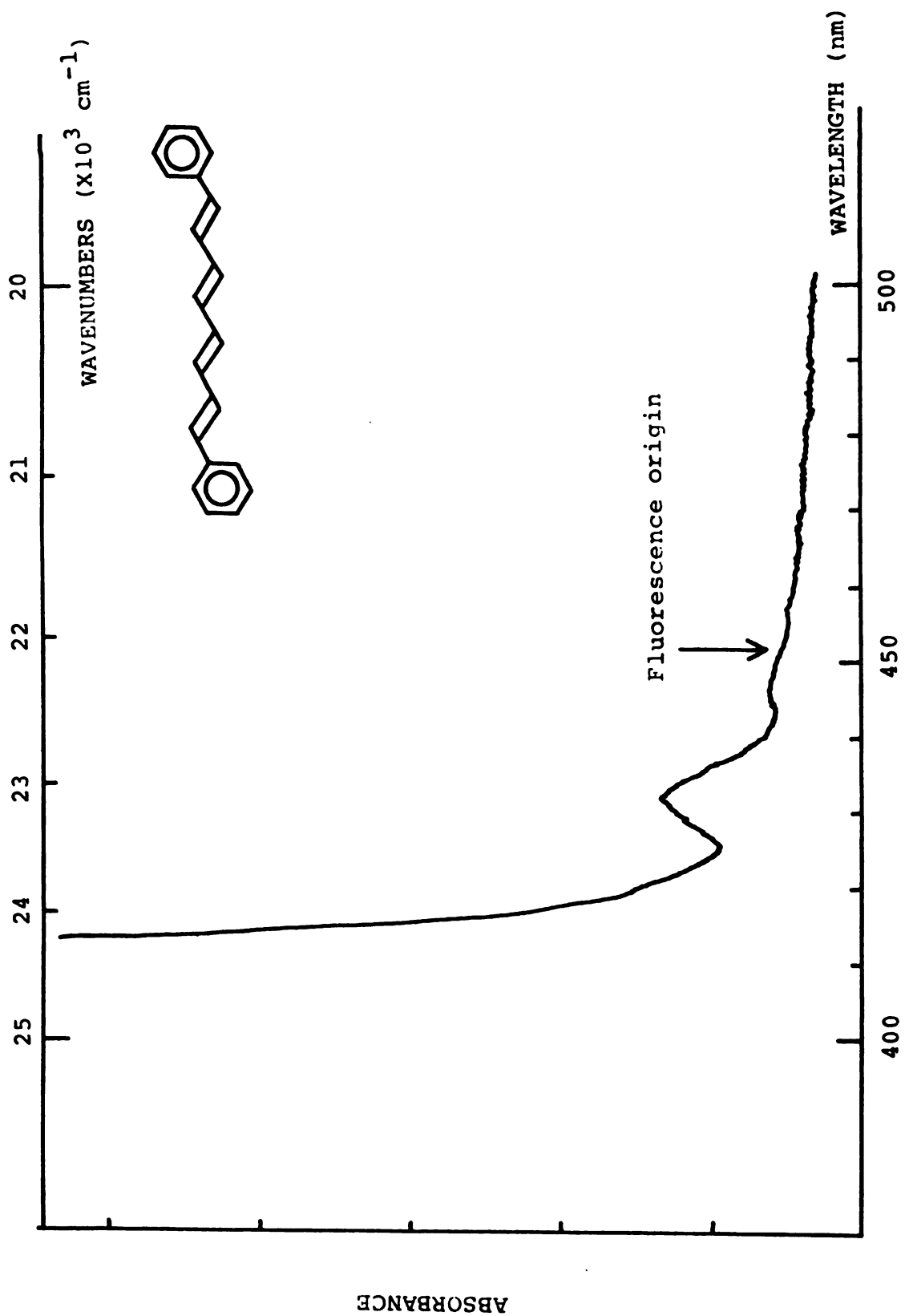


Figure 31. Diffuse Band Appears on the Low Energy Side of the Absorption Origin of DPO at High Concentration ($C = 2 \times 10^{-4} \text{ M}$ in EPA at 77° K).

According to Strickler and Berg's (Birks and Dyson's)²⁸ formula, the intrinsic fluorescence lifetime of an excited state can be calculated from the oscillator strength of the measured absorption spectrum, subject to certain approximations. This formula, which is related to the integrated absorption spectrum by an extension of the derivation of Einstein's A and B coefficients, can be approximately reduced to $\frac{1}{\tau_0} = 1.3 f \bar{\nu}^2$ where f is the oscillator strength and $\bar{\nu}$ is an average frequency for the absorption transition in cm^{-1} . This relationship has been extensively tested, and the accuracy for most organic molecules is within 80%. However the intrinsic fluorescence lifetime of DPO in benzene at room temperature is 49 nsec, which is almost 21 times longer than the 2.3 nsec value calculated from the formula.²⁸ In cyclohexane, the measured intrinsic fluorescence lifetime of DPO is 69 nsec, also 17 times longer than calculated value of 4.1 nsec.¹¹⁷ As described in chapter 1, all these discrepancies support the hypothesis of the existence of a low-lying symmetry forbidden state in DPO.

The two-photon excitation spectrum of DPO ($\sim 2 \times 10^{-4} \text{M}$) in EPA at 77°K has been obtained over the spectral range 10500-12700 cm^{-1} . A sharp origin and distinct vibrational structure are observed in the TPE spectrum, which is shown in Figure 32. These features were not discernible in the polarized TPE spectra of DPO in cyclohexane at

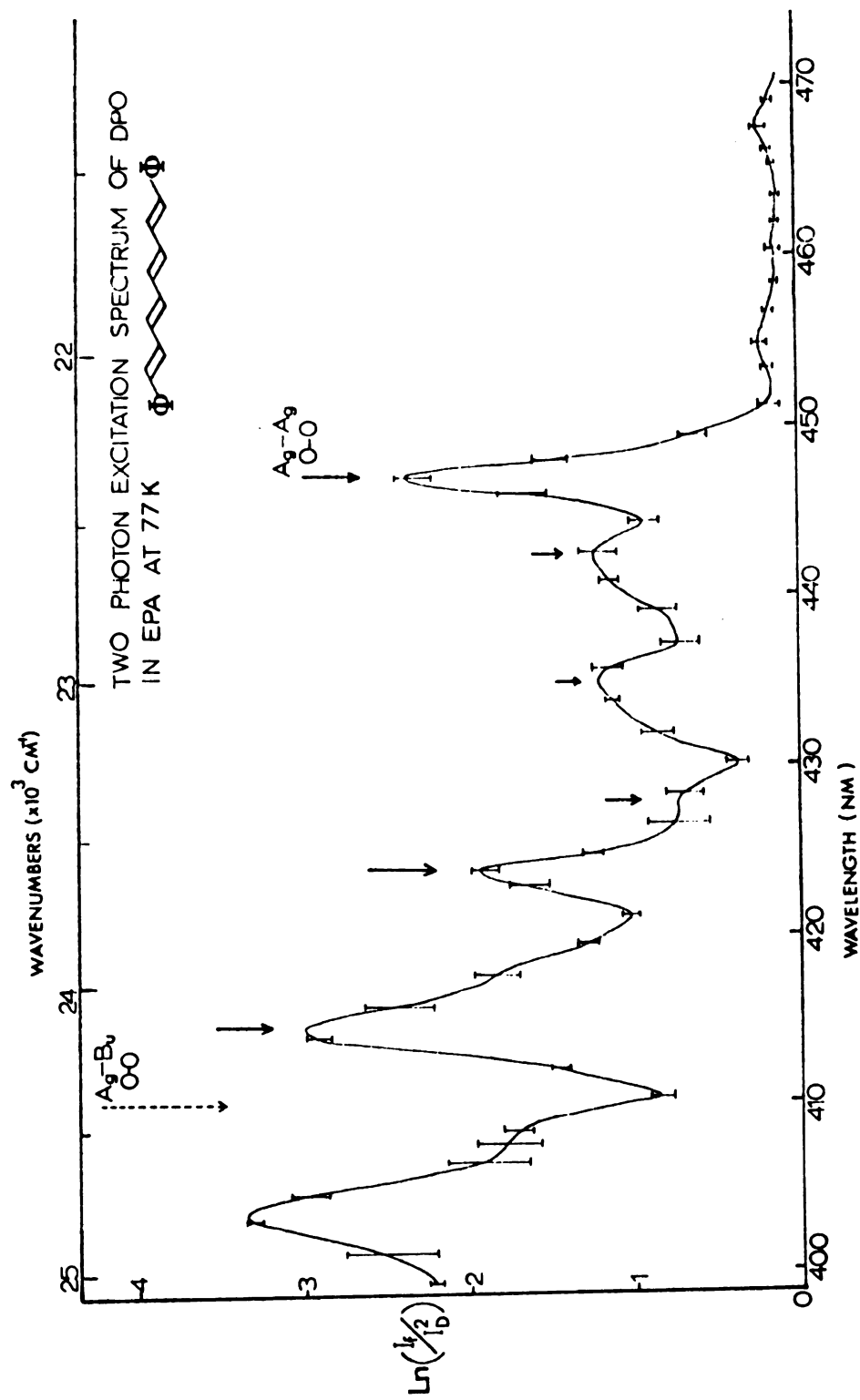


Figure 32. Two-Photon Excitation Spectrum of DPO in EPA at 77°K.

room temperature reported by Holtom and McClain. However, their polarization ratio measurements indicate that the low-lying state in this energy region has A_g symmetry.

Two-photon excitation requires that the fluorescence intensity be proportional to the dye laser intensity. This necessary condition was checked at several incident wavelengths by plotting $\ln I_f$ vs. $\ln I_D$; straight lines with slopes ~ 2 were obtained. An example is shown in Figure 33.

The lowest energy two-photon transition, $2h\nu = 22360 \text{ cm}^{-1}$ is assigned as the origin of a 1A_g excited electronic state of DPO. It lies 2060 cm^{-1} below the origin of the first allowed $^1B_u + ^1A_g$ transition. This origin is about 80 cm^{-1} to the blue of the fluorescence origin, but this difference (about twice the experimental uncertainty) is considered minor. The essential coincidence of the 1A_g origin with the fluorescence origin confirms the suggestion that the fluorescence originates from a lower-energy hidden state.

Two-photon selection rules require that the vibronic symmetry of the excited state be g. Thus the origin of the 1B_u state is symmetry-forbidden in the TPE spectrum; a minimum is observed in that region (dotted arrow in Figure 32). Transitions to symmetric vibrational states of the 1A_g electronic state account for the remaining

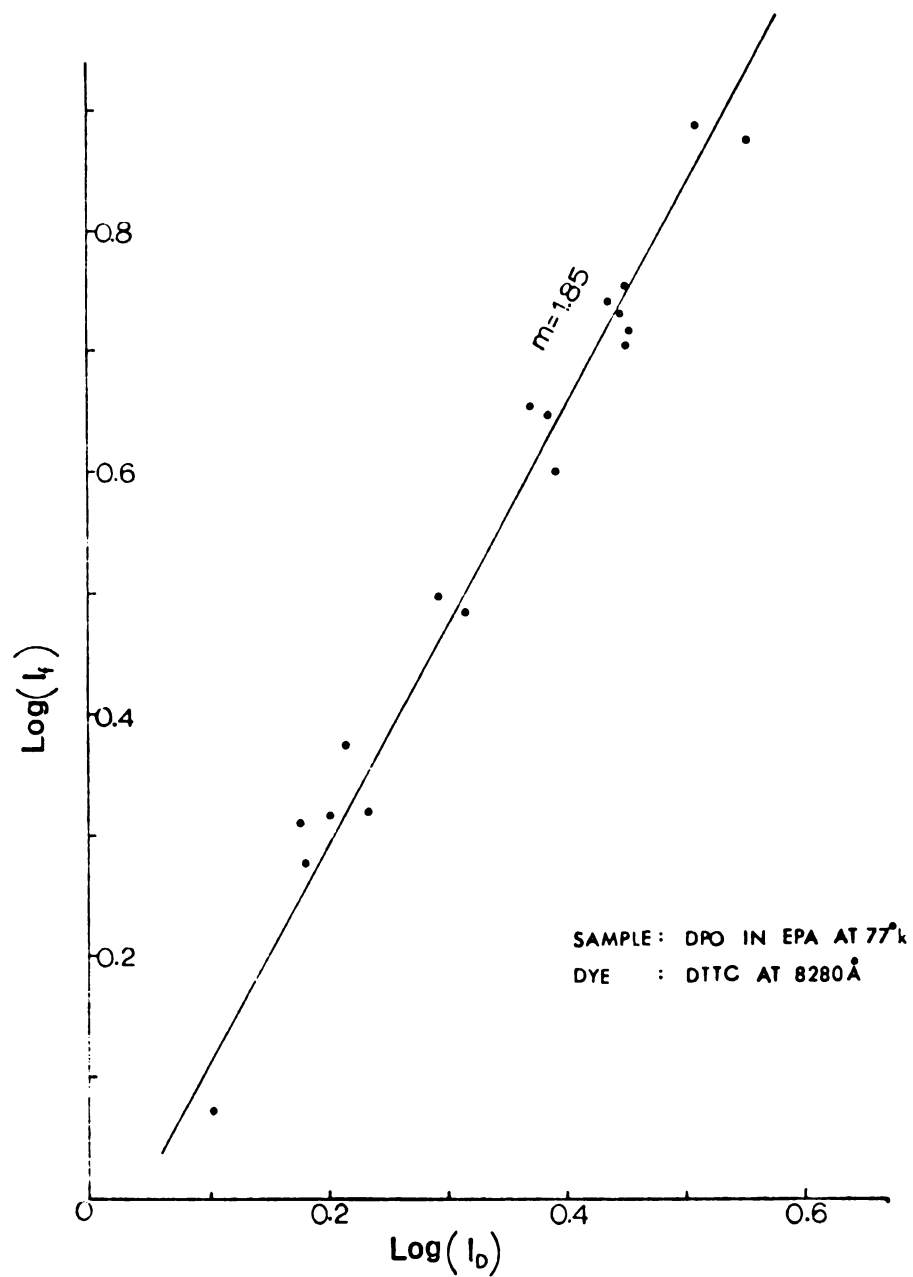


Figure 33. Square Dependence of Two-Photon Induced Fluorescence of DPO.

peaks in the TPE spectrum (solid arrows in Figure 32). Assignments are based on comparisons with low-temperature, high resolution absorption spectra of isolated DPO²⁶ and 2,10-dimethylundecapentaene,³⁴ and approximate correlations with the ground state vibrational frequencies obtained in emission or by Raman spectroscopy.²⁶ The vibrational assignments are listed in Table 1 and discussed below.

(1) The low frequency region (up to 400 cm^{-1} from the origin) consists of a broad band at about $230\text{--}315\text{ cm}^{-1}$. This is possibly due to skeletal bending or to torsional modes of the polyene chain. The fluorescence spectrum of stilbene shows a band at 211 cm^{-1} which has been assigned as the in-plane bending mode of the ethylene bond.¹⁰⁹ Also, 2,10-dimethylundecapentaene in a nonane Shpolskii host shows a 220 cm^{-1} vibration mode in the absorption spectrum.³⁴ The fluorescence spectrum of DPO in a pentadecane Shpolskii host shows several low frequency modes, at 154 cm^{-1} and 257 cm^{-1} .²⁶ Therefore this $230\text{--}315\text{ cm}^{-1}$ broad band in the TPE spectrum of DPO may be the counterpart of those low frequency modes in the DPO ground state.

(2) The next broad feature ($550\text{--}780\text{ cm}^{-1}$) is attributed to vibrational modes of the benzene rings, since no corresponding vibrations are noted for the methyl substituted polyenes.³⁴ Ground state vibrational intervals

of 612 and 726 cm^{-1} have been observed for DPO in the fluorescence spectrum.²⁶ Toluene has a normal mode at 622 cm^{-1} which has been assigned to a ring mode by Dyck and McClure.¹⁰⁹

(3) The relatively weak band at 980 cm^{-1} can be assigned either as a symmetric ring mode, or a C-H bending mode of the polyene moiety,^{118,119} or the combination of these two possibilities. (The a_g symmetric stretching mode of benzene is at 992 cm^{-1} .¹⁰⁹) For all polyenes, including those without benzene substituents, the IR spectra show a 995 cm^{-1} C-H bending mode.¹¹⁹

(4) The remaining features, shifted about 1230 cm^{-1} and 1600-1760 cm^{-1} from the band origin, are due to C-C and C = C symmetric stretching vibrations, respectively.

Their frequencies are higher in the excited 1A_g state than in the ground state (see Table 1). The same effect has been noted for undecapentaene,^{34,35} benzene,¹²⁰ and naphthalene,¹²¹ and explained on the basis of vibronic coupling between the ground and excited states.^{121,122}

The ground state vibrational intervals of DPO in the high resolution, low temperature fluorescence spectrum^{26,34} are also listed in Table 1 for comparison.

Table 1. Comparison of Vibrational Intervals Observed in TPE Spectrum with Those Observed in Fluorescence Spectrum for Diphenyloctatetraene.

Ground State Vibrational Intervals from Fluorescence Spectrum in Bibenzyl Host	Excited 1A_g State Vibrational Intervals from TPE Spectrum in EPA	Assignment
Origin at 22112 cm^{-1}	Origin at 22360 cm^{-1}	
19		
164		
255, 337	230-315	Skeletal Bending or Torsion
612, 726	550-780	Phenyl Ring
995	980	Ring Mode C-H Bending
1144	1230	C-C Stretching
1575	1600-1700	C=C Stretching

C. Conclusion and Implications

The origin of the transition to a low-lying "hidden" excited electronic state in DPO has been found through the two-photon excitation technique. It lies 2060 cm^{-1} below the $^1B_u + ^1A_g$ origin, and is essentially coincident with the one-photon fluorescence origin. Since it is a two-photon allowed transition, the symmetry of this state

is most probably 1A_g . Polarization measurements on the TPE spectrum of DPO at room temperature substantiate the A_g character of this electronic state.⁷⁶ The coincidence with the fluorescence origin supports the notion that the one-photon fluorescence originates from this state.²⁶ It is concluded that a low-lying 1A_g state of DPO has been confirmed by this work. The location of this low energy state removes several discrepancies between the expected and observed fluorescence properties of DPO. The existence of this 1A_g state not only provides a fundamental modification of electronic state ordering over the traditional picture of electronic structure of linear polyenes but also contributes some implications in understanding the photochemistry of polyene molecules.

It was pointed out by Dyck and McClure¹⁰⁹ that isomerization proceeded by two paths - one with an activation energy in the singlet manifold and the other with a singlet-triplet crossing. There is evidence that the photochemistry of polyenes occurs in the singlet manifold rather than the triplet manifold. Since the internal conversion is extremely fast, the lowest excited singlet state must be the one responsible for photochemistry. If the lowest excited singlet state is a symmetry forbidden 1A_g state, the lifetime of this state is long which is favorable for photochemical change. Additionally, a calculation of the bond orders for this

low energy 1A_g state indicates some possibilities for cis-trans isomerization. For example, the bonds in octatetraene in the 1B_u excited state have bond orders²⁶ of 0.79, 0.48, 0.55, 0.59, 0.55, 0.48 and 0.79. The

C1-2	C2-3	C3-4	C4-5	C5-6	C6-7	C7-8
------	------	------	------	------	------	------

bond orders of 1B_u state are almost constant for all bonds except the terminal bonds which are slightly higher.

The bond orders of octatetraene in the low energy 1A_g excited state are 0.64, 0.56, 0.41, 0.63, 0.41, 0.56, 0.64

C1-2	C2-3	C3-4	C4-5	C5-6	C6-7	C7-8
------	------	------	------	------	------	------

which shows a strong central bond (C4-5) and relatively weak bonds (C3-4 and C5-6) on either side of the center. This indicates that cis-trans isomerization will occur preferentially at those two bonds (C3-4 and C5-6) in this low-lying 1A_g state. Obviously, an understanding of the connection between the observed photochemistry and the electronic characteristics of the excited states in linear polyenes depends on an understanding of the reordering of their electronic states.

CHAPTER V

THE RETINYL POLYENES

A. Introduction

It has long been known that vitamin A deficiency is accompanied by visual deterioration.¹²⁴ It has also been found that 11-cis retinal, one of the isomers of vitamin A aldehyde, is the chromophore of visual pigments in vertebrate and many invertebrate retina.¹²⁵ All visual pigments in vertebrate retina are composed of a low molecular weight chromophoric molecule (retinal or its derivatives) and a protein (rod or cone opsin). The combination of retinal and rod opsin is called rhodopsin. The retinal-opsin linkage is a protonated Schiff base to the ϵ -amino group of lysine in the protein.^{126,127} Visual pigments of different species vary only in the nature of their protein, opsins, not in their chromophores. Spectra of visual pigments are usually broad and structureless, and absorption maxima of different rhodopsins range from about 430 nm to 620 nm. This variation is entirely due to differences in the opsins of different species. Retinal has an absorption maximum at about 370 nm in ethanol solution. Upon binding with opsin, the absorption maximum shifts

to the red. Many spectroscopic and theoretical models have been suggested to explain this large bathochromic shift. The initial step in visual excitation is light absorption by 11-cis retinal, the chromophore of the visual pigments. This light absorption by visual pigments initiates a series of events which by a still unknown mechanism leads to the triggering of the photoreceptor cells. Presumably, one of these primary events is a photochemical isomerization of the 11-cis isomer to the all-trans isomer of retinal, as postulated by Wald.¹²⁸ The isomerization leads to the release of a transmitter substance that subsequently decreases the Na^+ current across the photoreceptor cell membrane.¹²⁵

Although the detailed mechanism of vision is still unknown, one experimental fact is that the optical excitation of the visual pigment results in a cis-trans isomerization of the visual chromophore, a linear polyene, and provides a coupling between the electronic structure and molecular motions in this chromophore. An understanding of this vibronic coupling depends on an understanding of the electronic structures of retinyl polyenes. However, the spectroscopic information available on the excited electronic states of the retinyl family is quite limited due to their broad and vibrationally unresolved spectra. This diffuseness unfortunately precludes accurate assignment of the electronic origins. The discovery that

diphenyloctatetraene has a symmetry-forbidden excited singlet state below the 1B_u state responsible for the strongly allowed visible absorption suggests a reexamination of the traditional picture of the electronic energy level ordering of polyene molecules. Retinyl polyenes have a very similar polyene structure to DPO, except for the presence of the β -ionylidene ring in place of one of the terminal phenyl groups, and a carbonyl or hydroxyl group at the other terminus. (See structures shown in Figure 26.) The existence of low-lying 1A_g state in several dimethyl substituted polyenes³⁴⁻³⁷ also indicates that this level order might be general for all polyene molecules. Thus, a search for such hidden electronic states in the retinyl polyenes by the TPE measurement technique is worthwhile not only to reexamine the electronic energy ordering, but also to find a possible way to understand the vision mechanism.

The absorption and emission spectra of retinol and retinal in EPA glass at 77°K are shown in Figures 34 and 35. All show a remarkably diffuse nature, and present substantial difficulty to spectroscopic analysis. Several possibilities have been suggested to explain the broadness. Some authors indicate that the diffuseness in retinal is due to the near degeneracy of the $n\pi^*$ and $\pi\pi^*$ transitions.¹²⁹ Blout and Fields¹³⁰ found that the polyene aldehydes $CH_3 - (CH = CH)_n - CH = O$, for $n = 2, 3,$

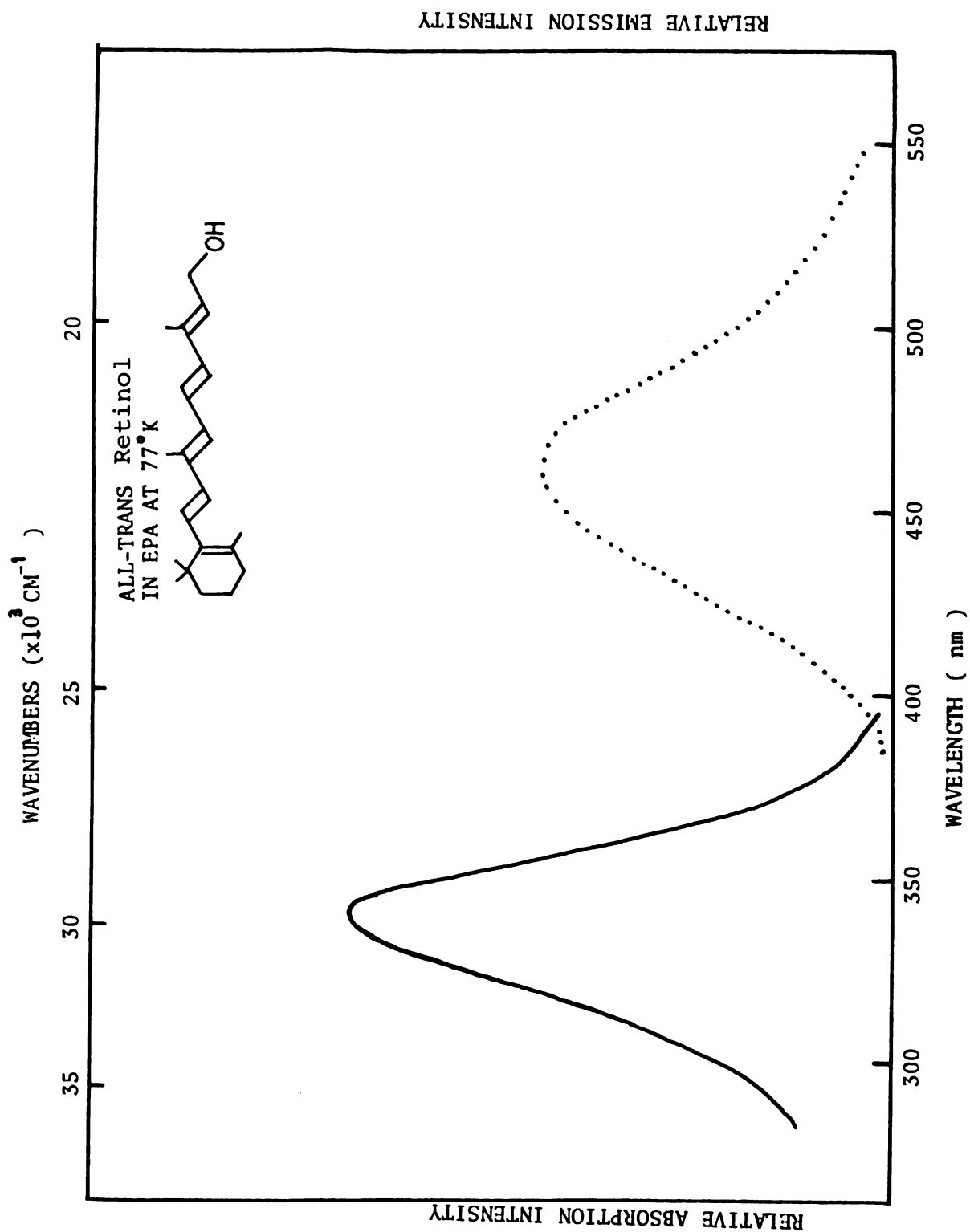


Figure 34. Absorption and Emission Spectra of All-trans Retinol in EPA at 77°K.

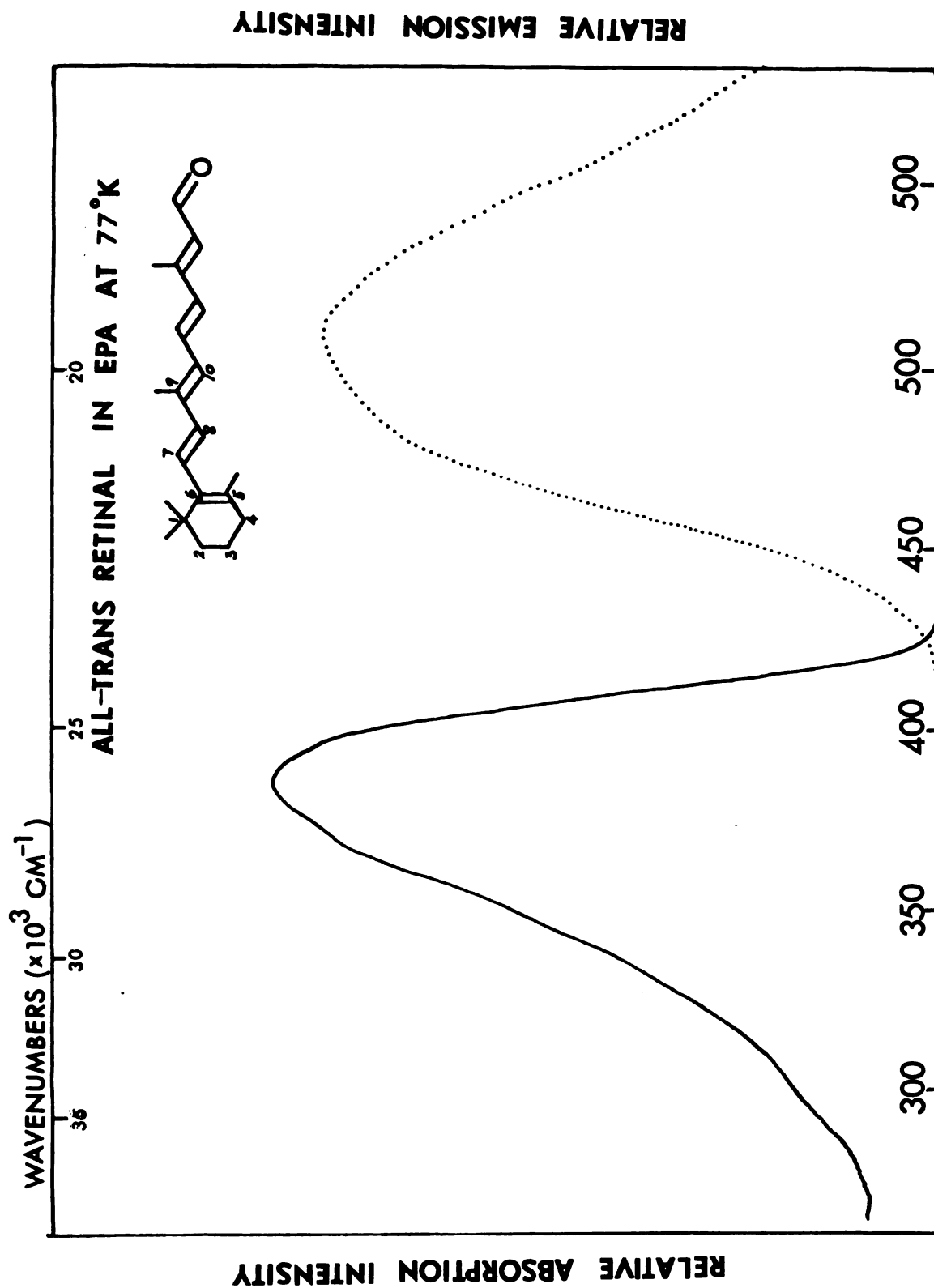
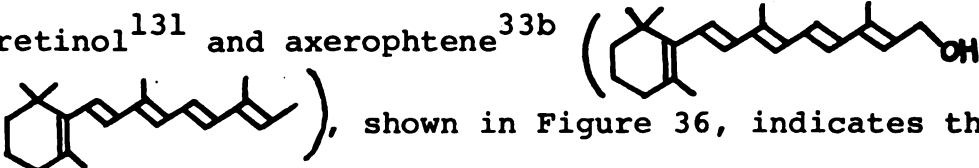
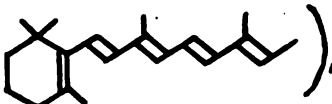


Figure 35. Absorption and Emission Spectra of All-trans Retinal in EPA at 77°K.

showed a weak absorption band on the red shoulder of their strong $\pi\pi^*$ transitions, which was attributed to a transition to an $n\pi^*$ state. They also found that the energy separation between $\pi\pi^*$ and $n\pi^*$ decreased as the chain length (the number of double bonds, n) increased. An extrapolation to $n = 4$ or 5 , as would apply to retinal, showed that the $n\pi^*$ and $\pi\pi^*$ transitions are almost degenerate. This degeneracy is thought to cause interaction between different electronic states and result in vibrational congestion which leads to the diffuse breadth of the absorption spectrum. However, comparison of the retinal spectrum with the absorption spectra of similar retinyl polyenes without a carbonyl group ($>C=O$), such as retinol¹³¹ and axerophytene^{33b} () and , shown in Figure 36, indicates that the degeneracy of $n\pi^*$ and $\pi\pi^*$ states cannot be the only reason for the broadness. The absorption spectra of retinol and axerophytene are still diffuse and broad, despite the absence of an $n\pi^*$ transition in these two compounds. In other words, the existence of an $n\pi^*$ absorption might to some extent be responsible for the breadth, but the removal of this possibility is not sufficient to provide a resolved spectrum. Another source of broadness is conformational disorder caused by non-bonded interactions between the β -ionylidene ring and the methyl substituents on the polyene chain.

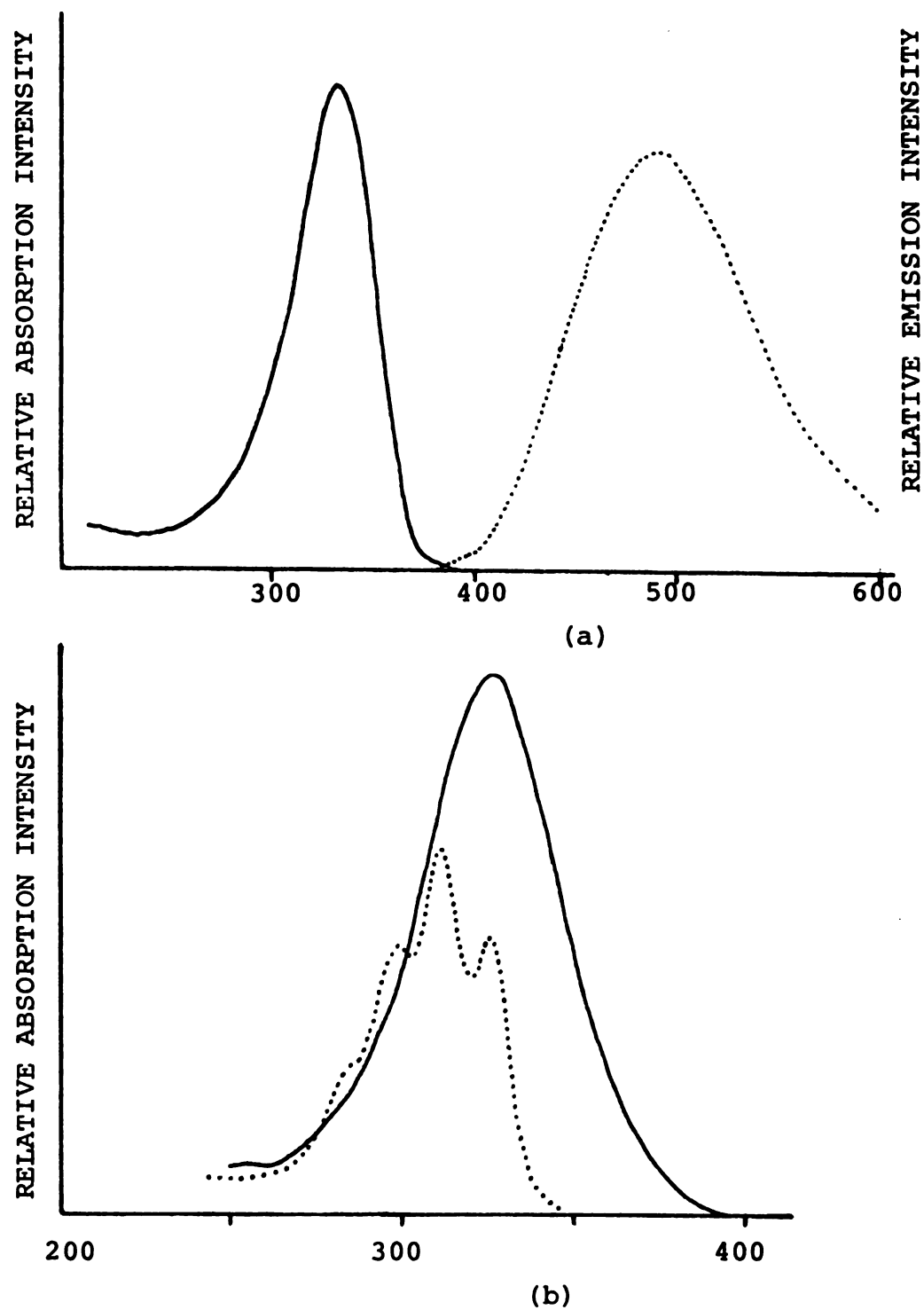
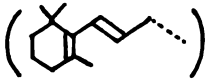
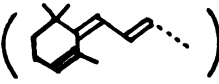
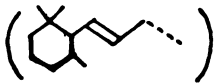


Figure 36. (a) The Absorption and Emission Spectra of Axerophytene in EPA at 77°K (ref. 33). (b) The Absorption Spectra of Retinol (—) and 5.6-dihydroretinol (---) in Ethanol of Room Temperature (ref. 132).

From the absorption spectra of retinol, retinal, axerophthene, 5,6-dihydroretinol and anhydrovitamin A (Figures 34 to 37), one could conclude that diffuseness is correlated with the presence of the β -ionylidene ring. Retinol, retinal and axerophthene contain the β -ionylidene ring. When the ring is transformed from β -ionylidene () to retro β -ionylidene () , such as in anhydrovitamin A,^{33b} or is changed to 5,6-dihydro β -ionylidene () , such as in 5,6-dihydroretinol,¹³² the absorption spectra are well resolved. A theoretical calculation by Honig and Karplus^{124b,133} showed that the ground state energy of retinal is a function of the torsional angle between the ring and the polyene plane (Carbons 6 and 7 shown in Figure 35). The potential as a function of torsional angle θ is shown in Figure 38. From this calculation, which was supported by magnetic resonance measurements of the nuclear overhauser effect, two results can be used to help explain the broadness of the retinyl polyene spectra. One feature is that the β -ionylidene ring does not lie in the same plane as the polyene chain, and the single bond between C-6 and C-7 is free to rotate over a wide torsional angle. Another is that the potential minimum is rather broad and flat, extending over a wide range ($40^\circ < \theta < 120^\circ$). This broad minimum causes the absorption or emission transition to encompass not only one, but several molecular

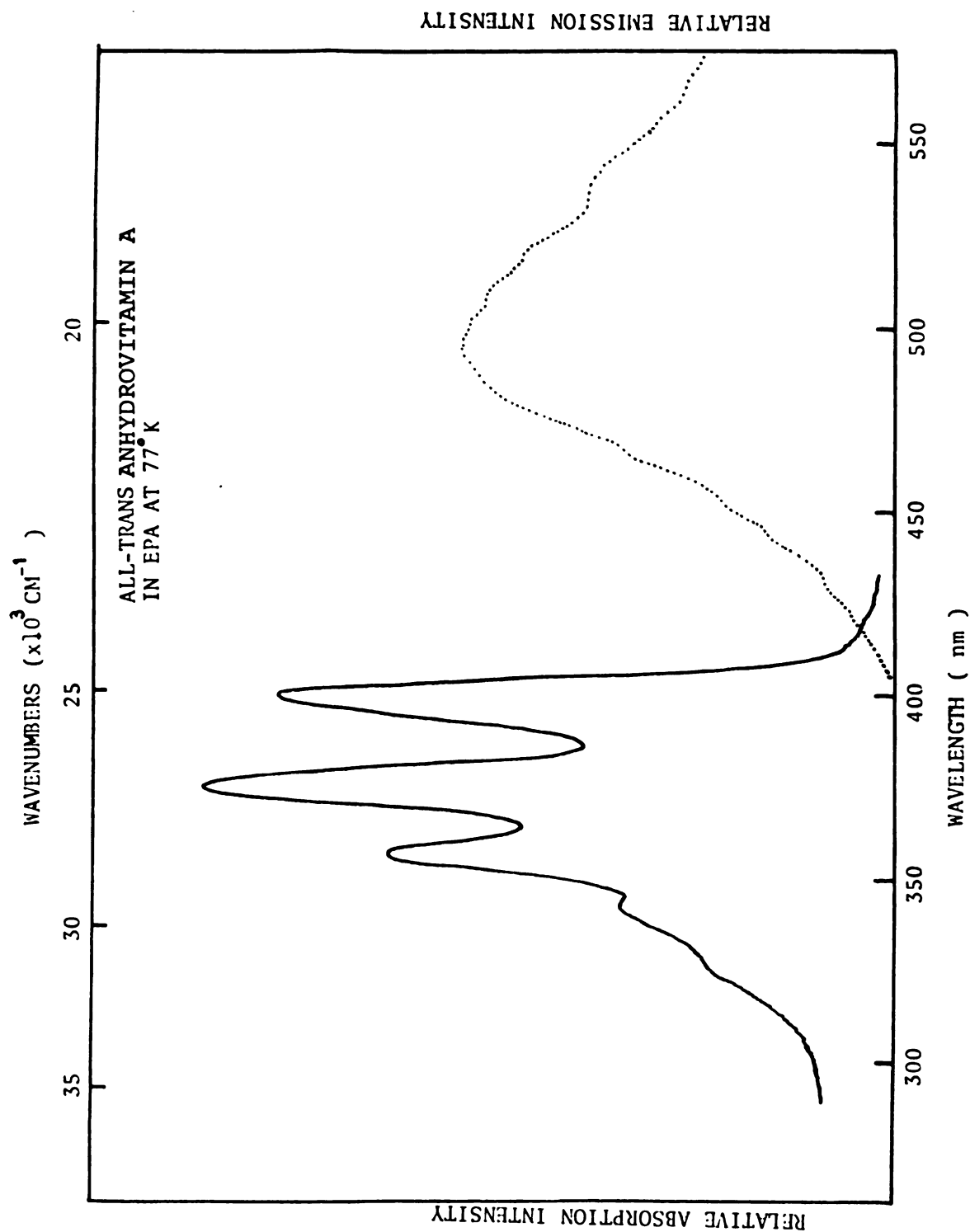


Figure 37. Absorption and Emission Spectra of All-trans Anhydrovitamin A in EPA at 77°K.

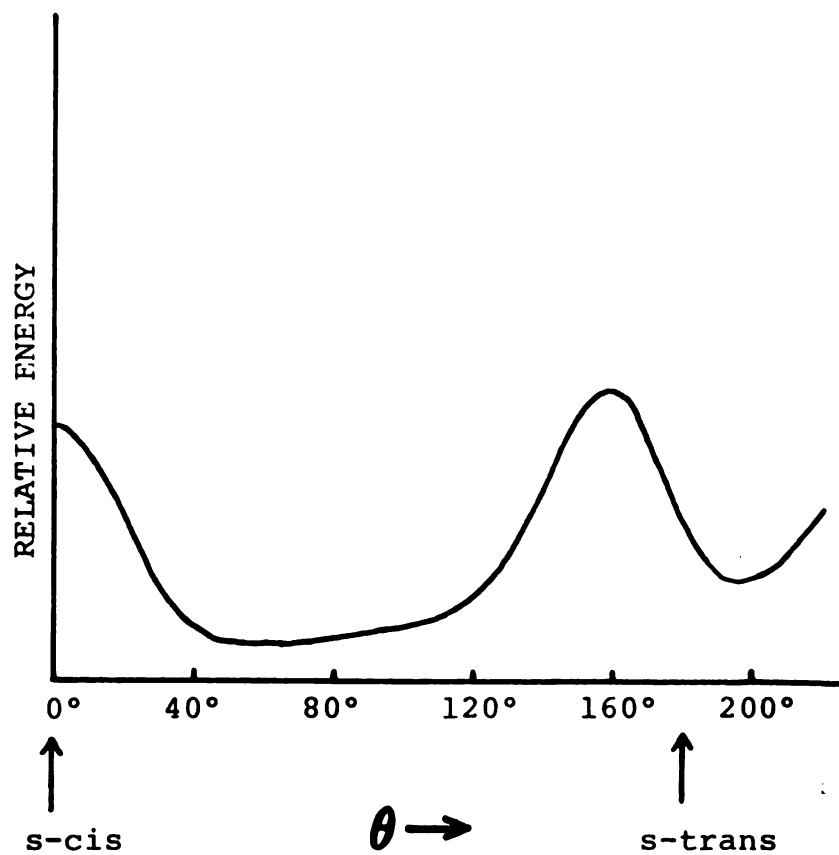


Figure 38. Torsional Potential for the β -ionylidene Ring in Retinal (Ref. 124b).

conformations which are superimposed to account for at least some of the observed broadness. An X-ray crystallographic study of all-trans retinoic acid¹³⁴ has shown that there are two kinds of crystals, one with s-cis for the C-6 and C-7 bond and the other with s-trans. This indicates that rotation around the C6-C7 bond is relatively free. The torsional motion will be more pronounced as the temperature increases.

Since the potential energy surface of the ground state of the retinyl polyenes is broad and has a wide torsional minimum, it would be reasonable to expect their excited states, both 1B_u and low-lying 1A_g states (assuming the chromophore of retinyl polyenes is of C_{2h} symmetry), to have broad potential energy surfaces also. Therefore, the characterization of "hidden" low-lying 1A_g states in these molecules by TPE measurements may well lead to the observation of broad two-photon allowed bands without any resolved vibrational structure. That result would provide only an approximate position of a new 1A_g state, and would still preclude accurate spectroscopic analysis such as the location of the absorption and fluorescence origins.

As discussed earlier, there are several requirements for suitable molecules for TPE measurements: a reasonably high two-photon cross-section, a relatively high fluorescence quantum yield, a fair photochemical stability, and

a wavelength-independent fluorescence quantum yield. The retinyl family, such as retinol and retinal, are fairly stable polyenes with reasonable values of fluorescence quantum yield. Like DPO and unsubstituted polyenes, they also show discrepancies between the expected and observed fluorescence properties. The overlaps between absorption and emission spectra of the retinyl polyenes are very small, even though their broadness precludes the accurate location of their origins. The measured intrinsic fluorescence lifetimes^{117,135} of retinyl polyenes are 80 to 100 times longer than the expected values. This information indicates the likelihood of a low-lying excited 1A_g state in these retinyl polyenes. However, in addition to the problems stemming from the broad spectroscopic transitions, the TPE spectra of the retinyl polyenes will be complicated by the wavelength dependence of the fluorescence quantum yields. Christensen and Kohler^{33a} reported that the fluorescence quantum yield of retinal is approximately ten times higher in its low energy absorption tail than at the absorption maximum, as shown in Figure 39. Becker et al.¹³⁶ have found that the quantum yield of retinal fluorescence decreases by a factor of four in going from an excitation wavelength of 440 nm to 360 nm. For retinol, the wavelength dependence of the fluorescence quantum yield is still uncertain. Thompson¹³⁷ found no indication of wavelength-dependent fluorescence

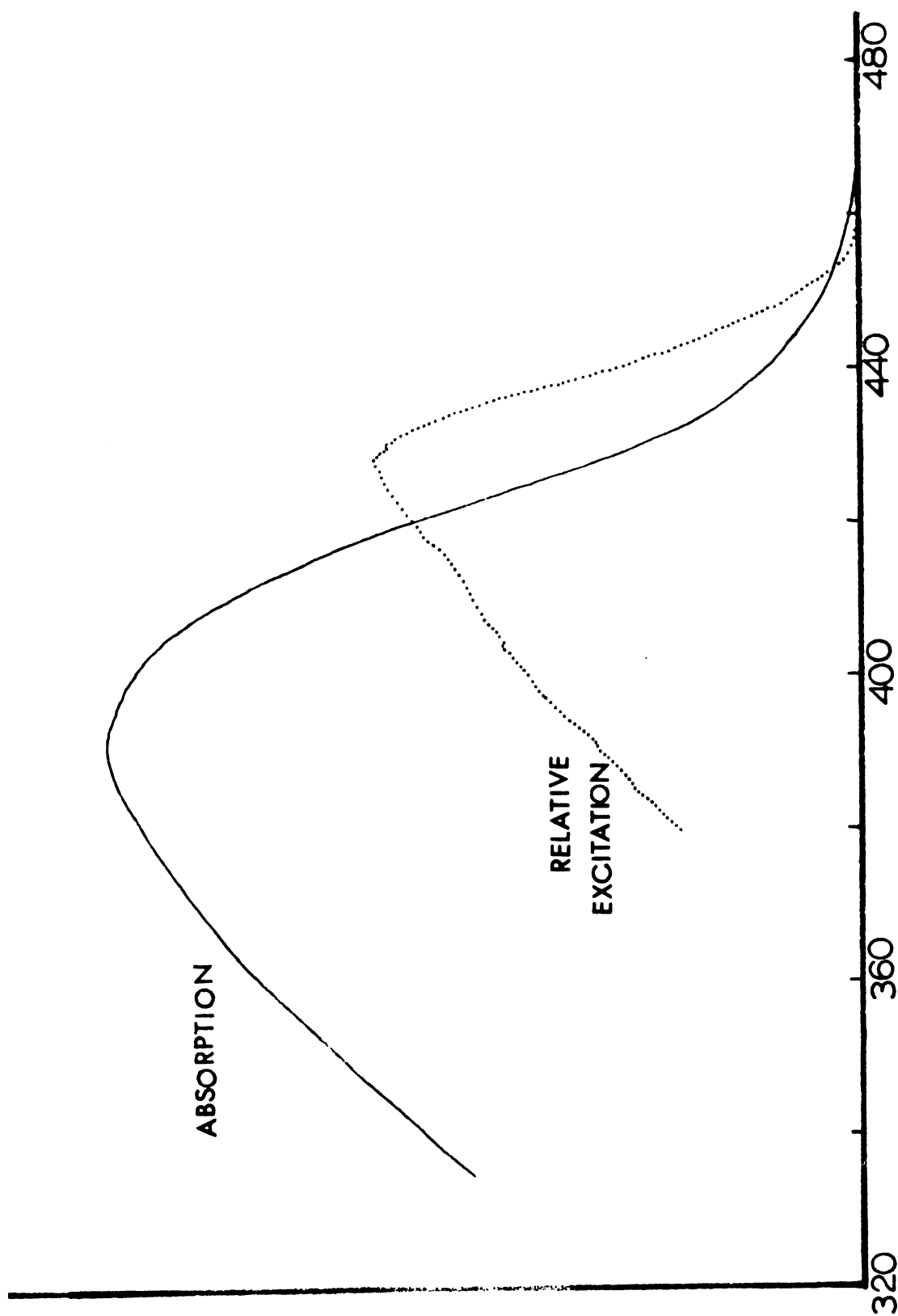


Figure 39. One photon excitation spectrum of all-trans retinal in EPA at 77°K

in retinol, but Mousseron-Canet et al.¹³⁸ claimed a wavelength dependent fluorescence quantum yield. Even if the latter report is correct, the extent of the dependence is much less than that of retinal.

The wavelength dependence of the fluorescence quantum yield of retinal can be explained by the existence of an $n\pi^*$ transition which lies very close to the energy of $\pi\pi^*$ transition. This nearly degenerate $n\pi^*$ transition provides a fast radiationless process which competes with internal conversion at higher vibronic levels of the first excited singlet state responsible for the strongly allowed transition (1B_u).^{33a} An alternative explanation of the wavelength dependence of the fluorescence is that it is the result of competition between photochemistry and internal conversion at high vibronic levels of the first excited state.¹³⁹ However, the nature of this competitive radiationless process, of course, cannot be deduced from either one-photon or TPE experiments.

Thus, the plethora of torsional conformers, the non-bonded interactions between the β -ionylidene ring and the polyene chain, and the vibronic interactions among closely packed excited states all contribute to the diffuse nature of the absorption and emission spectra of the retinyl polyenes. The additional complication of a wavelength dependent fluorescence quantum yield marks retinal as an unlikely candidate for TPE experiments.

This effect is smaller, or absent, for retinol, suggesting greater promise for that molecule.

In order to obtain some insight to the energy level description of retinal, a model compound which is similar in molecular geometry, but which shows vibrationally resolved spectra is needed. The best candidate is the retro-retinyl polyene,¹⁴⁰ anhydrovitamin A,^{33b} which is one of the retro-retinyl polyenes reported to show considerable vibrational structure in its absorption spectrum. The vibrational resolution permits the absorption origin to be accurately located and thus provides a more precise spectroscopic analysis of this model compound, considered to be most similar to retinal because they both have 12π electrons in the polyenic framework and their $\pi\pi^*$ energy schemes are expected to be nearly identical.

B. Results and Discussion

The absorption and emission spectra of an EPA solution of all-trans anhydrovitamin A at 77°K are shown in Figure 37. The absorption band corresponds to the ${}^1B_u \leftarrow {}^1A_g$ transition; well-resolved vibrational levels with origin at 3990 \AA (25063 cm^{-1}), followed by a progression separated by about 1550 cm^{-1} , are observed. At least four quanta of the C = C stretching vibration can be seen in the absorption spectrum. As the

concentration of anhydrovitamin A in EPA was gradually increased, a weak but diffuse band was found on the low energy side of the absorption origin at about 4230 \AA (Figure 40). The emission spectrum of anhydrovitamin A measured by the component system described in chapter III-B is poorly resolved (see Figure 37). The fluorescence started at 4060 \AA and reached a peak at 4900 \AA . The diffuse nature of the emission spectrum of anhydrovitamin A can be explained by postulating that the lowest excited 1A_g state (from which the fluorescence is thought to emit) has a broad potential energy minimum. This wide potential minimum would give rise to many conformational isomers in the 1A_g excited state, and the fluorescence emission from several conformers is superimposed to produce the observed broadness. The wavelength dependence of the fluorescence quantum yield was checked by using the fast scan fluorimeter in the Biochemistry Department. The excitation and absorption spectra are almost identical, and show no evidence for a wavelength dependence of the fluorescence quantum yield. This result is in agreement with Kohler's work.^{33a}

The two-photon excitation spectrum of all-trans anhydrovitamin A ($\sim 10^{-4} \text{ M.}$) in EPA at 77°K has been obtained over the excitation spectral range: $10630\text{--}13150 \text{ cm}^{-1}$. The TPE spectrum and the lowest energy one-photon absorption band ($^1B_u + ^1A_g$) are compared in Figure 41.

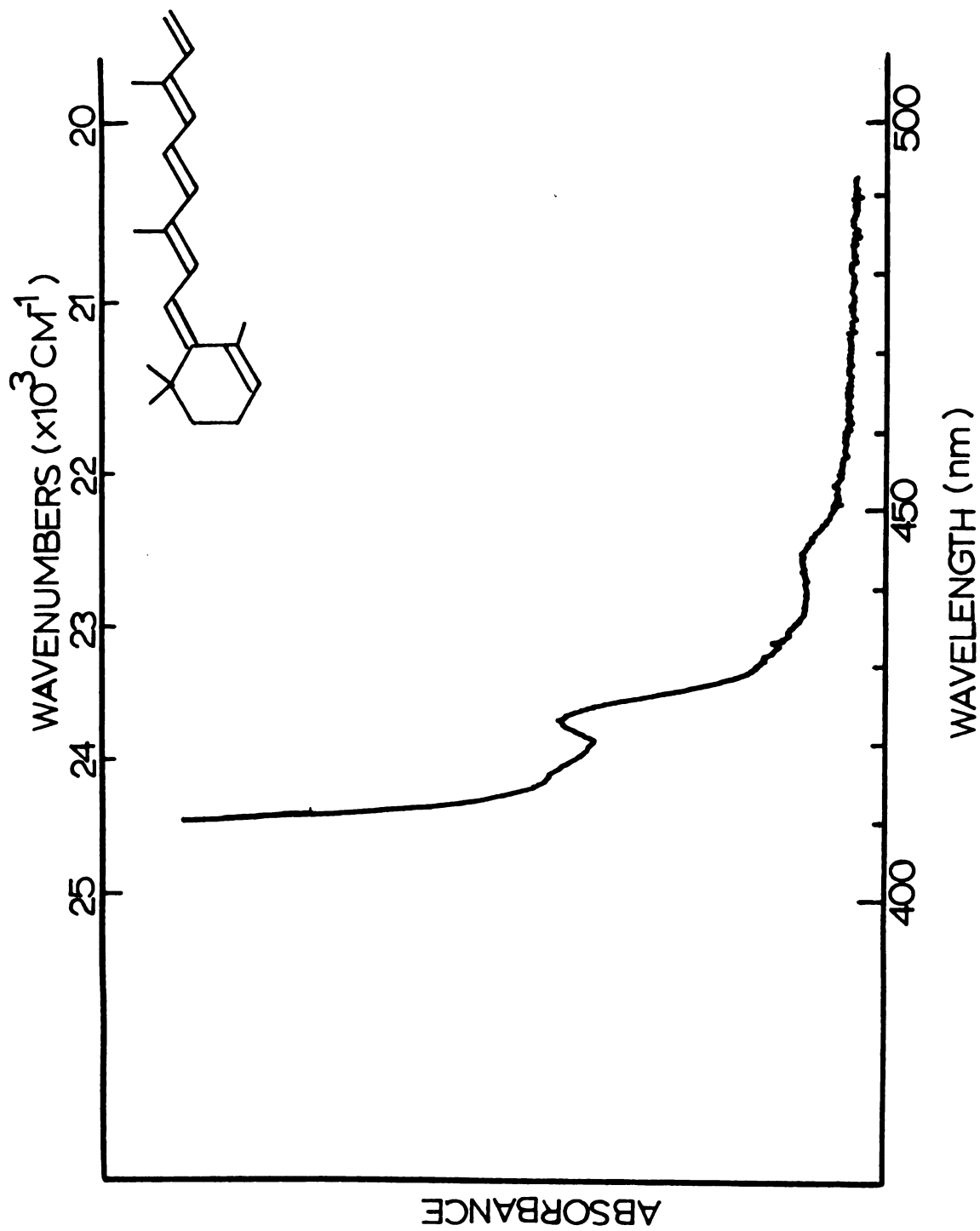


Figure 40. The Absorption Spectrum of All-trans Anhydrovitamin A in EPA at 77°K as Concentration Increases ($\sim 5 \times 10^{-5} \text{ M}$).

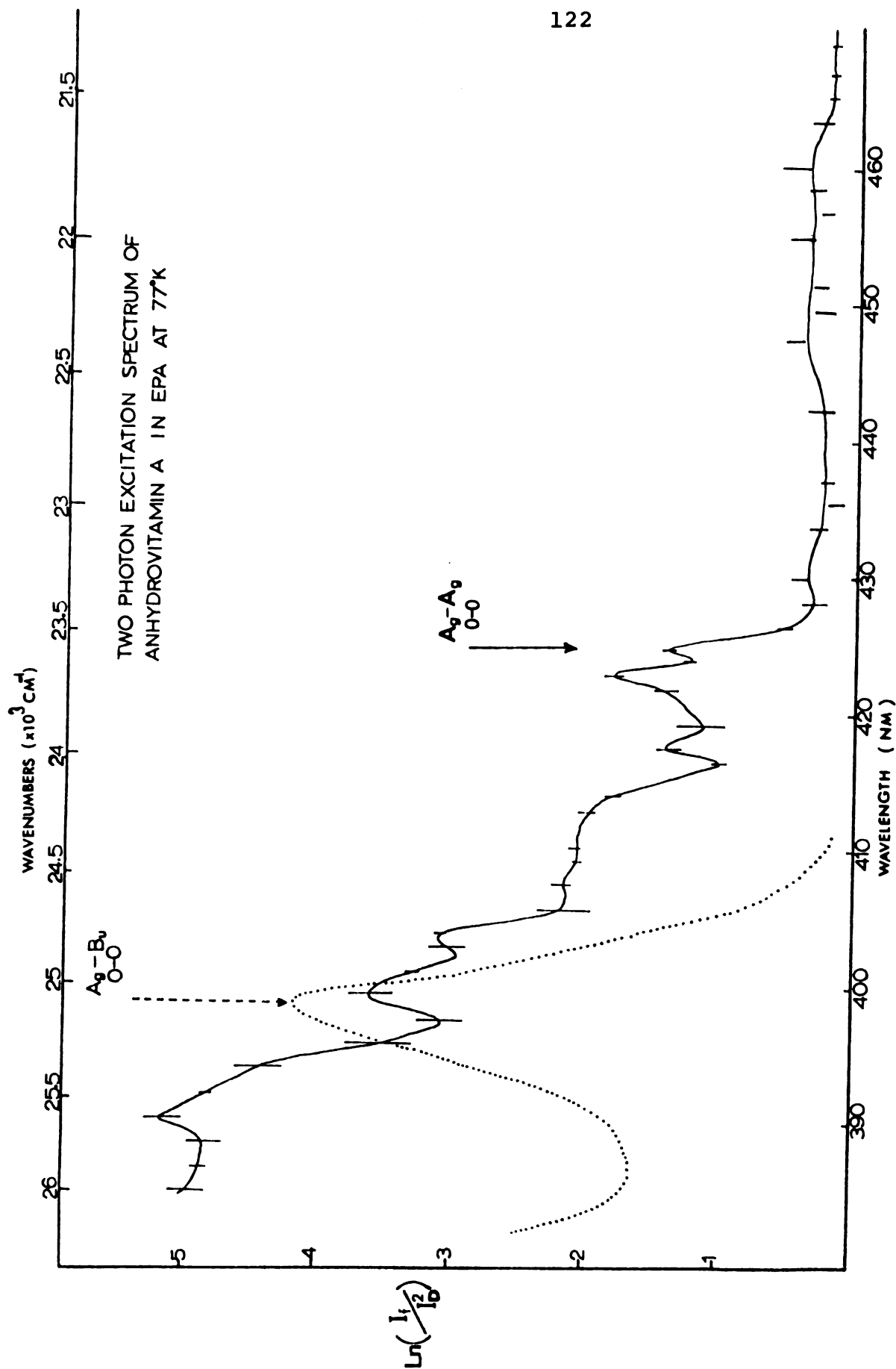


Figure 41. Two-Photon Excitation Spectrum (in unit of $\ln(I_f/I_D^2)$) and the Lowest Energy One-Photon Absorption Band (in unit of relative absorbance) in EPA at 77°K.

The most prominent feature in the TPE spectrum is a strong two-photon allowed band in the region 25120 - 26000 cm^{-1} , which falls in the minimum between the $^1\text{B}_u \leftarrow ^1\text{A}_g$ origin (3970 Å) and the second vibrational quantum in one-photon absorption spectrum. The TPE spectrum also shows a minimum at 3980 Å, which is roughly the one-photon absorption origin. This arises because the origin of the $^1\text{B}_u$ state is symmetry-forbidden in the TPE spectrum. On the red shoulder of $^1\text{B}_u \leftarrow ^1\text{A}_g$ transition, several broad and diffuse two-photon allowed bands are observed, which are interpreted as vibrational structure of a low-lying excited $^1\text{A}_g$ state. The sharp onset at 23500 cm^{-1} , the lowest-energy two-photon transition ($2h\nu = 23500 \text{ cm}^{-1}$), is assigned as the origin of this $^1\text{A}_g$ electronic state. It lies about 1560 cm^{-1} below the origin of the first allowed $^1\text{B}_u \leftarrow ^1\text{A}_g$ transition. No two-photon allowed peak is found at energies below this origin, and only background noise is observed in the region 21300-23300 cm^{-1} .

Up to about 1000 cm^{-1} above the origin, the TPE spectrum is broad and diffuse. This shows that anhydrovitamin A probably has a wide (or multiple) potential minimum in the lowest excited $^1\text{A}_g$ state; this is entirely consistent with the diffuse fluorescence spectrum, mentioned earlier. Although the diffuse nature of the TPE spectrum precludes precise assignments for the

vibrational structure, several features still can be identified by comparisons with low temperature absorption spectra of stilbene, diphenylbutadiene, diphenyl-octatetraene, and 2,10-dimethylundecapentaene, and through approximate correlations with ground-state vibrational frequencies obtained in fluorescence spectra. The broad band about $80\text{--}450\text{ cm}^{-1}$ from the origin probably involves low frequency torsional and skeletal bending modes. The assignment is based partially on analogy to the DPO fluorescence spectrum (in a pentadecane Shpolskii host) which has a strong vibrational mode at 77 cm^{-1} , and several medium intensity modes between $257\text{--}410\text{ cm}^{-1}$.²⁶ Stilbene also shows a strong 211 cm^{-1} normal mode,¹⁰⁹ which has been assigned as the in-plane bending vibration of the ethylene bond, and several low frequency modes between $129\text{--}297\text{ cm}^{-1}$. Diphenylbutadiene shows ground state vibrational intervals at 140 and 360 cm^{-1} .¹⁰⁹ The fluorescence spectrum of 2,10-dimethylundecapentaene also exhibits several modes³⁴ in this region (105 , 256 , 335 , and 435 cm^{-1}) and its absorption spectrum in a nonane Shpolskii matrix shows excited state vibrational modes in the range $220\text{--}400\text{ cm}^{-1}$.³⁴ The next broad feature ($710\text{--}1000\text{ cm}^{-1}$) may possibly be attributed to CH out-of-plane bending vibrations;^{118,119} the IR spectra of all linear polyenes show such a fundamental vibration in the neighborhood of 995 cm^{-1} .¹¹⁹

Beyond this diffuse region, two distinct TPE features, a C-C symmetric stretching vibration ($\sim 1200\text{ cm}^{-1}$ from the origin), and a C = C symmetric stretching vibration ($\sim 1530\text{ cm}^{-1}$ from the origin), are observed.

The fluorescence spectrum of all-trans anhydrovitamin A is broad and fairly structureless which precludes accurate location of the fluorescence origin. Its general shape differs markedly from the usual "mirror image" of the absorption spectrum (see Figure 37), which suggests that the emission originates from a different excited electronic state than the upper state of the absorption transition. The TPE spectrum definitely shows a two-photon allowed band on the red shoulder of $^1B_u \leftarrow ^1A_g$ origin, and this two-photon allowed band has a broad low frequency intensity distribution, similar in breadth to the fluorescence spectrum. Apparently electronic excitation into the strongly absorbing 1B_u state can rapidly decay to two or more of the 1A_g excited state conformational isomers, and the fluorescence emission from several such conformers is superimposed to produce the observed broadness.

The two-photon excitation spectrum of all-trans retinol ($\sim 5 \times 10^{-4}\text{ M.}$) in EPA at 77°K is shown in Figure 42. The main feature is a strong two-photon allowed band in the region $23250\text{--}24390\text{ cm}^{-1}$, with the maximum at 23800 cm^{-1} . This band is broad and structureless. The

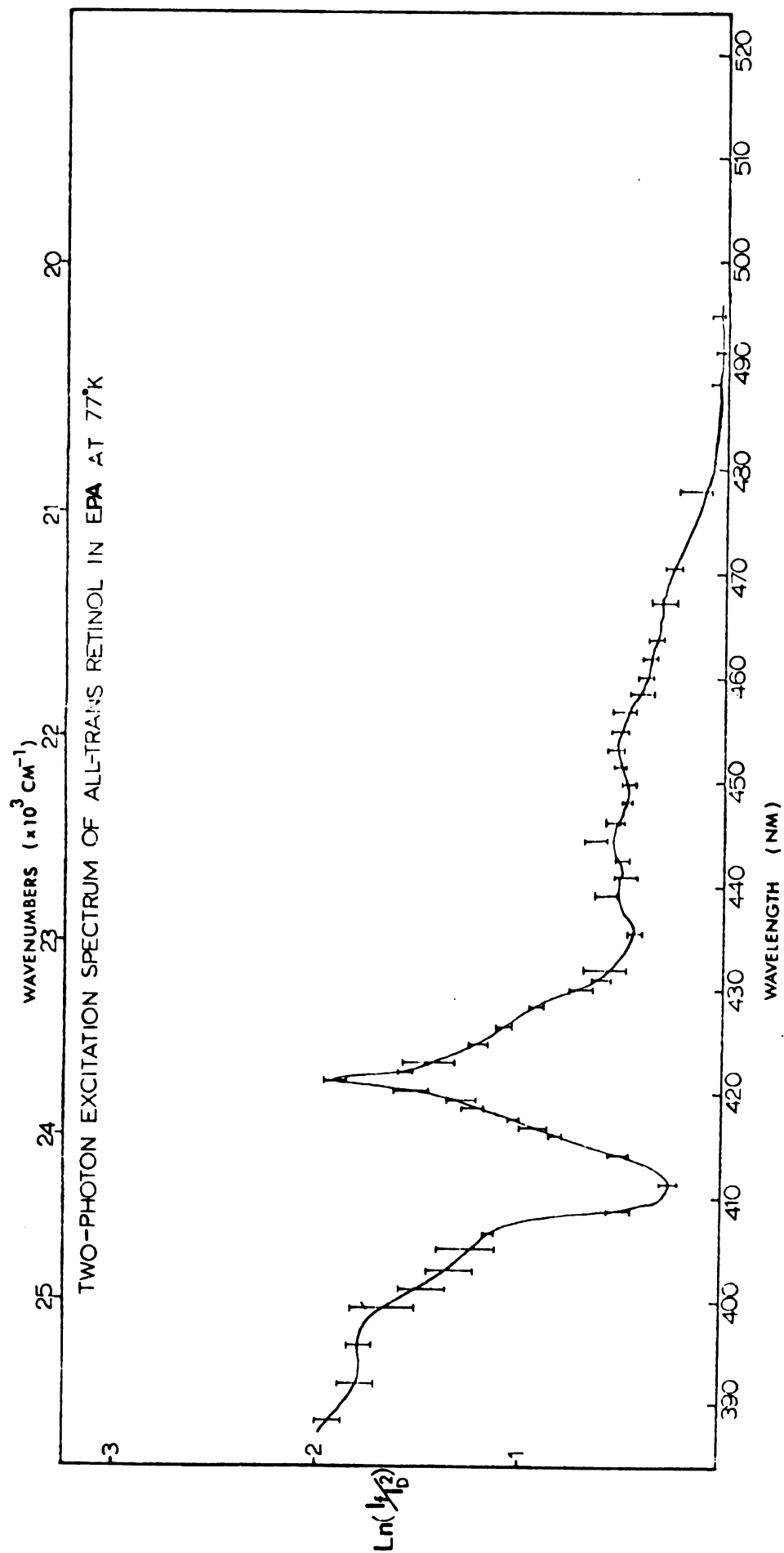


Figure 42. TPE Spectrum of All-trans Retinol in EPA at 77°K.

one-photon absorption and fluorescence spectra of all-trans retinol in EPA at 77°K are both broad (Figure 34). The separation between the maximum of the one-photon absorption band, 340 nm, and the TPE absorption maximum, 420 nm, is almost 5600 cm^{-1} . If the $^1B_u + ^1A_g$ transition origin is assumed to lie at the red edge of the one-photon absorption band, 370 to 380 nm, then the separation between the 1B_u origin and this two-photon allowed band is on the order of $2500\text{--}3200\text{ cm}^{-1}$. Due to its diffuse nature, little more can be said of this TPE spectrum than that it shows the probable existence of a low-lying " 1A_g " state. In the region bluer than 4100 Å , the TPE spectrum shows another diffuse two-photon allowed transition which might be attributed to the vibronically induced $^1B_u + ^1A_g$ transition.

Figures 43 and 44 show the square dependence of two-photon induced fluorescence and the TPE spectrum of all-trans retinal in EPA at 77°K. As mentioned above, retinal is not a good candidate for TPE measurement because of its wavelength-dependent fluorescence quantum yield. Nevertheless, it is interesting to note that the TPE spectrum shows a shift of the intensity maximum (423 nm) from that of the one-photon absorption band (390 nm). This shift is similar to the one-photon excitation spectrum shown in Figure 39.

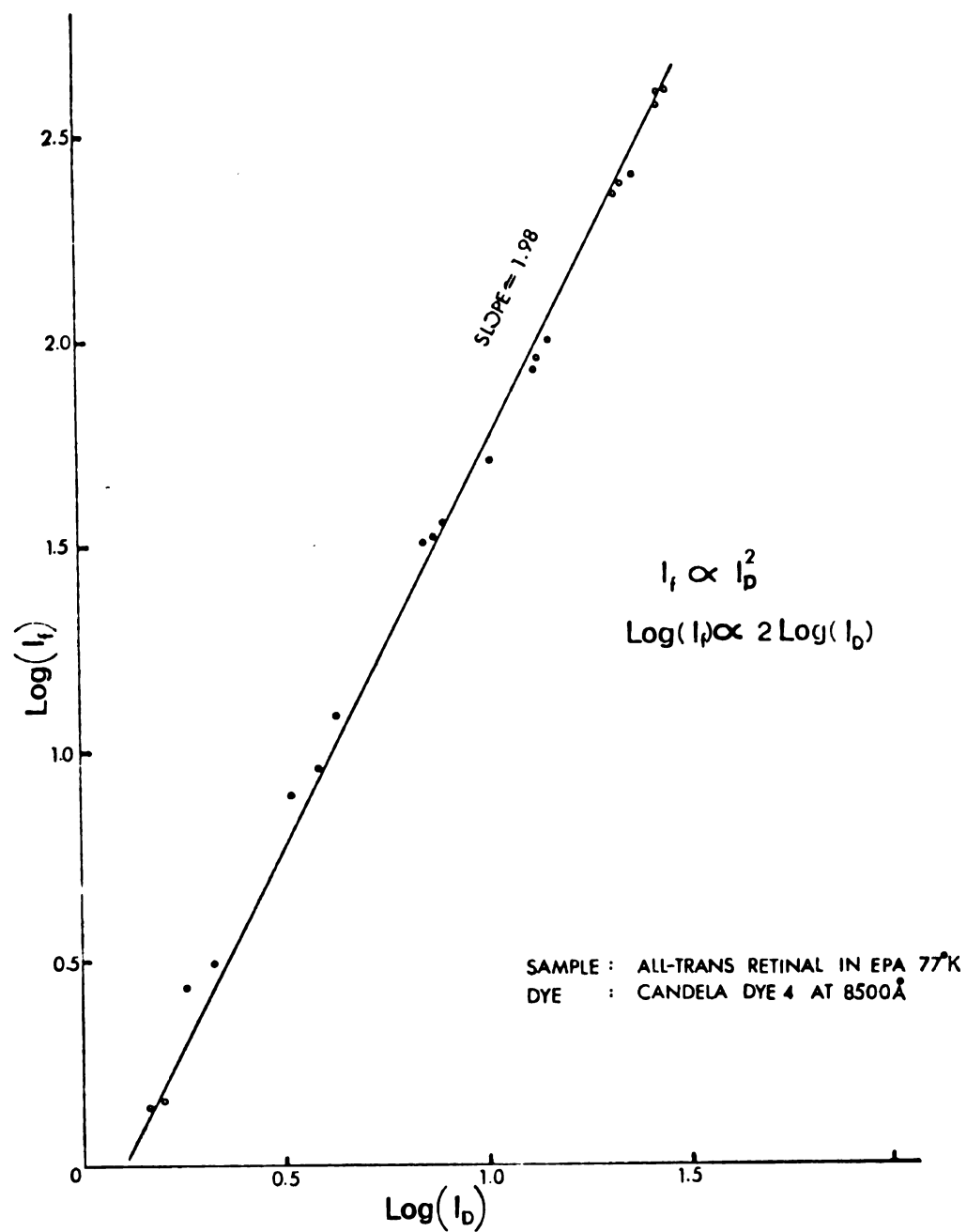


Figure 43. Square Dependence of Two-Photon Induced Fluorescence of All-trans Retinal.

C. Summary and Conclusions

The presence of an excited singlet state in linear polyenes at an energy below that of the lowest 1B_u state indicates that it is possibly a general occurrence. For diphenyl-substituted and dimethyl-substituted polyenes, the existence of low-lying 1A_g states explains the apparently anomalous fluorescence properties such as the large Stokes shift, long fluorescence lifetime and abnormal solvent shift behavior of these molecules. For retinyl polyenes, this low-lying symmetry-forbidden state not only removes these discrepancies in the fluorescence characteristics, but also helps explain other unusual spectroscopic properties such as the broadness of the transitions.

It has been shown that the optical spectra of the retinyl polyenes are remarkably diffuse when compared to those of other polyenes of approximately the same size. The most reasonable explanation is that the potential energy minima of the retinyl polyenes are very broad. Molecules in slightly varying local environments might have minima over a range of several different torsional angles. Electronic transitions from many conformers are superimposed to yield a rather diffuse spectrum. The low-lying 1A_g states are possibly involved in this broadness too. For C_{2h} symmetry polyenes such as DPO, which have a real center of inversion, the low-lying 1A_g states are very forbidden in one-photon spectroscopy;

they can be observed, presumably slightly perturbed, only in low temperature Shpol'skii matrices under high resolution. For retinyl polyenes, the substitution of several methyl groups on the chain and of the β -ionylidene ring on one end reduces the symmetry and makes retinyl polyenes only marginally " C_{2h} like". Therefore the forbidden nature of such a 1A_g state is not as restricted as that of diphenyl substituted polyenes. The out-of-plane distortion associated with rotation around the C6-7 bond between the β -ionylidene ring and the polyene chain provides additional reduction in symmetry. Then this "less forbidden" 1A_g state might couple more strongly with the " 1B_u " state and give rise to vibrational congestion and an extremely complicated pattern of strongly coupled vibronic components, which contribute to the broadness of the optical spectra. According to the recent calculation by Birge, *et al.*,¹⁰⁸ the one-photon oscillator strength for the $^1A_g \leftarrow ^1A_g$ transition of all-trans retinal is remarkably high. This indicates that the 1A_g state might contribute to the one-photon absorption and help account for its breadth.

If the fluorescence of polyene molecules originates from a low-lying excited 1A_g state, the energy gap between the two lowest excited singlet states, $^1B_u - ^1A_g$, must be essentially equal to their corresponding Stokes shift (the energy difference between the absorption and emission

origins). This energy gap is a function of not only the polyene chain length but also of the molecular geometric configuration and molecular environment. The energy separation is solvent dependent. As the solvent polarizability increases, the separation decreases. Changing the temperature is similar to a change of solvent. As temperature decreases, the volume of the solvent contracts which increases the polarization density. For example, changing the solvent from EPA (77°K) to a bibenzyl matrix matrix (4°K), the energy gap between the two lowest excited singlet states, 1B_u - 1A_g of DPO shifts from $\sim 2000 \text{ cm}^{-1}$ to 1300 cm^{-1} .²⁶ Similarly, a molecular structure change might more or less perturb the molecular energy levels. This perturbation may not alter the energy ordering of the lowest excited 1B_u and 1A_g states, but it definitely influences the energy separation between them. Anhydrovitamin A has an effective number of double bonds n between 5 and 6, but its energy gap of $\sim 1560 \text{ cm}^{-1}$ is smaller than that observed in the analogous linear polyene, 2,10-dimethylundecapentaene. Perhaps the small energy gap is due to the substituent effects which reduce the energy separation.

REFERENCES

1. B. Hudson and B. Kohler, *Ann. Rev. Phys. Chem.* 25, 437 (1974).
2. L. Salem, The Molecular Orbital Theory of Conjugated Systems (Benjamin, New York, 1966).
3. J.N. Murrell, The Theory of the Electronic Spectra of Organic Molecules (Chapman and Hall, London, 1963).
4. E. Rabinowitch and Govindjee, Photosynthesis (John Wiley and Sons, Inc., New York, 1969), p. 152.
5. J.H. Burnett, in Chemistry and Biochemistry of Plant Pigments, T.W. Goodwin, ed. (Academic Press, New York, 1976), 2nd ed., Vol. I.
6. B. Wald, *Nature* 134, 65 (1934).
7. E.W. Abrahamson and S.E. Ostroy, *Prog. in Biophys.* 17, 181 (1967).
8. R. Callender and B. Honig, *Ann. Rev. Biophys. Bioeng.* 6, 33 (1977).
9. K.W. Hausser, R. Kuhn, A. Smakula and K.H. Krenchen, *Z. Phys. Chem.* B29, 363 (1935).
10. K.W. Hausser, R. Kuhn, A. Smakula and M. Hoffer, *Z. Phys. Chem.* B29, 371 (1935).
11. K.W. Hausser, R. Kuhn, A. Smakula and A. Deutsch, *Z. Phys. Chem.* B29, 278 (1935).
12. K.W. Hausser, R. Kuhn and A. Smakula, *Z. Phys. Chem.* B29, 384 (1935).
13. K.W. Hausser, R. Kuhn and G. Seitz, *Z. Phys. Chem.* B29, 391 (1935).
14. K.W. Hausser, R. Kuhn and E. Kuhn, *Z. Phys. Chem.* B29, 417 (1935).

15. N.S. Bayliss, J. Chem. Phys. 16, 287 (1948).
16. R.S. Mulliken, J. Chem. Phys. 7, 121 (1939).
17. C. Sandorfy, Electronic Spectra and Quantum Chemistry (Prentice-Hall, Inc., New Jersey, 1964).
18. H. Kuhn, J. Chem. Phys. 17, 1198 (1949).
19. J.A. Pople and D.L. Beveridge, Approximate Molecular Orbital Theory (McGraw-Hill, Inc., New York, 1970).
20. J.W. Sidman, J. Chem. Phys. 27, 429 (1957).
21. R.J. Buenker and J.L. Whitten, J. Chem. Phys. 49, 5381 (1968).
22. R.S. Mulliken, Rev. Mod. Phys. 14, 765 (1942).
23. Reference 17, chapter 8.
24. H.H. Jaffe and M. Orchin, Theory and Application of Ultraviolet Spectroscopy (Wiley, New York, 1962).
25. B.S. Hudson and B.E. Kohler, Chem. Phys. Lett 14, 299 (1972).
26. B.S. Hudson and B.E. Kohler, J. Chem. Phys. 59, 4984 (1973).
27. L.J. Parkhurst and B.G. Anex, J. Chem. Phys. 45, 862 (1966).
28. The intrinsic fluorescence lifetime can be calculated from Birks and Dyson's formula (or Stickler and Berg's formula). (a) J.B. Birks and D.J. Dyson, Proc. R. Soc. Lond. A 275, 135 (1963). (b) S.J. Strickler and K.A. Berg, J. Chem. Phys. 37, 814 (1962).
29. (a) Reference 17, chapters 6 and 7. (b) G. Herzberg, Electronic Spectra of Polyatomic Molecules (Van Nostrand Reinhold, New York, 1966), p. 133.
30. K. Schulten and M. Karplus, Chem. Phys. Lett. 14, 305 (1972).
31. T.H. Dunning, Jr., R.P. Hosteny, I. Hsavitt, J. Am. Chem. Soc. 95, 5067 (1973).
32. B. Honig, A. Warshel and M. Karplus, Accts. Chem. Res. 8, 92 (1975).

33. (a) R.L. Christensen and B.E. Kohler, Photochem. Photobiol. 19, 401 (1974). (b) R.L. Christensen and B.E. Kohler, Photochem. Photobiol. 18, 293 (1973).
34. R.L. Christensen and B.E. Kohler, J. Chem. Phys. 63, 1837 (1975).
35. R.L. Christensen and B.E. Kohler, M. Kasha Symposium on Energy Transfer in Organic, Inorganic and Biological Systems, Florida State University, Tallahassee, Florida, January, 1976.
36. J.R. Andrews and B.S. Hudson, Paper MG-7, 32nd Symposium on Molecular Spectroscopy, Columbus, Ohio, June, 1977.
37. W.M. Hetherington, III and B.S. Hudson, Paper MG-6, 32nd Symposium on Molecular Spectroscopy, Columbus, Ohio, June, 1977.
38. (a) O.A. Mosher, W.M. Flicker and A. Kuppermann, Chem. Phys. Lett. 19, 332 (1973). (b) F.W.E. Knoop, L.J. Oosterhoff, Chem. Phys. Lett. 22, 247 (1973).
39. C. Djerassi, E. Bunnenberg and D.L. Elder, Pure Appl. Chem. 25, 57 (1971).
40. H.L.B. Fang, R.J. Thrash and G.E. Leroi, J. Chem. Phys. (1977), to be published.
41. H.L.B. Fang and G.E. Leroi, Paper MG-9, 32nd Symposium on Molecular Spectroscopy, Columbus, Ohio, June, 1977.
42. R.J. Thrash, H.L.B. Fang and G.E. Leroi, J. Chem. Phys. submitted.
43. R.J. Thrash, Ph.D. Thesis, Michigan State University (1977).
44. N. Bloembergen, Nonlinear Optics (Benjamin, New York, 1965).
45. A. Yariv, Quantum Electronic (Wiley, New York, 1967).
46. M. Goeppert-Mayer, Ann. Phys. 9, 273 (1931).
47. (a) P.R. Monson and W.M. McClain, J. Chem. Phys. 53, 29 (1970). (b) K.B. Eisenthal, M.W. Dowley and W.L. Peticolas, Phys. Rev. Lett. 20, 93 (1968).
48. W.M. McClain, J. Chem. Phys. 55, 2789 (1971).

49. (a) W.M. McClain, J. Chem. Phys. 57, 2264 (1972)
(b) W.M. McClain, *ibid*, 58, 324 (1972). (c) R.P. Drucker and W.M. McClain, Chem. Phys. Lett. 28, 255 (1974) (d) R.P. Drucker and W.M. McClain, J. Chem. Phys. 61, 2616 (1974).
50. W.M. McClain, Acc. Chem. Res. 7, 129 (1974).
51. W. Kaiser and C.G.B. Garrett, Phys. Rev. Lett. 7, 229 (1961).
52. D. Fröhlich and M. Mahr, Phys. Rev. Lett. 16, 895 (1966).
53. A. Gold, Proc. Int. School Phys. Enrico Fermi, Course 42: Quantum Optics, R.J. Glauber, ed. (Academic Press, New York, 1969).
54. W.L. Peticolas, Ann. Rev. Phys. Chem. 18, 233 (1967).
55. (a) A. Bergman and J. Jortner, Chem. Phys. Lett. 15, 309 (1972). (b) A Bergman and J. Jortner, Chem. Phys. Lett., 26, 323 (1974).
56. H. Mahr, Quantum Electronics, H. Rabin and C.L. Tang, ed. (Academic Press, New York, 1975), Vol. 1, p. 285.
57. M.D. Levenson and N. Bloembergen, Phys. Rev. B10, 4447 (1974).
58. (a) R.T. Lynch, Jr. and H. Lotem, J. Chem. Phys. 66, 1905 (1976). (b) H. Lotem, R.T. Lynch and N. Bloembergen, Phys. Rev. A14, 1748 (1976).
59. (a) R.L. Swofford and W.M. McClain, J. Chem. Phys. 59, 5740 (1973). (b) R.L. Swofford and W.M. McClain, Rev. Sci. Instr. 46, 246 (1975).
60. R.L. Swofford and W.M. McClain, Chem. Phys. Lett. 34, 455 (1975).
61. R.G. Kepler, Phys. Rev. B9, 4468 (1974).
62. R.C. Miller and W.A. Nordland, Jr., J. Appl. Phys. 46, 2177 (1975).
63. J.R. Whinnery, Acc. Chem. Res. 7, 225 (1974).
64. (a) P.M. Rentzepis and Y.H. Pao, J. Chem. Phys. 44, 2931 (1966). (b) C.E. Bell and J.A. Landt, Appl. Phys. Lett. 10, 46 (1967). (c) E.F. Carome, E.M. Carreira and C.J. Prochaska, App. Phys. Lett. 11, 64 (1967). (d) P.A. Barnes and K.E. Rieckhoff, Appl. Phys. Lett. 13, 282 (1968).

65. N. Mikami and M. Ito, Chem. Phys. Lett. 31, 472 (1975).
66. J. Krasinski and W. Majewski, Opt. Commun. 14, 187 (1975).
67. P.M. Johnson, M.R. Berman and D. Zakheim, J. Chem. Phys. 62, 2500 (1975).
68. R.V. Ambartsumyan and V.S. Letokhov, Appl. Opt. 11, 354 (1972).
69. W.C. Lineberger and T.A. Patterson, Chem. Phys. Lett. 13, 40 (1972).
70. W.C. Lineberger and B.W. Woodward, Phys. Rev. Lett. 25, 424 (1970).
71. (a) H. Zipin and S. Speiser, Chem. Phys. Lett. 31, 102 (1975). (b) N.Y.C. Chu and K. Weiss, Chem. Phys. Lett. 27, 567 (1974).
72. J.P. Hermann and J. Duening, Phys. Rev. A 5, 2557 (1972).
73. L. Hudley, T. Coburn, E. Garwin and L. Stryer, Rev. Sci. Instr. 38, 488 (1967).
74. S. Brody, Rev. Sci. Instr. 28, 1021 (1957).
75. Handbook of Mathematical Functions, ed. M. Abramowitz and I.A. Stegun, Dover, New York, 1970.
76. G.R. Holtom and W.M. McClain, Chem. Phys. Lett. 44, 436 (1976).
77. M. Dowley, K. Eisenthal and W. Peticolas, J. Chem. Phys. 47, 1609 (1967).
78. A. Aleksandrov and V. Genkin, Opt. Spectry. 30, 37 (1971).
79. G. Koren, C. Cohen and W. Low, Solid State Commun. 16, 257 (1975).
80. R.M. Hochstrasser, H.-N. Sung and J.E. Wessel, J. Chem. Phys. 58, 4694 (1973); J. Am. Chem. Soc. 95, 8179 (1973); J. Chem. Phys. 60, 317 (1974); Chem. Phys. Lett. 24, 168 (1974).
81. R.M. Hochstrasser and J.E. Wessel, Chem. Phys. Lett. 24, 1 (1974).

82. P.D. Maker, and R.W. Terhune, Phys. Rev. 137, A801 (1965).
83. C. Flytzanis and N. Bloembergen, Prog. Quantum Electr. 4, 271 (1976).
84. R.J.N. Anderson, G.R. Holton and W.M. McClain, J. Chem. Phys. 66, 3832 (1977).
85. I. Webman and J. Jortner, J. Chem. Phys. 50, 2706 (1969).
86. D. Fröhlich, Festkörperprobleme (Vieweg Verlag, Braunschweig, 1970), Vol. X, p. 227.
87. J.M. Worlock, Laser Handbook, ed. Arecchi and Schulz-Dubois (North Holland, Netherlands, 1972), Vol. II, p. 1323.
88. P. Kush and V.W. Hughes, Encyclopedia of Physics (Springer-Verlag, Berlin and New York, 1959), Vol. XXXVII/1, Sect. 30.
89. D.L. Rousseau, Ph.D. thesis, Princeton University (1966).
90. B.A. Lengyel, Introduction to Laser Physics (Wiley, New York, 1966).
91. (a) P. Kafalas, J.I. Masters, and E.M.E. Murray, J. Appl. Phys. 35, 2349 (1964). (b) D. Hull, Appl. Opts. 5, 1342 (1966). (c) R.M. Brown and R.J. Stone, Appl. Opts. 8, 2356 (1969).
92. M.E. Mack, IEEE Quantum Electronics, QE-4, 1015 (1968).
93. G. Mouron, IEEE Quantum Electronics, QE-11, 1. (1975).
94. F.P. Schafer, Dye Lasers, F.P. Schafer, ed. (Springer-Verlag, Berlin and New York, 1973), Chap. 1 and 2.
95. P.P. Sorokin, J.R. Lankard, V.L. Moruzzi and E.C. Hammond, J. Chem. Phys. 48, 4726 (1968).
96. H.W. Furumoto and H.L. Ceccon, Appl. Optics 8, 1613 (1969).
97. P.P. Sorokin and J.R. Lankard, IBM J. Res. Develop. 11, 148 (1967).

98. R. Pappalardo, H. Samelson and A. Lempicki, IEEE J. Quantum Electronics QE-6, 716 (1970).
99. J.B. Marling, D.W. Gregg and L. Wood, Appl. Phys. Lett. 17, 527 (1970).
100. F.C. Strome, Jr. and S.A. Tuccio, Opt. Commun. 4, 58 (1971).
101. (a) A.E. Siegman, An Introduction fo Lasers and Masers (McGraw-Hill, New York, 1971). (b) A. Maitland and M.H. Dunn, Laser Physics (North-Holland Co., Amsterdam, 1969).
102. B.B. McFarland, Appl. Phys. Lett. 10, 208 (1967).
103. (a) Y. Muyazoe and M. Maeda, Appl. Phys. Lett. 12, 206 (1968). (b) C.F. Dewey and L.O. Hocker, Appl. Phys. Lett. 18, 58 (1971). (c) F.C. Strome, Eastman Organic Chemical Bulletin 46, No. 2 (1974). (d) J.P. Webb, F.G. Webster and B.E. Plourde, Eastman Organic Chemical Bulletin 46, No. 3 (1974). (e) P. Oettinger and C.F. Dewey, Jr., IEEE J. Quantum Electronics QE-12, 95 (1976). (f) C.P. Decker and F.K. Tittel, Opt. Comm. 7, 155 (1973).
104. (a) C.P. Wang, Rev. Sci. Instr. 47, 92 (1976). (b) J. Itani, K. Kagawa and Y. Kimura, Appl. Phys. Lett. 27, 503 (1975). (c) J.H. Crouch and W.S. Risk, Rev. Sci. Instr. 43, 632 (1972).
105. (a) E.T. Gerry, Appl. Phys. Lett. 7, 6 (1965). (b) D.A. Leonard, Appl. Phys. Lett. 7, 4 (1965).
106. T.W. Hänsch, Appl. Opt. 11, 895 (1972).
107. E.M. Shantz, J.D. Cawley and N.D. Embree, J. Am. Chem. Soc. 65, 901 (1943).
108. R.R. Birge, J.A. Bennett, B.M. Pierce and T.M. Thomas, to be published.
109. R.H. Dyck and D.S. McClure, J. Chem. Phys. 36, 2326 (1972).
110. G.V. Gobov, Opt. Spectrosc. 15, 194 (1963).
111. D.S. McClure, Solid State Phys. 8, 1 (1959).
112. C. Tric and V. Lejeune, Photochem. Photobiol. 12, 339 (1970).

113. R.M. Gavin, Jr., S. Risemberg, and S.A. Rice, J. Chem. Phys. 58, 3160 (1973).
114. T.S. Sorenson, J. Am. Chem. Soc. 87, 5075 (1965).
115. A.D. Mebane, J. Am. Chem. 74, 5227 (1952).
116. G.R. Holtom, R.J.M. Anderson and W.M. McClain, Paper WE-9, 32nd Symposium on Molecular Spectroscopy, Columbus, Ohio, June 1977.
117. I.B. Berlman, Handbook of Fluorescence Spectra of Aromatic Molecules, 2nd Ed. (Academic Press, New York, 1971), p. 322.
118. L.J. Bellamy, The Infrared Spectra of Complex Molecules (wiley, New York, 1954).
119. E.R. Lippincott and T.E. Kenney, J. Am. Chem. Soc. 84, 3641 (1962).
120. D.M. Friedrich and W.M. McClain, Chem. Phys. Lett. 32, 541 (1975).
121. N. Mikami and M. Ito, J. Chem. Phys. 64, 3077 (1976); Chem. Phys., to be published.
122. R.M. Hochstrasser and C.A. Marzzacco in Molecular Luminescence, E.C. Lim, ed. (W.A. Benjamin, New York, 1969).
123. R.M. Hochstrasser, Acc. Chem. Res. 1, 266 (1968).
124. Special Issue on the Chemistry of Vision, ed. E.L. Menger, Acc. Chem. Res. 8, 81-113 (1975): (a) D.S. Kliger and E.L. Menger, p. 81; (b) B. Honig, A. Warshel and M. Karplus, p. 92; (c) E.W. Abrahamson, p. 101.
125. R. Callender and B. Honig, Ann. Rev. Biohpys. Bioeng. 6, 33 (1977).
126. G.A.J. Pitt, F.D. Collins, R.A. Morton, and P. Stok, Biochem. J. 59, 122 (1955); R.A. Morton and G.A.J. Pitt, *ibid.*, p. 128 and references cited therein.
127. (a) M. Akhtar, P.T. Blosse, and P.B. Dewhurst, Life Sci., 4, 1221 (1965). (b) D. Bownds and G. Wald, Nature 205, 254 (1965).
128. G. Wald, Science 162, 230 (1968).

129. P. Naylor and M.C. Whiting, J. Chem. Soc. 1955, 3037 (1955).
130. E.R. Blout and M. Fields, J. Am. Chem. Soc. 70, 189 (1948).
131. T.A. Moore, Ph.D. Thesis, Texas Tech. University (1975).
132. P.E. Blatz, P.B. Dewhurst, V. Balasubramaniyan, P. Balasubramaniyan and M. Lin, Photochem. Photobiol. 11, 1 (1969).
133. B. Honig, B. Hudson, B.D. Sykes, and M. Karplus, Proc. Natl. Acad. Sci. U.S.A., 68, 1289 (1971).
134. C.H. Stam and C.H. MacGillavry, Acta Cryst. 16, 62 (1963).
135. J.P. Dalle and B. Rosenberg, Photochem. Photobiol. 12, 151 (1970).
136. R.S. Becker, K. Inuzuka, J. King and D.E. Balke, J. Am. Chem. Soc. 92, 43 (1971).
137. A.J. Thompson, J. Chem. Phys. 51, 4106 (1969).
138. D.A. Lerner, J.-C. Mani and M. Mousseron-Canet, Bull. Soc. Chim. France, 1968 (1970).
139. W.H. Waddell, A.M. Schaffer, and R.S. Becker, J. Am. Chem. Soc. 95, 8223 (1973).
140. W. Oroshnik, G. Karmas, and A.D. Mebane, J. Am. Chem. Soc. 74, 295 and 3807 (1952).



1. The first part of the document is a list of names, each followed by a date in parentheses. The names are: John A. Smith (1845), John B. Smith (1846), John C. Smith (1847), John D. Smith (1848), John E. Smith (1849), John F. Smith (1850), John G. Smith (1851), John H. Smith (1852), John I. Smith (1853), John J. Smith (1854), John K. Smith (1855), John L. Smith (1856), John M. Smith (1857), John N. Smith (1858), John O. Smith (1859), John P. Smith (1860), John Q. Smith (1861), John R. Smith (1862), John S. Smith (1863), John T. Smith (1864), John U. Smith (1865), John V. Smith (1866), John W. Smith (1867), John X. Smith (1868), John Y. Smith (1869), John Z. Smith (1870).